Cantilever systems for the next generation of biomechanical sensors

Marco Lazzarino

University of Groningen
Zernike Institute
for Advanced Materials

Cover: Artistic variations of a scanning electron micrograph of oscillating cantilevers. Fabricated, imaged and elaborated by the author.

Printed by: Facilitair Bedrijf RuG, Groningen

ISBN 978-90-367-5818-5

ISSN 1570-1530

Zernike Institute for Advanced Materials Ph.D.-thesis series 2012-24

RIJKSUNIVERSITEIT GRONINGEN

Cantilever systems for the next generation of biomechanical sensors.

Proefschrift

ter verkrijging van het doctoraat in de

Wiskunde en Natuurwetenschappen

aan de Rijksuniversiteit Groningen

op gezag van de

Rector Magnificus, Prof. Dr. E. Sterken,

in het openbaar te verdedigen op

dinsdag 04 december 2012

om 09:00 uur

door

Marco Lazzarino

geboren op 18 april 1966

te Savona, Italië

Promotor:	Prof. dr. P. Rudolf
Beoordelingscommissie:	Prof. dr. F. Parmigiani
	Prof. dr. J.T.M. De Hosson
	Prof. dr. E. Van der Giessen

CONTENTS:

CHAPTER 1

Introduction

Micro-Electro-Mechanical Systems, or MEMS, is a technology that in its most general form can be defined as miniaturized mechanical and electro-mechanical elements (*i.e.* devices and structures) that are made using the techniques of microfabrication. The critical physical dimensions of MEMS devices can vary from well below one micron on the lower end of the dimensional spectrum, all the way to several millimeters. Likewise, the types of MEMS devices can vary from relatively simple structures having no moving elements, to extremely complex electromechanical systems with multiple moving elements under the control of integrated microelectronics. The one main criterion to define a MEMS device is that there are at least some elements having some sort of mechanical functionality whether or not these elements can move. The term used to define MEMS varies in different parts of the world. In the United States they are predominantly called MEMS, while in some other parts of the world they are called "Microsystems Technology" or "micromachined devices". A recent development of MEMS are NEMS, or nano-electromechanical systems, in which the moving parts are nanometric in size and have peculiar properties which derive from their nano-character.

While the functional elements of MEMS are miniaturized structures, sensors, actuators, and microelectronics, the most notable (and perhaps most interesting) elements are the microsensors and microactuators. Microsensors and microactuators are appropriately categorized as "transducers", which are defined as devices that convert energy from one form to another. In general sensors convert a measured mechanical signal into an electrical signal; in the case of biosensors, a biological interaction first translates a biological signal, typically the presence of biological molecules, into a mechanical signal which is then transduced into an

electronic signal. Since the second part is common to all microsensors and realatively mature, research has been mainly focussed on the first step.

The field of micromechanical biosensors originated about 10 years ago. A paper entitled: “Translating biomolecular recognition into nanomechanics” appeared in the April 2000 issue of Science magazine [Fritz 2000], and the main message of that paper, namely that it was possible to transduce a biomolecular interaction into a nanomechanical motion, envisioned all the potential implications of this message. After 12 years this article has been cited more than 1000 times and can probably be used to identify the birth of micromechanical biosensors. Several papers were published before, and many others have been published later. In the last 10 years, several approaches have been proposed, several different environments have been tested and the average performances have been improved by many orders of magnitude. The mass sensitivity has been improved from single cell, single, virus, single molecule, to nearly single atom detection. The latter was obtained using carbon nanotubes–based nanomechanichal oscillators which have a mass sensitivity in the zeptogram range (zepto = 10^{-21}). Original read-out strategies have been proposed, coupling mechanical, electrical, dielectrical, piezoresistive, piezoelectrical and optical properties of resonating elements and the integration with CMOS platform have been proposed.

In spite of the huge effort and the excellent results obtained so far, the arrangement of the mechanical microstructures used for biosensing did receive a very limited attention. The different typologies of micro- and nanomechanical systems used in biosensing can be gathered in three main categories:

- static sensors

These are flat and thin beams, clamped at one end, that bend upon the adsorption of a molecule on one side, which has been previously functionalized. They can be made of silicon, silicon nitride and a large choice of polymeric materials and have typical in plane size in the hundreds of micron range, and thickness in the micron range.

- dynamic cantilevers

These are flat and thin beams, clamped at one end, that oscillate at a very specific resonance frequency that depends on the size and the material properties. The cantilever mass increase after a biomolecular recognition induces a change in the resonance frequency proportional to the increase of mass. The smaller the size of the cantilevers the better is the mass sensitivity, therefore the cantilever size has been shrunk down to submicron range.

- double clamped beams

Thin beam clamped at both ends, are operated in dynamic mode as for cantilevers but being much stiffer, they may reach much higher resonance frequencies and offer a higher sensitivity. The record in mass sensitivity for a microfabricatred NEMS has been reached using double clamped beams. The presence of two terminals offers further advantage in the actuation and detection, which here can be also magnetic and electric, since a current can flow through the beam.

In this thesis work I resume my activity devoted to the investigation of alternative geometries of nanomechanical oscillators. Complex system can, in principle, improve the simple micromechanical systems described above, by extending their basic operation to more complex transfer functions and to more challenging environments. The vision of this work is that cantilevers and double clamped beams can be the building blocks for more complex devices that offer pre-defined functions and improved performances.

The main topic of this thesis work, entitled “Cantilever systems for the next generation of biomechanical sensors” can be subdivided in two parts:

- twin cantilevers

These are couples of cantilevers facing each other that change their resonance response when one or more molecules react on the gap. Two different geometries have been fabricated and tested. One, with identical cantilevers, takes advantage of the shift in resonance frequency occurring

upon molecular detection; the second with asymmetrical cantilevers, uses the shortest one to actuate the motion of the longer one through a molecular link.

- self-aligned chemomechanical functionalization

Here the structure of twin cantilevers is the starting point for creating a spatially confined chemical functionalization in the gap between two cantilevers facing each other. This original process is extremely precise and represents an important milestone toward the future realization of complex micro- and nanomechanical systems for biomolecular detection.

Chapters 2, 3 and 4 introduce the main concepts in micromechanical sensors, a short description of microfabrication techniques and a short review of the main results published so far in the field. Chapter 5 and 6 describe the twin cantilevers system and are based on two original publications. Chapters 7 and 8 describe the chemomechanical functionalization process and are based on three original publications

Conclusion and future perspectives will resume the main results obtained in these years.

CHAPTER 2

Micromechanical resonators

The invention of the field effect transistor in 1947 gave rise to the beginning of integrated circuit (IC) technology which is the machining of complex electronic circuits on a small piece of a semiconductor [Lojek 2006]. It was immediately clear to that this technology would be a revolution, so big efforts have been made in order to shrink the dimensions and to increase the quality of the microstructures on a chip.

Since the fifties, physicists, chemists and engineers joined up because of the necessity of broad interdisciplinary competences and many materials, processes and tools have been invented and deeply studied. Nowadays, it is possible to realize chips with an area of around 350 mm^2 and with almost 1 million of transistors per mm^2. This allowed shrinking computers which had dimensions of a room into devices which can be kept in one hand. Indeed, "shrink" is the keyword of IC industry because smaller means cheaper and faster because less material, power and space are required.

In thirty years, the minimum printed line widths (*i.e.* transistor gate lengths) has reduced from 10 μm (1971) to 32 nm (2010) and the International Technology Roadmap for Semiconductors (ITRS) estimates that 11 nm will be reached in 2022 (www.itrs.net). It will be the ultimate step of the miniaturization of silicon devices: smaller than this will be forbidden by quantum mechanics laws.

However, all the know-how accumulated in decades was not confined only in the electronic industry but several and different applications have been proposed. In the 1970s, the concept of micro-electro-mechanical systems (MEMS) was introduced and now this technology is widespread in many devices, from inkjets printers to automotive applications, and has conquered an important market share [Kajakaari 2009]. In MEMS

mechanical elements and electronics are integrated on a common substrate through the utilization of microfabrication technology. The mechanical part, which can move, has two main functions: sensing and actuating. MEMS are used as accelerometers, gyroscopes, pressure or flow sensors and, as actuators, in micromotors, mirror mounts, micro pumps and more.

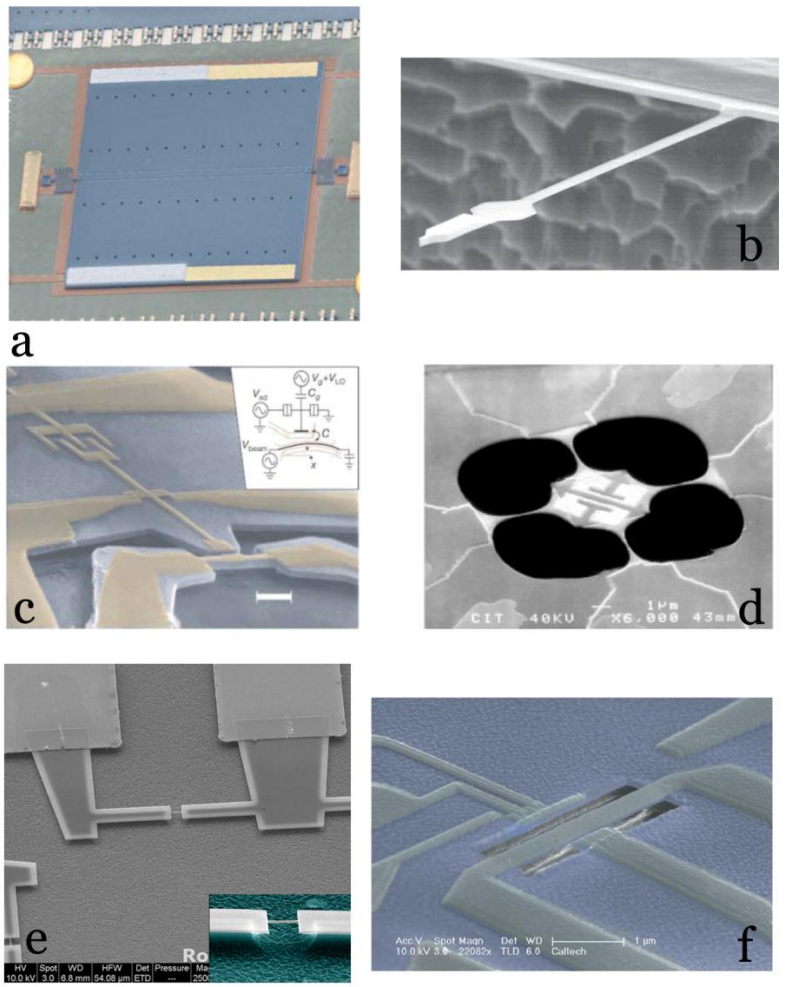

Figure 2.1: *NEMS device. (a) A torsional resonator used to study Casimir forces. (b) An ultrasensitive magnetic force detector that has been employed to detect a single electron spin. (c) A 116-Mhz resonator coupled to a single-electron transistor. (d) Suspended mesoscopic device used for measuring the quantum of thermal conductance. (e) Zeptogram-Scale Nanomechanical Mass sensor. (f) Nanomechanical resonator coupled to qubits*

The reasons of their success are basically three:

- They are cheap. Due to the "batch processing" many devices are made in parallel reducing the price of a single component.
- They are extremely sensitive. In fact, as rule of thumbs, in many applications the smaller sensor, the less it is affected by external perturbation. Moreover as actuator, precision down to nanometer scale is achievable.
- They are small. It is possible to integrate many sensors in a single functional circuit.

Besides these commercial applications which we use every day, MEMS have attracted the interest of some researchers in field of fundamental research.

Due to a constant effort to shrink the device size and to improve the measurement techniques, force and mass sensitivities of the order of zeptonewtons and zeptogram (zepto = 10^{-21}) have been demonstrated. In general, these devices are called nanoelectromechanical systems (NEMS) to stress the difference with the micro-device, but usually only one of three dimension (*i.e.* thickness) is less than 100 nanometers. It became possible to design experiments which in the past were considered only *gedanken experiments* because a huge sensitivity is required. Now, thanks to NEMS some fundamental laws of Physics can be explored. Currently, one of the most important goals is to observe the quantum fluctuations of a mechanical system, due to zero point energy. In figure 2.1 the nanomechanical devices used to produce some of the most important result are shown. [Decca 2003] [Rugar 2004] [Knobel 2003] [Schwab 2000] [Lahaye 2009] [Yang 2006].

However, this kind of measurements requires extremely demanding conditions, like milliKelvin temperatures and ultrahigh vacuum; so with the present technology, they are confined in few high level laboratories and can hardly be employed for any commercial application. But if we accept the compromise of reducing the sensitivity in favour of increasing the feasibility, we can still use the MEMS approach for developing tools and applications for different fields of science, including biology and medicine.

2.1 BioMEMS

The term BioMEMS was introduced to identify a class of MEMS used for biological application but nowadays it has a more broad and general meaning. R. Bashir in his review about BioMEMS [Bashir 2004] gives the definition *"devices or systems, constructed using technique inspired from micro/nano-scale fabrication, that are used for processing, delivery, manipulation, analysis, or construction of biological and chemical entities"*. According to this classification, for example, also force microscopy based on atomic forces or microfluidics devices can be categorized as "BioMEMS". Surely, this definition can appear strange because it includes devices which do not possess any mechanical component or do not integrate directly an electrical part but after all it is just a semantic question. In figure 2 some examples of microfluidic and non-mechanical BioMEMS are shown. [Burns 1998] [Thorsen 2002] [Levene 2003] [Armani 2007] [Prausnitz 2004]

However in this introduction and in the rest of the thesis we shall focus on devices based on the mechanical detection of chemical interaction like adsorption or chemical reactivity. Besides the general advances in using a MEMS technology, there are some which are peculiar to biological and clinical applications.

High sensitivity - In general, biological materials (DNA, protein) are present in very low amounts inside a single cell or even in the entire body. Standard biotechnological approaches need amplification of the material of interest using protocols like polymerase chain reaction (PCR). The main drawback is that an exponential amplification may propagate errors. The alternative approach consists in avoiding duplication by means of a highly sensitive MEMS.

Label Free - Most of the used techniques are based on optical detection. This means that target molecules have to be functionalized with an optically active group (fluorescence). By using alternative detection schemes offered by MEMS this step is avoided and the probability of artefacts and errors reduced.

Parallelization - Biological systems are complex; a single process is often governed by many proteins or an illness can be due to the mutation of

several genes. To have a complete picture it is therefore necessary to measure many markers at the same time. One of the characteristics of MEMS is the possibility of integrate many sensors on the same device. Each sensor can be assigned to a specific molecule. In this way, due to high parallelization, it is possible to perform simultaneously a complex analysis, reducing significantly the time required for a complete diagnosis.

Integration - The idea of a lab-on-a-chip (LOC) is completely based on MEMS. LOC is a device that integrates many laboratory functions on a single chip of only millimeters to a few square centimeters in size. Sometimes the term "Micro Total Analysis Systems" (μTAS) is used as well.

Real time - The direct integration with electronics and microfluidic systems allows to design sensors which provide the results in a real time or in a very short time. From a clinical point of view the speed, together with the accuracy, are essential characteristics for any diagnostic tool.

2.2 Mechanical sensors

Atomic Force Microscopy was invented in 1986 as a tool for imagining of surfaces [Binnig 1986]. It is a complex instrument but the sensing element is completely mechanical. In fact, it is just a cantilever which bends because of interaction with the substrate. In the last few years non-imaging applications were developed and the AFM was used for studying inter- and intramolecular interactions down to the single molecule level. This became possible because force spectroscopy based on these new experimental tools allows to measure forces in the piconewton (even in femtonewton) range on a μs time scale. The AFM force spectroscopy is still a growing field but researchers have also began to develop the cantilever-like mechanical sensor. Cantilever is one of the possible geometries of a mechanical sensor but in this chapter it will be considerated as a benchmark model.

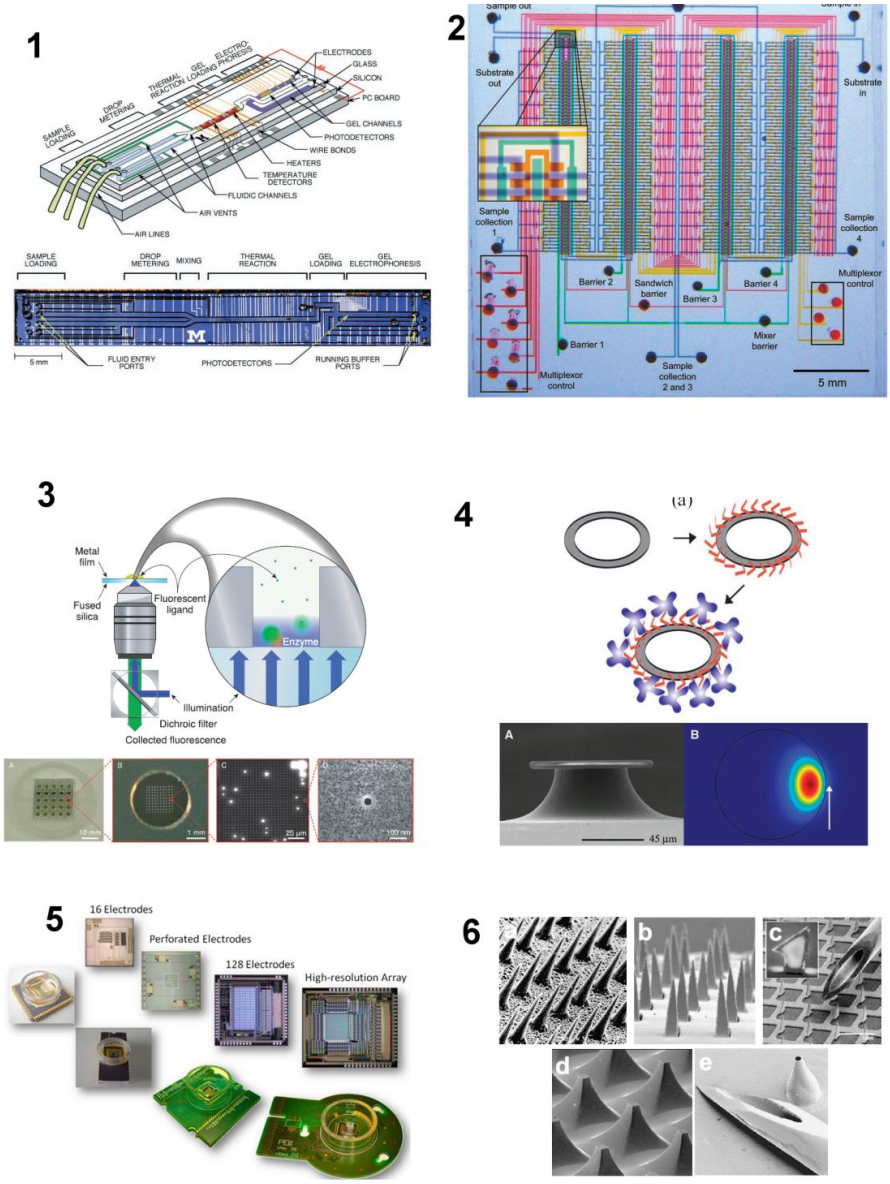

Figure 2.2: *BioMEMS (1) An Integrated Nanoliter DNA Analysis Device which has fluidic channels, heaters, temperature sensors, and fluorescence detectors to analyze nanoliter-size DNA samples. (2) Optical micrograph if an High-density microfluidic chips that contain plumbing networks with thousands of micromechanical valves and hundreds of individually addressable chambers. The various inputs have been loaded with food dyes to visualize the channels and subelements of the fluidic logic. (3) Zero-Mode Waveguides for Single-Molecule Analysis. (A) The coverslip, with overlying gasket to isolate arrays for individual*

experiments. Successive increases in scale are shown in (B) to (D). A scanning electron microscope image of an individual waveguide is shown in (D). (F) An apparatus for single-molecule enzymology using zeromode waveguides. (4) The microtoroid resonator biological sensor. The interaction of the whispering-gallery mode with the environment, specifically molecules bound on the surface of the toroid, enables the ultrasensitive detection .(5) Microelectrode arrays (MEAs) are arrangements of usually 60 electrodes that are used for multisite extracellular recordings from electrogenic cells. The high-density CMOS-based microelectrode array features 11,011 metal electrodes and 126 channels, each of which comprises recording and stimulation electronics, for extracellular bidirectional communication with electrogenic cells. (6) Images of microneedles used for transdermal drug delivery.

The adsorption of molecules on a cantilever sensor has two main effects: it increases the mass and changes the surface stress. There are three approaches to measuring which divide MEMS mechanical sensors in as many categories:

Static mode: the static deflection due to differential surface stress is measured.

Dynamic mode: the response to an external periodical force in frequency range around the resonance is measured. It gives information about the resonance frequency and the shape of the resonance curve.

Resonance Frequency PLL mode: the cantilever is kept at its resonant frequency by following the change in resonant frequency by means of a Phase Lock Loop.

2.2.1 Static Mode

The theory describing the static deflection due to differential surface stress is very simple. A generic beam which experiences a different surface stress on two opposite sides, bends and the deflection δ is proportional to the differential stress $\Delta\sigma$ according to Stoney's equation [Stoney 1909] [Butt 1996]:

(2.1) $$\delta = \frac{3(1-\nu)}{E}\left(\frac{L}{t}\right)^2 \Delta\sigma$$

where ν is Poisson's ratio, E Young's modulus, L the beam length and t the cantilever thickness. This model is valid also for a micrometer sized cantilever and by means of selective functionalization of one side of the cantilever, it possible to transduce molecular adsorption to mechanical bending. The selective functionalization is usually obtained by exploiting the gold-thiol interaction. Probe molecules are functionalized with a thiol group and one side of the cantilever is coated with gold. Thiolated molecules covalently bind with the gold substrate. Subsequently the target molecules bind to the probes. Each step induces a bending. Arrays of cantilevers allow for differential measurements to recognize different molecules. In 2000, Gerber and his collaborators published a milestone paper about the application of this technique for biomolecular recognition [Fritz 2000]. More detailed examples of static detection are reported in the chapter 4: "State of the art in 2012"

2.2.2 Dynamic mode

A mechanical system responds to an external oscillating force with different amplitude depending on the frequency. The spectral distribution is characterized by peaks which are known as resonant frequencies and correspond to oscillating modes. A small driving force at the resonance frequency can induce a large oscillation. The dynamics of the cantilever is described in a simplified model where the cantilever is approximated with a size-less mass linked to a spring (characterized by the spring constant k) which moves in a viscous medium. To describe all the geometrical effects due to the three-dimensional structure, the actual value of the mass is substituted by a reduced value. Each mode has different geometrical factors. A resonance curve is characterized by two parameters: the position of the peak (resonance frequency) and the width of the peak, which is generally calculated at the half maximum and indicated with FWHM (Full Width at Half Maximum). More often, a dimensionless parameter, the quality factor or Q-factor, defined as the ratio between the resonance frequency and the FWHM, is used. The Q-factor also has a physical interpretation since it is proportional to the ratio between the energy stored and the energy lost in one cycle.

There are many sources of energy loss but the most critical one is damping by the medium in which the resonator oscillates. In figure 2.3, some curves

of resonance with different Q-factor are shown. As a general rule of thumbs, in vacuum Q as high as several 10,000 can be reached, in air few hundreds and in liquids it is hard to get Q-factors better than 10.

If the damping is negligible, the peak position of the lowest mode corresponds to the natural frequency and is given by:

(2.2) $$f_0 = \frac{1}{2\pi}\sqrt{\frac{k}{m^*}} = \frac{1}{2\pi}\sqrt{\frac{E}{\rho}}\frac{t}{L^2}$$

where ρ is the density, E Young's modulus, L the beam length and t the cantilever thickness, k the spring constant, m the reduced mass. If the damping is not negligible the peak it is not at the natural frequency but reduced by the factor $\sqrt{1-\frac{1}{4Q^2}}$. For a Q-factor of 10 the reduction is 0.12%, for Q-factor of 1000 is 0.12 ppm. The adsorption of molecules changes the

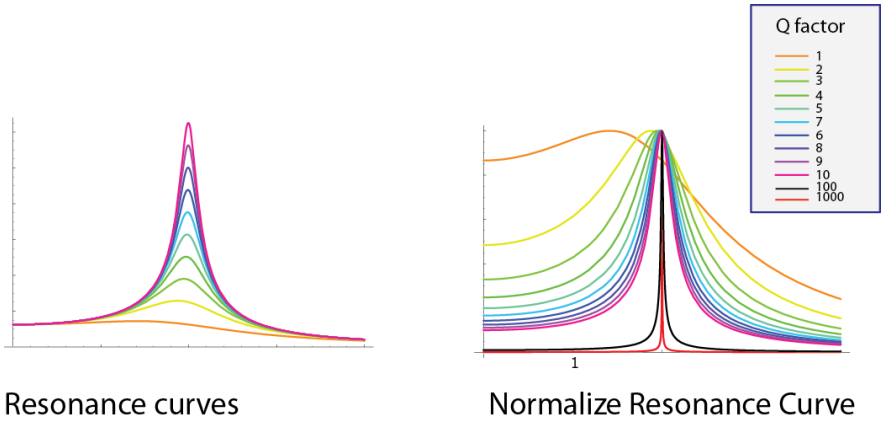

Figure 2.3 *Amplitude (left) and width (right) of the frequency spectrum at the resonance for increasing Q-factors.*

shape of the resonance curves. The main effect is to shift the resonance frequency. In first approximation, the mass of the resonator increases by the quantity Δm, which corresponds to the mass of adsorbed molecules.

According to equation 2.3, the resonance changes to the value

(2.3) $$f_{\Delta m} = \frac{1}{2\pi}\sqrt{\frac{k}{m^* + \Delta m}}$$

assuming that the elastic constant does not change. If the added mass is much smaller than the mass of the resonator, a linear relation between the shift in frequency and the variation of mass is obtained:

(2.4) $$\frac{\Delta f}{f_0} = -\frac{1}{2}\frac{\Delta m}{m^*}$$

Alternatively, it is possible to focus on the change of other parameters such as the change of the device compliance or the Q-factor. This technique is extremely sensitive in vacuum, where attogram resolution is routinely achieved, but has the big disadvantage of losing its power in a liquid environment where due to viscous effects, the width of the resonance increases and the amplitude decreases dramatically. The main consequence is that the minimum detectable frequency shift becomes very large and this approach becomes useless. For biological applications this is a huge limitation but one possible solution is to separate the functionalization and adsorption phase from the measurement phase. This approach is commonly known as "dip and dry". All the chemical reactions are performed in liquid, then the device is dried and placed in a vacuum chamber, where the resonance frequency is measured. With this procedure high sensitivity is

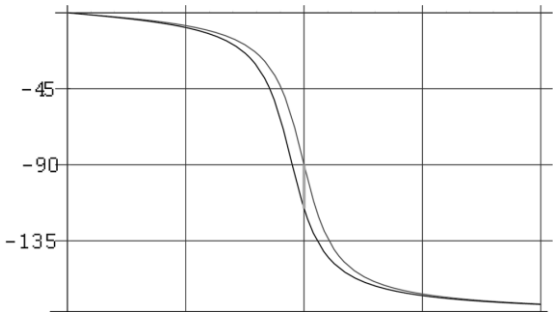

Figure 2.4: *Two curves of phase shift in function of frequency with different resonance frequency.*

preserved but it is necessary to renounce to real time detection. In 2001, Ilic *et al.* reported the detection of a single *Escherichia coli* cell (665 fg) by

means of silicon nitride cantilever with a sensitivity of 7.1 Hz/fg. [Ilic 2001] After three years, the adsorption of a single *vaccinia* virus (9.5 fg) was measured by Gupta *et al* [Gupta 2004]. They used a silicon cantilever with a sensitivity of 6.3 Hz/ag. In 2005, Ilic *et al.* were able to count single dsDNA molecules (999 KDa = 1.6 ag) bound to a nanomechanical oscillator with a sensitivity of (194 Hz/ag). More details will be provided in chapter 4.

2.2.3. Resonance Frequency PLL mode

This mode is usually included in the dynamic mode because the cantilever is kept in oscillation; however it differs from the former in that this approach does not provide information about the spectral response but only about the shifts of the resonance peak. If an oscillator is actuated there is a phase difference $\Delta\phi$ between the actuation and the amplitude oscillation and it is function of the actuation frequency f:

(2.5) $$\varphi = \tan^{-1}\frac{-f_0 f}{Q(f_0^2 - f^2)}$$

At resonance, the phase difference is -90^o. As the name suggests, this detection mode is based on a phase lock loop circuit [Best 2007]. The cantilever is actuated by an electronic signal with frequency f. The actuating signal is -90^o shifted and continuously compared to the signal of the cantilever deflection. If f is set to be equal to f_0, the phase difference of the two signals is zero. If the resonance frequency changes for any reason, the phase difference (error signal) will be different from zero. The error signal controls the actuating signal and changes it in order to cancel itself like in a negative feedback system. This method, like any PLL control, can be implemented both with an analogue circuit and with digital (software) control. It is possible to track the variation in resonance frequency continuously and very quickly. This method has the big advantages to allow for real time and very fast measurements but has the drawback of giving no information about the change of the device compliance or the Q-factor.

2.3 Detection and Actuation

The potential of mechanical resonator sensors is strictly connected to the effectiveness of the actuation and the detection of the movements because the translation from a mechanical response to a measurable signal will be more accurate. Therefore many efforts have been made in order to explore and develop new detection schemes. They can be optical or electrical. The most widely used is the optical lever method [Putman 1992]. Almost all commercial AFMs are based on this technique. The working principle is based on deflection of a laser spot focused on a cantilever. The angular deflection of the cantilever causes twice the angular deflection of the laser beam. The reflected laser beam strikes a position-sensitive photodetector consisting of two side-by-side photodiodes. The difference between the two photodiode signals indicates the position of the laser spot on the detector and thus the angular deflection of the cantilever. Since the cantilever-to-detector distance generally measures thousands of times the length of the cantilever, the optical lever greatly magnifies (~2000-fold) the motion of the tip. Photodiodes, divided into two or four independent areas, transduce the light into electrical signals that are amplified and elaborated to get the deflection of the beam. Optical lever detection is currently the most sensitive method for measuring deflection; vertical deflections as small as a few Ångstroms can be reliably measured with this technique. On the other hand the set up needs a laser source, some optics element (lens, mirrors) and a photodiode, therefore it is rather cumbersome and expensive. The reduction of the dimension of the cantilever is limited by optical diffraction. Moreover it has low degree of parallelization; in fact, by means of multiple sources and detectors it is possible to monitor different cantilevers but due to cost and complexity issues the number of detectors is not higher than ten.

A second optical detection method is a based on interference [Boef 1989]. As shown in the left panel of figure 2.5, the cantilever is used as the moving mirror in a Michelson interferometer. The movement of the cantilever causes a change in the optical path of one arm of the interferometer resulting in a change of intensity of the light at photodiode due to constructive or destructive interference. This method is extremely sensitive (deflection of the order 0.01 Å can be measured) and does not need an external height calibration. However it has the same practical

limitation of the optical lever method. Also detection methods based on a Fabry-Perot scheme have been developed.

The group of G. Nordin recently proposed an alternative optical detection [Noh 2008]. These authors developed a photonic microcantilever with in plane photonic transduction of deflection. In this approach the microcantilever is etched to form a single mode rib waveguide. Light propagates down the microcantilever and crosses a small gap at the free end of the microcantilever; a fraction of the light is captured by an asymmetrical multimode waveguide that terminates in a Y branch. The Y-branch output is used to form a differential signal that is monotonically dependent on microcantilever deflection.

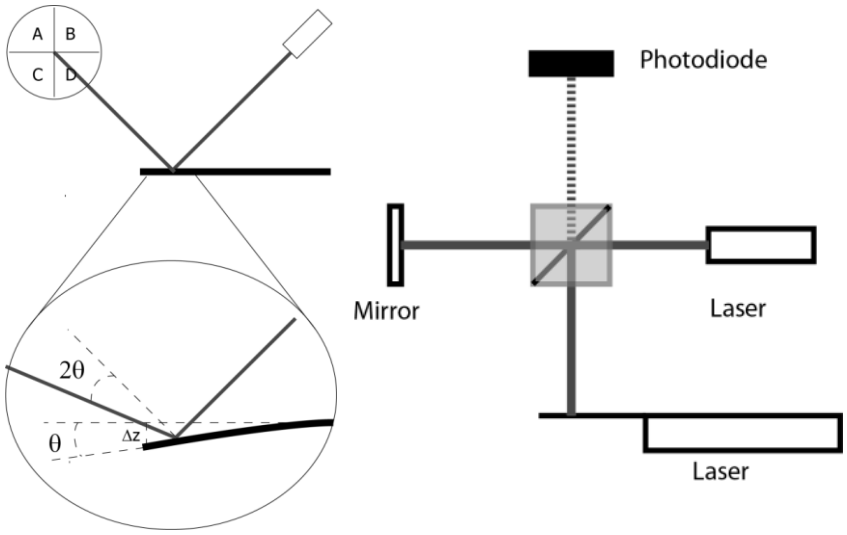

Figure 2.5 *left: optical lever method for the measure of cantilever deflection. A tilt of θ of the cantilever induces a tilt of 2θ in the optical path. If the ratio of the optical path versus cantilever length is 1000 (100 mm and 100 μm, respectively) a deflection of 1 nm of the cantilever translates into a shift of 2 μm in the beam position on the detector. Right: a Michelson interferometry scheme for cantilever movement detection. This method is used mainly inside cryostats, where the space is restricted.*

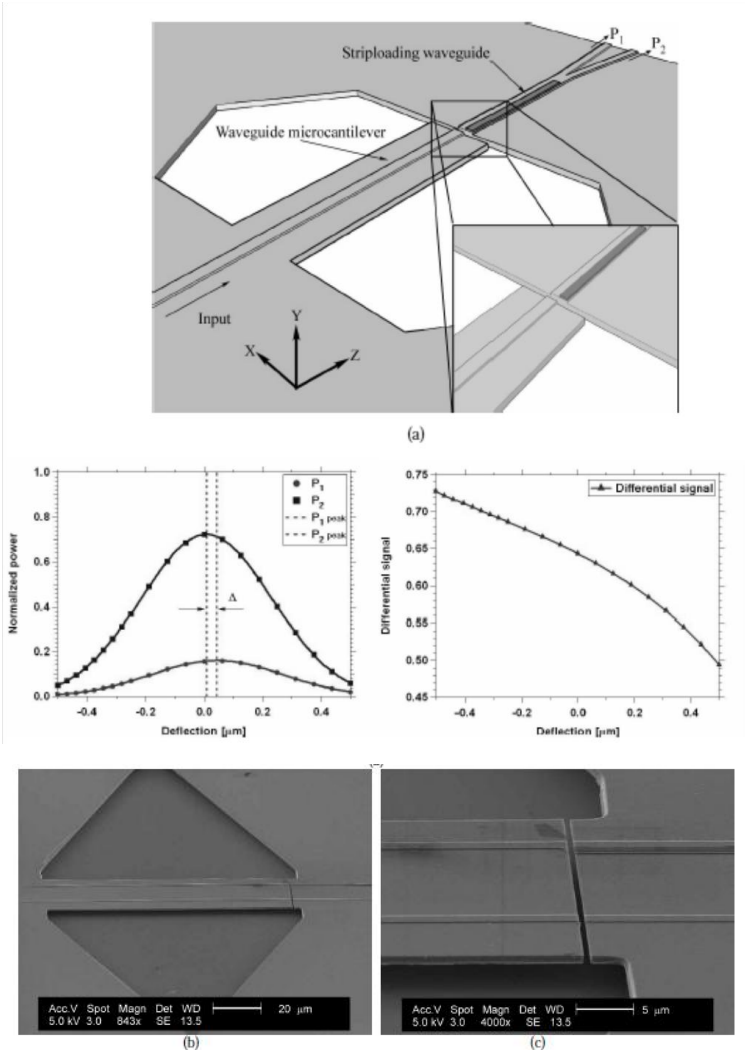

Figure 2.6: *Optical detection after [Noh 2008]. The cantilever has integrated an optical waveguide matching a second waveguide on the chip. When the cantilever does not move, all the light is transmitted across the gap. When the cantilever oscillates, the light is modulated at the oscillation frequency.*

A resonant sensor can also be placed inside an electrical circuit and act as variable resistor or capacitor. The strain can change the electrical resistance of metals or semiconductors. In the case of a metal the effect is totally geometric and is described by Ohm's law. By contrast, in semiconductors the change of resistance is principally given by the change

of the resistivity. This effect is called piezoresistivity and is due to the dependence of the bandgap on the inter-atomic spacing. By integrating a piezoresistive element onto a resonator or design a resonator in order to be a piezoresistive sensor, it is possible to detect the bending by measuring the change of resistance. This method is less sensitive than the optical ones and more affected by thermal fluctuations but it offers many advantages. There are no limitations on the size of the resonator, integration with the read-out electronic on the same silicon chip is possible and parallelization is only limited by wiring issues. Similarly, the piezoelectric effect is also used to correlate motion with an electric signal. Even if there are many limitations a capacitive detection method is also used. [Davies 2003] The cantilever and the substrate form a parallel plate capacitor if they are separated by an insulating layer as illustrated in figure 2.7. The capacity is proportional to the surface of the cantilever and inversely proportional to the distance between the cantilever and the substrate. This implies some limitations on the geometry. The gap between the cantilever and the substrate must be the smallest possible in order to enhance the sensitivity involving technical efforts from a fabrication point

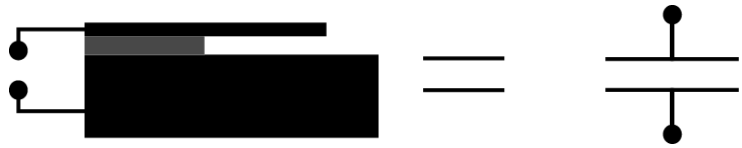

***Figure 2.7**: Cross section of a cantilever fabricated out of a silicon on insulator (SOI) wafer and its correspondence as a capacitor for capacitive actuation.*

of view. Also the miniaturization is limited by sensitivity because the cantilever surface must be large enough to allow a measurable variation of capacity. However the most crucial limitation is that this device is intrinsically a low pass filter (RC circuit) with frequency cut off inversely proportional to the capacity. This makes this scheme not particularly suited for high frequency dynamic measurements.

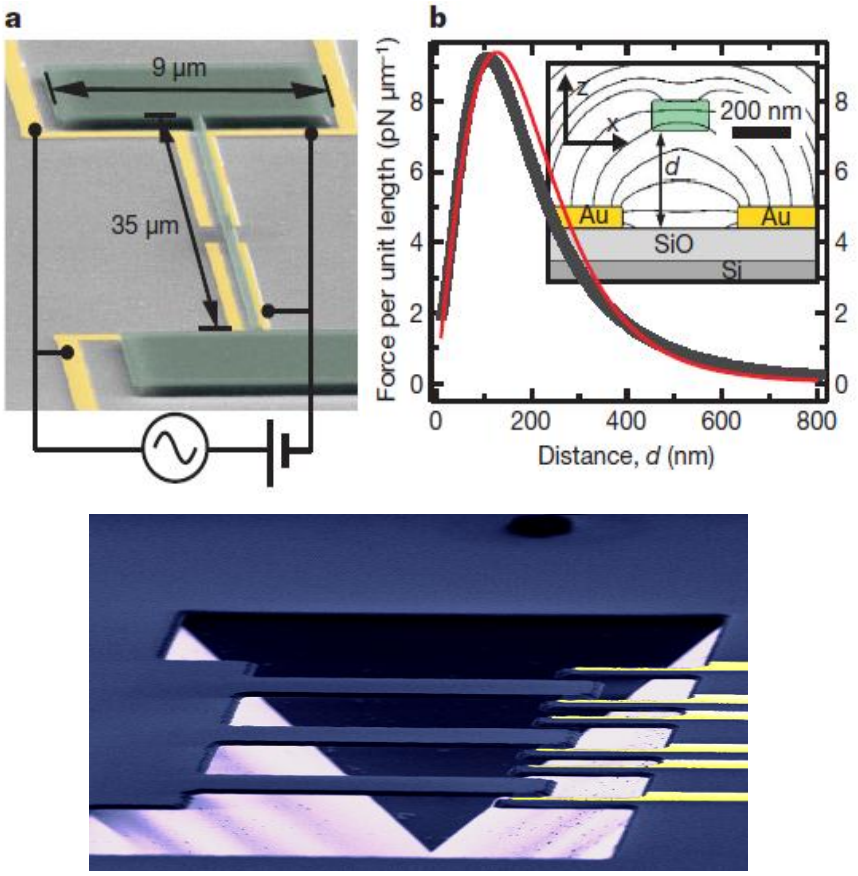

Figure 2.8: *Dielectric actuation. Top: device for excitation of a SiC microbridge, with a sketch of the electric field. Bottom: device for the individual actuation of cantilevers in a triple coupled cantilever system. [H. Pakdast and M. Lazzarino unpublished]*

In dynamical modes the resonators need to be actuated. In many applications, the thermal energy kT is enough to cause a measurable mechanical response but for highest sensitivity applications an external actuation is required to increase the signal to noise ratio. The most widely used technique, especially combined with optical detection, is to mount the chip with the resonator directly onto a piezoelectric crystal. In this method there is no direct force acting on the cantilever but rather a mechanical coupling between the movement of the piezo and the modes of the

cantilever. This technique is very simple to implement but able to actuate at frequencies lower than a few MHz due to the intrinsic frequency cut off the piezo. The capacity detection method can be adapted to be an actuator. In fact, by applying a bias, V, between the cantilever and the substrate an electrostatic force $F = \frac{\varepsilon_0 V^2}{2d^2} S$ is generated.

There are also other electrical methods based magnetomotive force [Ekinci 2004] or on electric displacement [Unter 2009]. They have less bandwidth limitations and allow accessing the GHz range. The latter does not require the control of any material properties of the cantilever, nor necessitate contacts or wiring. Moreover it can be realized in a very compact way and allows for separate actuation of individual resonators. It is therefore one of the most promising method to actuate the systems of cantilevers that are the subject of this work. Figure 2.8a show the basic principle of the method taken from [Unter 2009]. Figure 2.8b presents a structure developed in Trieste by our group to actuate individually each cantilever of a triple cantilever system.

The last actuation mechanism that is worth to mention is based on an optical-thermal mechanism [Ilic 2005]. A modulated laser illuminates one side and induces local heating of the cantilever. The resulting temperature gradient induces an inhomogeneous thermal expansion causing the cantilever to bend.

CHAPTER 3

Microfabrication

Microfabrication is at the basis of the MEMS technology and comprises all the techniques which permit to fabricate structures with dimensions from microns to nanometers. Microfabrication takes place in a particular environment called a "clean room", where air contamination, dust particles present, temperature and humidity are controlled. In fact, if dust particles with dimensions comparable with the microstructure land on a microfabricated device, they will ruin it. Moreover, to obtain robust and repeatable processes, temperature and humidity must have always the same value with very low fluctuations. The most studied and used material for fabrication is single crystalline silicon. Another common substrate in MEMS technology is silicon on insulator (SOI). It consists in a thick wafer of silicon covered by a thin thermal silicon oxide and of a thin crystalline layer of silicon which has the same crystallographic orientation of the substrate. It is widely used in MEMS because by removing the insulator layer (called in this contest sacrificial layer) it possible to make a suspended structure. There are three fundamental processes: lithography, etching and film deposition.

3.1 Optical Lithography

Optical lithography is the process used to transfer a pattern from a mask to a substrate. First, the substrate must be coated with a thin layer of polymer (known as a resist) that is sensitive to ultraviolet radiation. Similarly to photography, an image is projected onto the resist by directing light through a mask. The mask is a glass plate with transparent and opaque zones which draw the desired pattern. According to the type of resist, positive or negative, the illumination renders the polymer soluble or insoluble to a solution called developer. After the development the

substrate is coated with a patterned resist which protects locally the surface. Lithography requires the following steps:

- cleaning of the substrate
- resist deposition by spinning
- prebake for evaporating the resist solvent
- illumination in a mask aligner. The mask aligner permits to align the mask with previous features or with the crystallographic orientation of the substrate
- post exposure bake
- development

The resolution of this pattering process is limited by the light diffraction at the mask edges and, as a rule of thumb, is given by half the wavelength of the radiation used for the exposure. The main lines of a mercury vapour lamp are 365.4 nm, 404.7 nm and 435.8 nm and the maximum resolution amounts to around 150 nm. Using X-rays the resolution can be increased to below 10 nm but this is commonly used only in synchrotron facility.

Alternatively, there is another kind of lithography based not on electromagnetic radiation but on electron beams. A scanning electron microscope allows to focus electrons on spots of the order of 2 nm on a substrate. The process is similar to photolithography but a different resist, which is sensitive to electrons, is employed. Moreover there is no need of a mask because the pattern is created by moving the beam under control of a computer using a pattern generator. The final resolution is limited by the properties of the resist and resolution down to 10 nm can be routinely achieved. However, it is possible to push the resolution down to 5 nm. E-beam lithography offers higher resolution and greater flexibility with respect to standard optical lithography but it is very slow and the throughput is extremely low.

3.2 Chemical etching

Chemical etching is the second fundamental process and serves to remove material from the substrate. The patterned resist permits to control spatially the etching. There are two classes, wet etching and dry or plasma etching. In the wet etching process the wafer is put in a solution, where an active

component removes material by making it soluble. For example two very important reactions are:

$$SiO_2\,(s) + 6HF \rightarrow H_2SiOF_6\,(aq) + 2H_2O$$
$$Si\,(s) + 2OH^- + 2H_20 \rightarrow Si(OH)_2(O^-)_2\,(aq) + 2H_2\,(g)$$

In plasma etching the wafer is placed in a vacuum chamber where a plasma of a particular gas is created. In this case, the reaction with the plasma makes the material volatile, for example:

$$SiO_2\,(s) + CF_4\,(g) \rightarrow SiF_4\,(g) + CO_2\,(g)$$

The plasma of a heavy gas such as Argon can also be used to physically remove material by ion bombardment. This process, known as ion milling, is used especially with materials which are quite inert and hence cannot be removed by chemical etching.

The speed at which material is removed by etching is called the etching rate and ranges from 1 nm/min to 1 μm/s. The etching rate is not constant but depends on many factors which characterize each process:

Selectivity: this is the ratio between the etching speeds of different materials. For example, hydrofluoric acid removes silicon oxide one hundred times faster than silicon.

Isotropy: an etching can attack differently each crystallographic plane of a crystalline material. If the material is amorphous, the etching will be uniform and result in a spherical profile. On the contrary, anisotropic etching is characterized by being ineffective on some crystallographic planes and results in a profile with tilted, flat walls. For example potassium hydroxide etches fast the silicon (100) plane but extremely slowly the (111) plane.

Aspect ratio: it is the ratio between the lowest dimension of the pattern and the height of the etching. This parameter is important especially in anisotropic etchings where the target is to create a vertical wall. In fact, a perfect anisotropy is impossible to achieve and there is always some undercut or overcut which limits the aspect ratio.

3.3 Film deposition

The opposite of etching is the deposition of material. There are several techniques: chemical vapour deposition (CVD) with many variants (light-assisted, plasma assisted etc.), sputtering, thermal evaporation/ sublimation and electron beam evaporation. In CVD a heated wafer reacts with gaseous reactants in a vacuum chamber giving rise to growth of a thin layer of a desired material. CVD is usually employed to grow silicon oxide or silicon nitride. Sputtering is a process where a solid target material is bombarded by energetic and heavy particles causing the ejection of atoms of the target. The projectiles are often supplied by an argon plasma. Thermal and e-beam deposition are similar processes where a target material is heated up to cause evaporation/sublimation. The difference between the two is in how the heating is achieved; in thermal evaporation/sublimation the target are warmed by a standard heat source, while in e-beam deposition an energetic and intense electronic beam is focused on a target.

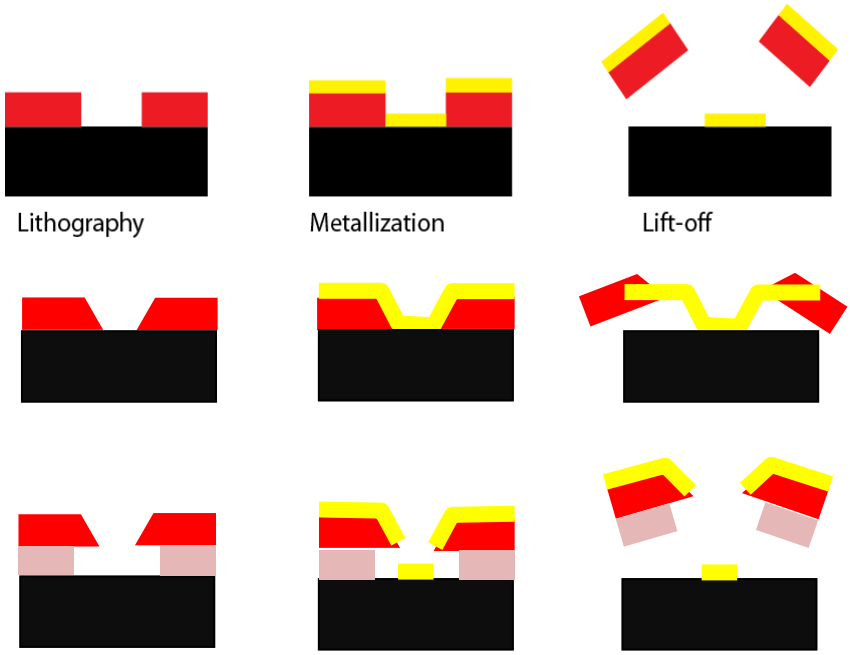

Figure 3.1 *Lift off process without and with the use of a two layer resist technique.*

Strictly connected with film deposition is the lift-off process which is the metallization after lithography and the removal of the resist. All metal deposited on the resist is removed but the metal adhering directly to the substrate remains and follows the pattern of the lithography as sketched in figure 3.1. However lift off is not a trivial process and much care must be taken to avoid retention and re-deposition of the unwanted metal sheet. A typical problem encountered in a lift off process arises when the lateral walls of the resist pattern are not vertical, so that the evaporated metallic film is continuous everywhere. To circumvent this problem, a two layers resist film is deposited, with the lower one overexposed, so that a significant undercut is realized and the deposited film is not continuous, as also sketched in figure 3.1.

3.4 Suspended structures release and critical point drying

Very often in surface micromachining processes, the moving parts, like cantilevers and suspended bridges, are obtained by the etching of an underlying sacrificial layer. In most cases the sacrificial layer is made of silicon oxide, which is etched selectively by HF or NH_4F aqueous solutions. However, when the suspended structures are thin and flexible, the process of drying after etching causes their collapse because of the capillary forces exerted by residual water after rinsing. The scheme of this phenomenon is

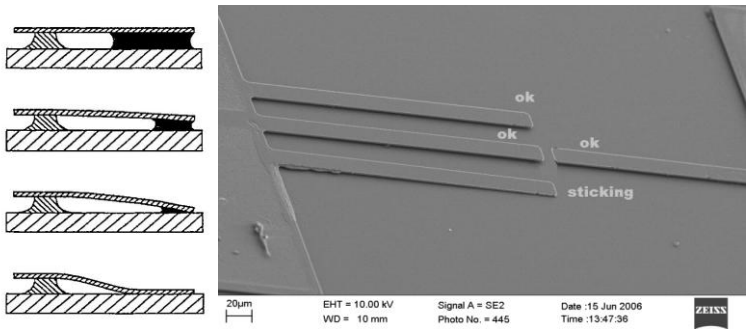

Figure 3.2 *Sticking effect after the release and drying process in the fabrication of a twin cantilever device from a silicon on insulator wafer.*

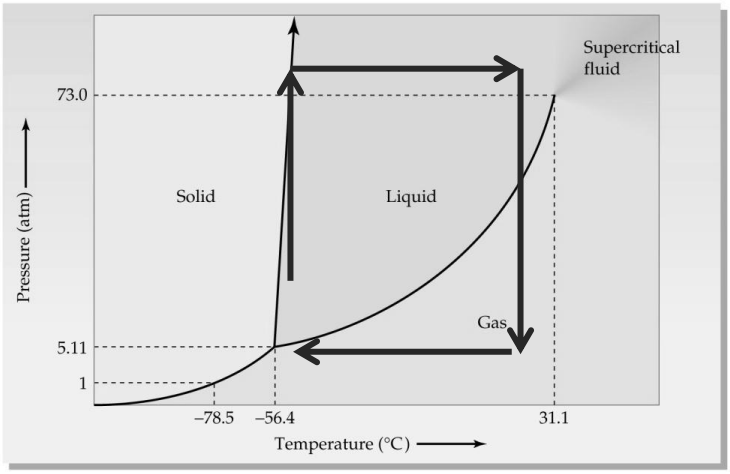

***Figure 3.3**: CO2 phase diagram with the path used to remove the liquid without crssing any phase boundary*

illustrated in figure 3.2a and the effect on a cantilever system is shown in figure 3.2b.

To circumvent this problem, critical point drying can be used. It takes advantage of the peculiar phase diagram of CO_2 in which the critical point is at reasonably low temperature and pressure, within the reach of lab equipment (see figure 3.3 for an example of a CO_2 phase diagram).

Here, the water resulting from the post-etching rinsing is first substituted by ethanol and then by liquid CO_2 below 273 K but above the freezing point of ethanol. At this point both pressure and temperature are raised above the supercritical point, and finally the chamber is evacuated, thus avoiding crossing any phase boundary, with the related surface tension that may force the collapse of suspended structures.

CHAPTER 4

The state of the art in 2012

In this chapter I shall review the main achievements obtained in the field of micro- and nanomechanical biosensing. Some results have been already anticipated in the previous chapter but will be described with more detail here.

4.1 The static approach

The first remarkable report about the use of micromechanical systems to detect a molecular phenomenon dates back to 1997 [Berger 1997]. In this paper the deflection induced by the formation of a self-assembled monolayer (SAM) of alkanethiol molecules on top of a gold-coated atomic force microscope (AFM) cantilever was recorded as a function of time. Since self-assembly causes compressive surface stress that closely follows Langmuir-type adsorption kinetics up to monolayer coverage, the cantilever bends downwards following the formation of the SAM and this bending can be monitored using the deflection of a laser onto a four quadrant detector. Moreover, the surface stress at monolayer coverage was found to increase linearly with the length of the alkyl chain of the molecule, therefore both the formation of the monolayer and the length of the alkane chain can be determined. In left part of figure 4.1 the scheme of the experiment is shown, while in the right panels of figure 4.1 the response curves versus time are reported for different alkanethiol length. Using this approach the authors were able to determine variations above the readout noise that are attributed to local non-uniformity of the molecular solution due to thermal turbulence in the attomolar range.

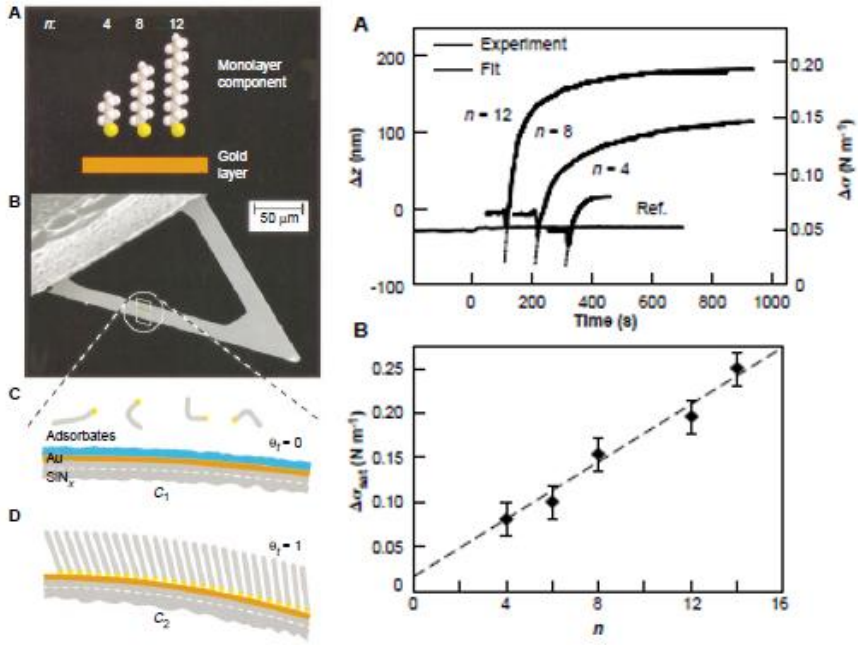

Figure 4.1. *The experiment conceived by Berger and coworkers using a commercial AFM cantilever and alkanethiols (Top left). The absorption on the top side of the cantilever induces its downward bending, mainly because of steric forces (Bottom left). The evolution of the bending with time reaches saturation when a complete monolayer is formed. The saturation bending value increases with molecular length (right).*

This approach was applied to molecular detection a few years later when the same effect, bending of a microcantilever following a molecular reaction, was used to determine the hybridization of a SAM of single strand DNA [Fritz 2000]. Differently from the previous work (from the same group), here the microcantilevers were fabricated on purpose, instead of using standard AFM sensors. A second remarkable improvement from a conceptual point of view was that the sensor could be operated in liquid, thus enabling real biosensing in biological conditions. The mechanism still relied on the increase of the steric hindrance induced by the volume increase of the hybridized DNA molecule with respect of the single strand

molecule. A cartoon of the working principle of the device is displayed in the left panels of figure 4.2. In panel (A), two cantilevers with different DNA functionalization are shown. In panel (B), ssDNA molecules complementary to only one of the strands grafted onto the cantilevers are introduced and only one cantilever deflects. In panel (C) the second complementary ssDNA is introduced and then also the second cantilever bends. The experimental results are displayed in the right panels of figure 4.2. Due to turbulence and thermal effects it was difficult to track unambiguously the movement of one cantilever at a time but the comparison with a reference cantilever provides the unequivocal signature of the hybridization effect.

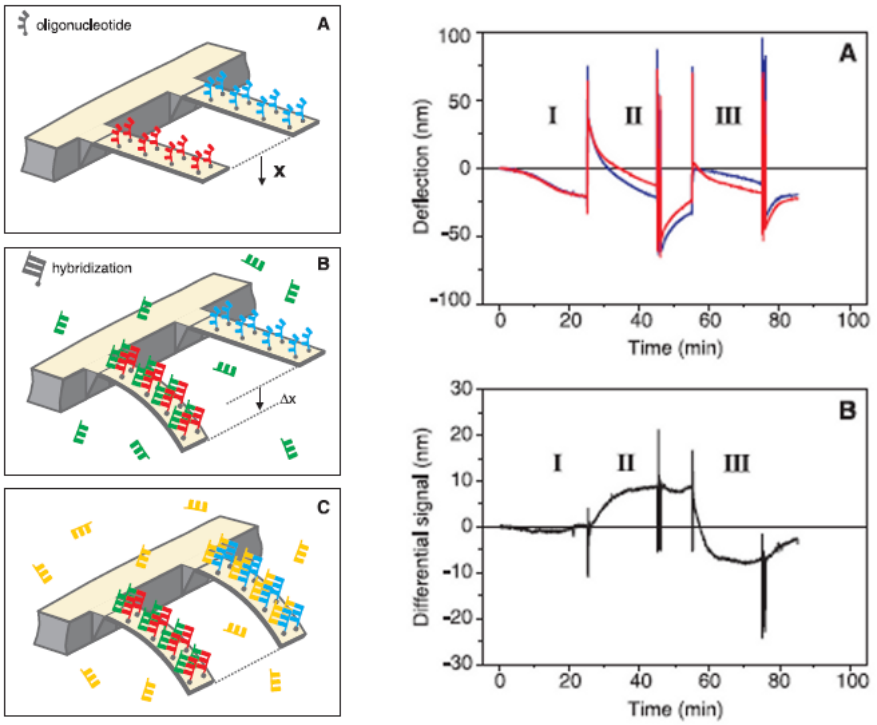

Figure 4.2. *Use of cantilevers to detect molecular recognition. Left: A) Two cantilevers are hybridized with different ssDNA sequences. B) Upon exposure to a solution with complementary strands of one type, one cantilever is hybridized and bends, while the other hosting a non-complementary sequence, remains unchanged. C) Exposing the cantilevers to the second complementary sequence, also the latter cantilever is bend. Right A) Individual bending signal as a function of time. B) Differential signal: the noise induced by flow and thermal drift is cancelled.*

The static approach has become quite broadly diffused and several groups used it in different fields to detect not only DNA hybridization but also antigene- antibody reactions, enzymatic reactions etc. For instance the Thundat group in Californa applied cantilever bending to investigate the detection of human prostate specific antigene (PSA) at low concentration (as low as 0.2 nM) in mM concentration of human serum albumin, showing a remarkable sensitivity and selectivity of the cantilever response [Wu 2001]. Concentris, a company based in Basel distributes a platform for the use of microcantilevers with the static approach. Several companies including IBM provide chips with eight cantilevers 100x500x2mm^3 made of silicon nitride for this purpose.

The static approach however works only at relatively high concentrations (above the nM range) and for reactions involving a large number (10^7 to 10^{10}) molecules; it is therefore not adequate for high sensitivity applications.

4.2 The Dynamic Approach

The alternative to the static approach is the dynamic approach where, as already described in the previous chapter, the resonance frequency of a cantilever is monitored as its mass changes. In the late '90s several authors described the fabrication and measurements of devices, which were aimed at the detection of a mass increase by monitoring the change in resonance frequency. However the first application to real detection was demonstrated by the group of Harold Craighead at Cornell [Ilic 2001], who fabricated silicon nitride cantilevers with lengths and widths in the range of 5-50 and 15-400 μm, respectively and a thickness of 320 nm so that the resonance frequency was in the 10 kHz range. The cantilever surface was functionalized with a layer of purified goat *anti-Escherichia coli* O157:H7 antibodies to detect selective binding to *Escherichia coli* cells. Figure 4.3a shows a scanning electron microscope (SEM) image of a cantilever with a single cell adsorbed on its surface. The resonance frequency measurement was performed in air, and the quality factor was correspondingly low but the cell mass is large enough to induce a significant frequency shift. The frequency response before and after cell adsorption are displayed in figure 4.3b. By performing a statistical analysis the authors showed that counting of detected cells was indeed possible (see figure 4.3 panel c and d).

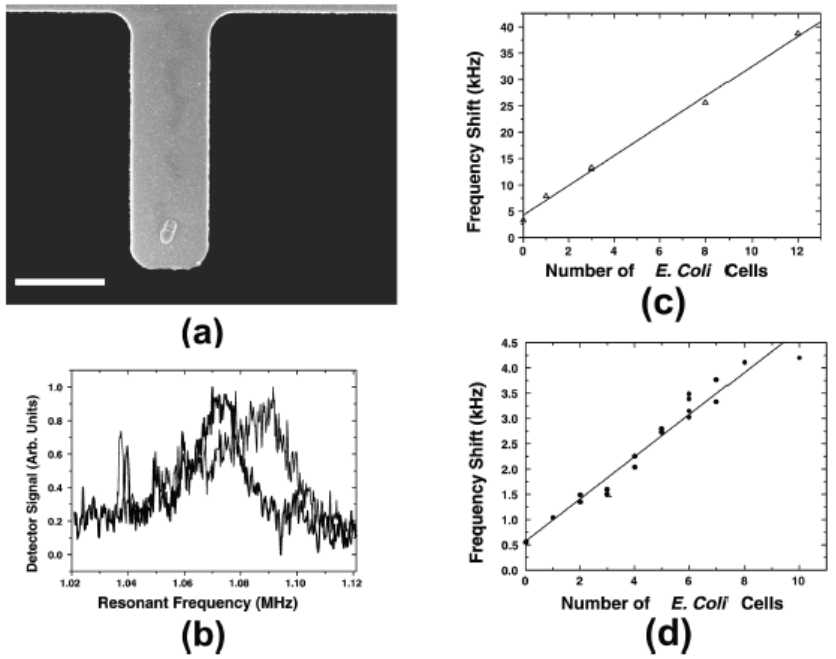

Figure 4.3 (a). *SEM image of a single Escherichia coli cell bound to the immobilized antibody layer on top of the oscillator. (b) The corresponding transverse vibration spectra of the cantilever due to the thermal and ambient noise before and after antibody immobilization and single cell attachment. The shift due to a single cell and an antibody coating was 7.9 kHz (Δ f cell 54.6 kHz and Δf antibody 3.3 kHz). In air, the mechanical quality factor, Q, is very low (Q=50) due to considerable air damping of the cantilever vibrations. Measured frequency shift vs the number of bound Escherichia coli cells for the l=15μm (c) and l=25μm (d) long cantilevers.*

Using smaller cantilevers, Gupta and coworkers were able to count smaller entities, namely *vaccinia* virus which is a member of the Poxviridae family and forms the basis of the smallpox vaccine. In general, they proved that decreasing the overall dimensions of the cantilever beams results in a corresponding increase in the mass sensitivity: they obtained a mass sensitivity of 9.5 pg at atmospheric pressure. [Gupta 2004] The next step was to introduce vacuum technology. Operating in vacuum at a pressure of

$3.3x10^{-7}$ Torr, the dissipation due to air interaction is removed and the quality factor of the resonator improves by several orders of magnitude up to 8500, which in turn allows the detection of smaller frequency shifts.

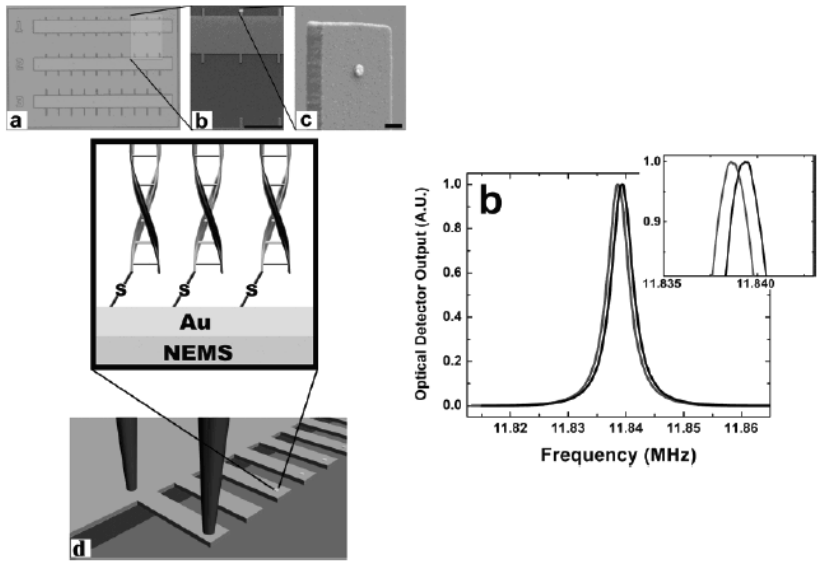

Figure 4.4 *Optical and SEM images of microcantilevers used to detect a single dsDNA molecule. The location of the molecular adsorption is defined by a Au dot defined lithographically (C panel). The cantilever oscillation is actuated by the photothermal effect generated by a pulsed laser at the base of the cantilever, and is read with a laser focused on the cantilever extremity forming a Fabry Perot cavity (Panel D). The resonance response with and without the adsorption of a dsDNA molecule with 1480 bp (red and black curves respectively). The cantilevers were operated in high vacuum conditions (10^{-7} torr) and showed Q-factors up to 5000.*

The group of Harold Craighead at Cornell first used this approach to investigate in detail the ultimate limit of detection of nanocantilevers [Ilic 2004]. They used a well-defined gold nanopad to localize molecular adsorption to avoid any possible effect related to the strain induced by the adsorption itself. This polycrystalline silicon device was 165 nm thick, 500 nm wide, and 4 μm long, with paddle dimensions of 1μm x 1μm and a gold pad with a diameter of 250 nm. Using a SAM of thiolated molecules (namely a dinitrophenyl polyethylene glycol undecanthiol-based molecule,

~DNP-PEG4-C11thiol) they were able to measure a mass change of 6.3 attograms with a minimum theoretical sensitivity of 0.63 ag. One year later they applied their device to measure and enumerate molecules of double strand DNA [Ilic 2005]. Figure 2.7 shows a cartoon in which the experimental apparatus is schematically depicted and SEM pictures of representative devices are reported. The devices shown are the same used in the previous experiments with thiolated molecules. Figure 2.8 shows the frequency spectra acquired before and after DNA molecule adsorption. It should be noted here that these measurements are remarkable from the technical point of view because of the high sensitivity obtained but they are not really relevant to the biological issue since the molecules used are artificially bound to the cantilever (*i.e.* a synthetic thiol binder is used instead of exploiting a biological recognition process) and measured in vacuum, which is not an immediate biological environment.

The rush toward increasing sensitivity continued across the first decade of this century and the detection of single Xe atoms first [Yang 2006] and single gold atoms later [Jensen 2008] was soon demonstrated, using SiC double clamped beams and a one-end clamped carbon nanotube, respectively. Finally, using a SiC double clamped beam mounted on a high vacuum, low temperature cryostat, a single molecule mass spectrometer was proposed, able to distinguish proteins with few Dalton of difference [Naik 2009]

4.3 Operation with liquids

The urge for a more applicative evolution forced many researchers entering in the field in the last 5 years to come up with new original solutions. One of the smartest ideas to merge microelectromechanical sensors and biological environment was proposeded first in 2003 by Thomas Burg and Scott Manalis and fully developed 4 years later [Burg 2007]. These authors just turned the problem around: if we cannot put a resonator into a biological fluid, why not put the biological fluid into the resonator? So they built a microfluidic channel, that after a number of microfabrication process was shaped into a normal cantilever beam. They showed that the presence of liquid does not change significantly the quality factor (i.e. the sharpness) of the resonance, thus keeping a sensitivity of 300 ag. On the other hand, filling the channel with liquids of different densities changes

the overall mass of the resonator, which in turn shifts the resonance frequency, as seen above. By first functionalizing the inner walls of the microfluidic channel and then flowing the proper antigens and antibodies, they demonstrated that sensing in a biological environment was possible. The frequency variation upon sequential exposure to a solution containing a 100 nM concentration of biotin, neutravidin and again biotin are shown in figure 4.5.

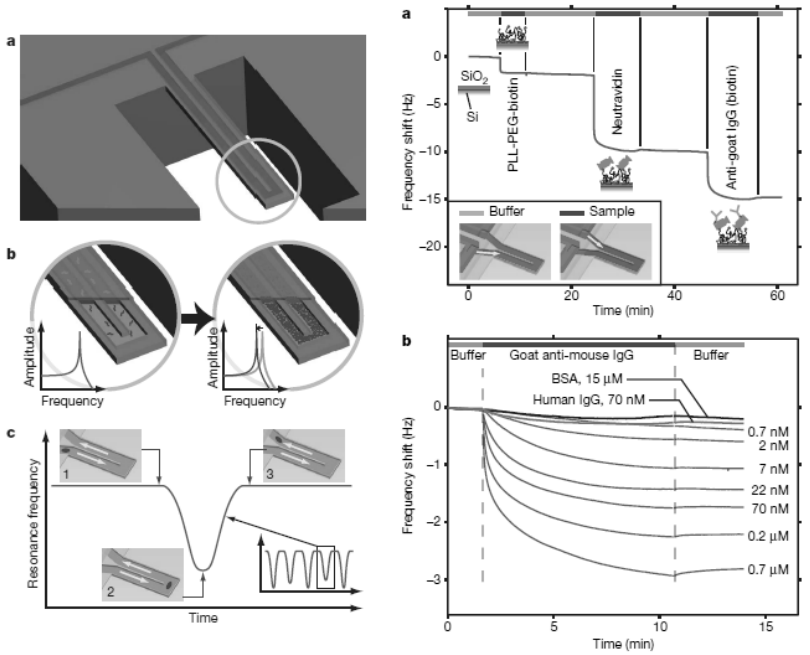

Figure 4.5*: Right panel: Cartoon depicting the main concept of a microchannel resonator. A microchannel is fabricated in the shape of a suspended cantilever. The frequency shifts occurring when different entities pass in the channel are also sketched. Left panel: The temporal evolution of the resonance frequency for different biochemical interactions within the channel, namely: PLL-PEG-biotin functionalization of the channel wall; recognition and immobilization of neutravidin on the channel walls. Recognition and immobilization of an anti-neutravidin antibody on the channel walls.*

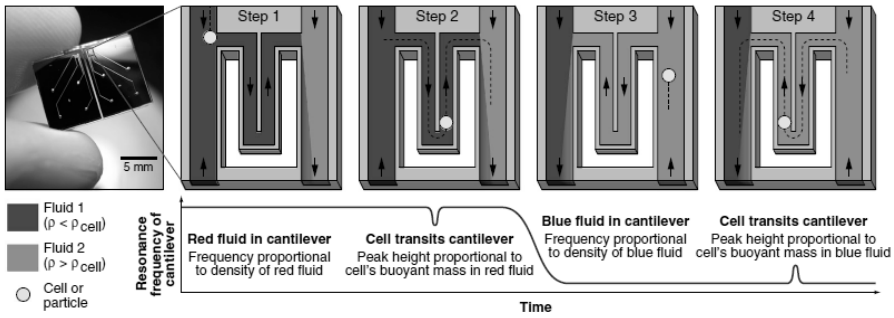

***Figure 4.6**: Application of microchannel resonator to measure the density of one single cell.*

The group of Scott Manalis has recently applied this technology to several biological cases; the most relevant in my opinion, is the use of a suspended microchannel to measure the density of cells [Grover 2011]. In this setup the same cell is forced to flow back and forth in the suspended microfluidic resonator in solutions with different densities, one higher and one lower than the cell density. The measurement of the buoyant mass in the two cases provides a precise measurement of the cell density, which is only slightly affected by experimental errors and calibration uncertainty. A sketch of the measurement principle is provided in figure 4.6. This method is extremely promising for detecting cells that have similar chemical and biological character but different density such is the case of malaria-infected red blood cells or circulating tumors cells.

An alternative geometry, distinct from cantilevers and double clamped beams, are micro and nanopillars, which share with the cantilevers the same working principle, actuation scheme and read out strategies and differ in orientation, which is vertical with respect of the substrate, and arrangement, since micropillars can be assembled in very dense arrays. Micropillars were first proposed by the Oesterschultze group in Kaiserslautern [Kerbush 2008] and developed there and in my group in Trieste [Melli 2010, Melli 2011].

A very peculiar property of micropillars is that, by choosing carefully the geometrical spacing and the surface termination of the pillar lateral walls, it is possible to obtain a superhydrophobic surface, like that shown in figure 4.7, in which only the top side of the pillar is in contact with

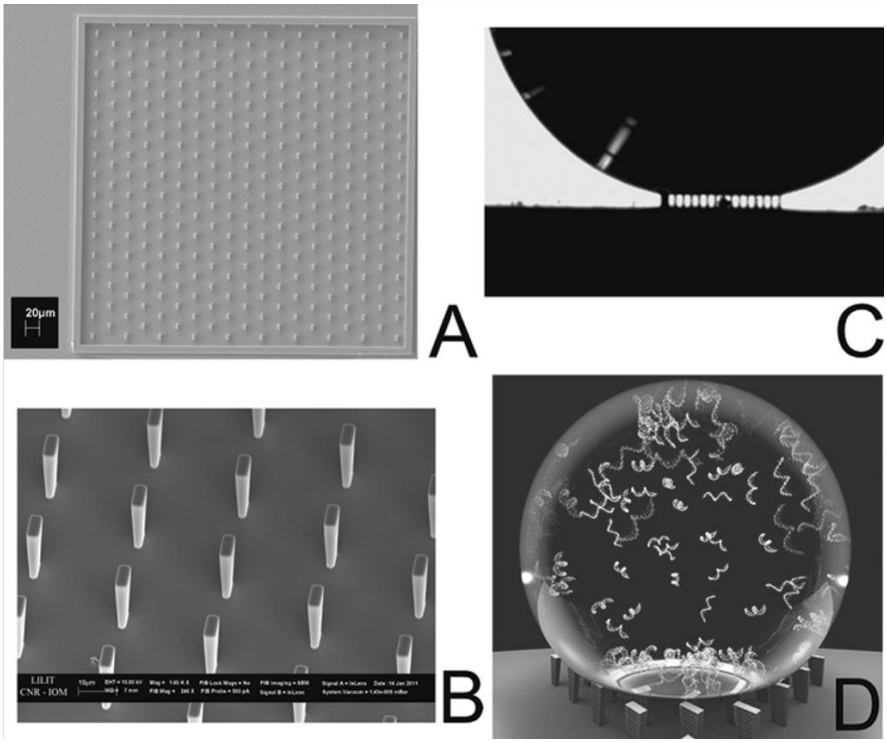

***Figure 4.7**: Micropillar resonators. Micropillars are fabricated in dense arrays (A, B) and functionalized to be superhydrophobic, so that water cannot penetrate in between. (C) In this way the pillar top is in contact with the analyte containing solution, while the pillar oscillates in air with relatively high Q-factor (D).*

the liquid droplet while the rest of the resonator lies in air or in a controlled atmosphere [Melli 2011].

As a consequence, the oscillator maintains the air-behaviour, resonance frequency and quality factor, allowing a more precise measurement of the mass variation induced by analyte adsorption on the top surface of the pillars [Oesterschultze 2012].

4.4. Systems of cantilevers

The field of single microresonators is nowadays rather mature and a trend towards a more effective integration in real devices with wafer scale production is emerging [Bargatin 2012] as illustrated in figure 4.8.

In the meantime some work appeared proposing alternative geometries, materials and arrangements of micromechanical resonators, with interesting and promising performances. Alex Zettl's group in Berkely and Adrian Bachtold's group in Barcelona demonstrated carbon nanotube oscillators at extremely high frequencies, 1.8 GHz [Peng 2006] and 4.2 GHz [Chaste 2011] respectively. The same approach was used to detect single Au atoms [Jensen 2008]. Daniel Ramos and colleagues fabricated a silicon nanowire oscillator which exhibits two perpendicular oscillation modes and a very peculiar optical confinement that can be exploited to actuate selectively the oscillation modes and to cool down the thermal vibrations [Ramos 2012].

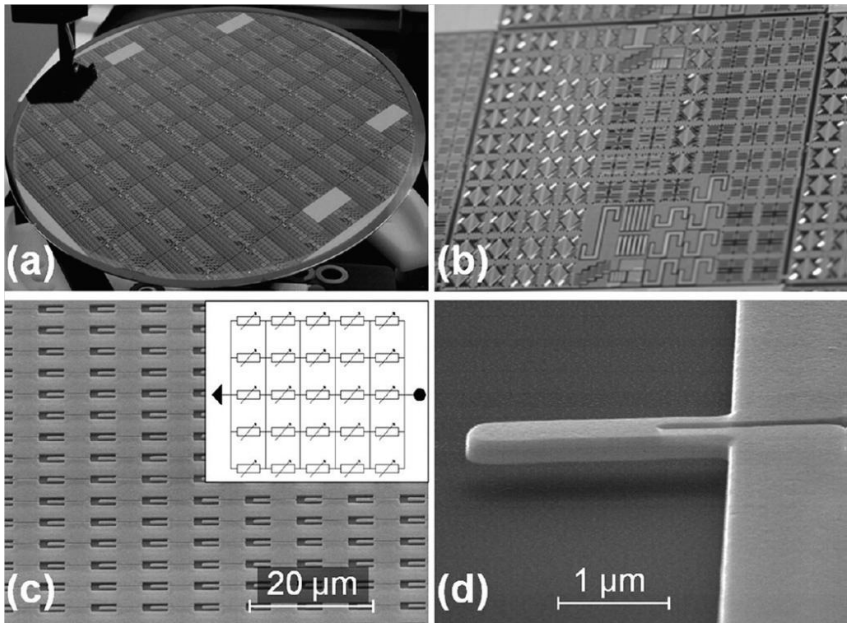

Figure 4.8: *Wafer-size array of microresonators with fully integrated control circuitry.*

A topic of particular interest for this dissertation is that of coupled cantilevers. The first work addressing the use of coupled cantilevers for mass sensing appeared in 2006 [Spletzer 2006] and described two gold cantilevers which were mechanically coupled by using an "overhang" microfabricated between the two. The two cantilevers, which are in principle undistinguishable, oscillate at the same resonance frequency, and thus can be described as a degenerate system.

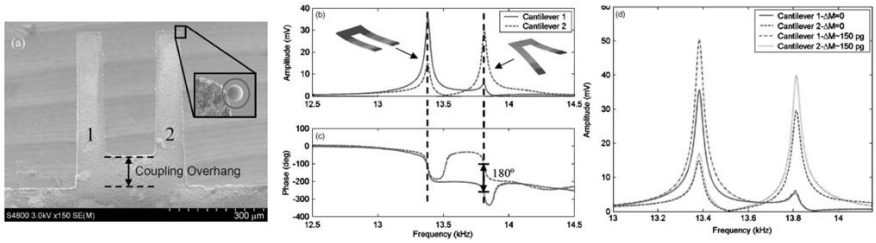

Figure 4.9*: Coupled cantilevers. In the top panel an SEM image of two gold cantilevers with a coupling overhang in between is shown. A small Au bead is also shown in the inset. In the lower left panel the resonances of the two modes (symmetric and anti-symmetric) are shown. The phase record, in particular highlights how the cantilevers are n phase in the first mode and 180^o out of phase in the second. The right panel illustrates that the motion becomes more localized after nanoparticle adsorption.*

The coupling introduces an interaction between the two and removes the degeneracy splitting the energy levels. A symmetric and an antisymmetric mode are generated, with the second having higher resonance frequency, and for the equipartition of energy, slightly lower amplitude, likewise to what happens for the electronic energy levels of the hydrogen molecule. The adsorption of a mass on one of the two cantilevers introduces an element of asymmetry, and the modes become partially localized. The amount of the localization is proportional to the adsorbed mass and can be used to quantify it, while the cantilever with the adsorbed mass allocates the higher energy mode. Figure 4.9 shows the structure of the device and typical response curves.

The same concept was developed by Gil Santos *et al.*, who fabricated smaller and better defined devices, in which localization was observed clearly [GilSantos 2008]. In their experiment they notice that thermal actuation provides a correct measure of localization, while external actuation excites preferentially symmetric modes. A very interesting implementation of this concept was proposed by the group of Yamaguchi at NTT-Tokyo [Okamoto 2009]. Here GaAs double clamped beams, instead of cantilevers, are coupled; this allows for the separate tuning of the elastic constant of each beam, thus realizing perfectly identical resonator. Finally, very recently in our laboratory, Hossein Pakdast and myself fabricated and tested the triple coupled cantilever shown in figure 4.10. In this configuration, in the second mode of oscillation the central cantilever

does not oscillate, when the structure is perfectly symmetric. Any deviation from symmetry, *e.g.* mass adsorption on one lateral cantilever, induces a detectable motion of the central cantilever. We were able to demonstrate the detection of 0.9 pg beads with 100 μm long cantilevers, with a sensitivity equivalent to that obtainable tracking the frequency shift in vacuum. [Pakdast 2012]

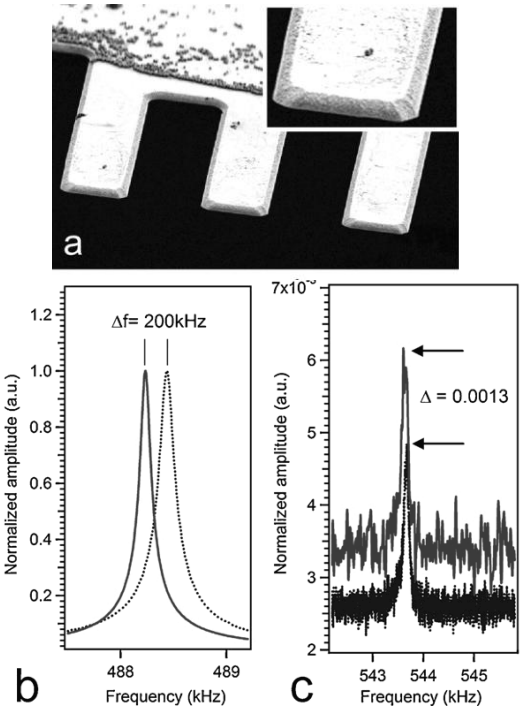

***Figure 4.10**. Triple coupled cantilever. Left panel: SEM image of the structure showing two nanoparticles located on the left cantilever. Right panel: frequency and amplitude measured before and after the adsorption of 1 pg bead (black and red curves respectively), showing that mode localization and frequency shift have comparable sensitivities.*

In the last years several review papers on micromechanical sensors have appeared. An exhaustive one by Arlett *et al.* [Arlett 2011] compares the performances of several families of micromechanical sensors, not in terms of ultimate sensitivity, which may be, after all, useless, but rather in terms of concentration and response time. All the sensor families are grouped in a single plot having concentration on Y axis and incubation time on the X

axis. All techniques ly above the line $C \bullet (T)^3 = 10^{-11}\ M \bullet min^3$. This curve will set a reference for all the sensors to be developed from now on.

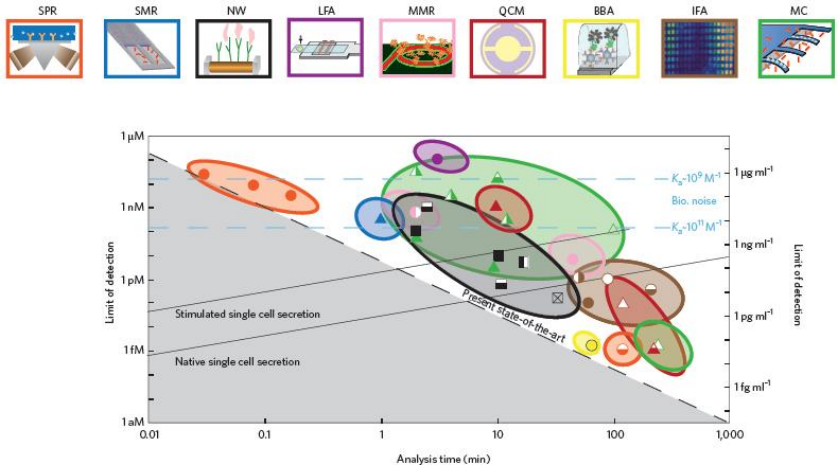

Figure 4.11 *An exhaustive comparison among all the family of sensors nanosensors in term of sensitivity and incubation time.*

CHAPTER 5

Twin cantilevers[*]

Single molecule experiments aimed both at fundamental investigation and applications, have been attracting a lot of attention recently. Most of the devices used for the detection and the manipulation of single molecules are based on very expensive lithographic tools, need a specific molecule labeling or functionalization and still show many limitations. In this chapter we present an alternative approach based on the fabrication of pair of identical silicon cantilevers (the twin cantilevers), separated by a gap that is tunable on the nanometric scale. The fabrication and operation of our twin cantilever device involves only the use of standard optical lithography and micrometric manipulation. We have investigated the frequency response of the twin cantilever device around its fundamental resonance and, by modeling its behaviour, we shoedw that a single molecule bridging the cantilever gap produces a detectable molecular shift.

[*] This chapter is based on: M. Lazzarino, E. De Marchi, M. Bressanutti, L. Vaccari, S. Cabrini, C. Schmid, R. Poetes and G. Scoles, Microelectron. Eng. **83**, 1309 (2006)

5.1 Introduction

Micro-electro-mechanical-systems have been demonstrated as effective tools for single molecule detection and nanoscale manipulation. Fritz and colleagues [Fritz 2000] have demonstrated the detection of DNA hybridisation through the measurement of the mechanical deflection of a silicon cantilever. More recently, Ilic and co-authors [Ilic 2005] were able to count the number of DNA molecules that are sticking on a nanocantilever by measuring the shift in the frequency response of the cantilever itself. On the other hand, single molecule experiments based on the use of atomic force microscope cantilevers such as protein unfolding [Fernandez 2001] or DNA unzipping [Krautbauer 2003] have also been reported. However, so far only isolated cantilevers or arrays of isolated cantilevers have been proposed. In this chapter we describe an alternative approach based on the fabrication of a pair of identical silicon cantilevers, the twin cantilevers, separated by a gap tunable with nanometric sensitivity. If we consider the frequency response of the twin cantilevers as a single system, the presence of a molecule connecting the two cantilevers across the gap acts as a perturbation of the system that shifts slightly its resonant frequency response. By measuring this shift we can obtain information on the mechanical properties and the number of linking molecule, while, by tuning the twin cantilever gap, we can select the size of the molecules of interest.

5.2 Device design

To define properly the device dimensions and to understand if our configuration is suitable for the use of a single molecule detector, we performed a numerical simulation to predict the mechanical behaviour of the system with and without a molecule. To simplify the problem we used a dsDNA molecule that is rigidly attached to the two facing ends of the two cantilevers.

The twin cantilever device, including the dsDNA molecule, has been simulated by a finite element analysis. We assumed the silicon is isotropic with Young's modulus E = 150 GPa, Poisson ratio of 0.17 and density 2.33 g/cm^3. The dsDNA molecule has been modelled as a uniform 50nm long rod with 1nm of diameter, Young modulus E = 300 MPa, Poisson ratio of

0.31 and density 1.20 g/cm^3. The values reported in the literature for these last parameters are characterized by a large variability, due to the different external conditions in which the mechanical properties of DNA are experimentally determined. The numbers we used have been taken from [Smith 1996] [Baumann 1997] [Gevorkian 1990].

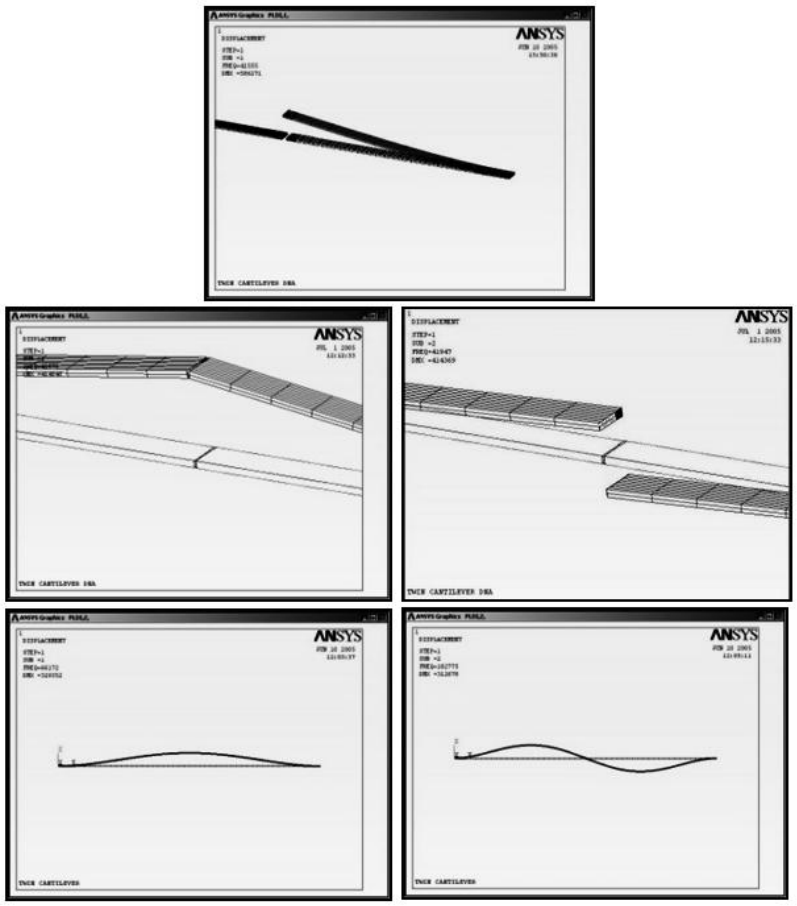

Figure 5.1: *(a) Finite element analysis output of a modal simulation. (a) twin cantilever with no DNA molecules bridging the gap. The two cantilevers oscillate independently at the same frequency. (b) 10 DNA molecules in the gap, in the symmetric mode the two cantilevers oscillate in phase (c) while in the antisymmetric mode the two cantilevers oscillate in antiphase (d) 1000 molecules. The system behaves like a doubled clamped beam in the fundamental mode. (e) same as in (d) but in the second mode.*

Cantilever length and width were chosen to be 250 μm and 20 μm, respectively. The cantilever thickness was varied from 0.5 μm to 4 μm.

In absence of molecules the two cantilevers oscillate independently at the same frequency, so that we can say that the lowest mode of the system is twofold degenerate. As soon as we introduce even a single molecule, the degeneracy is split and the two cantilevers oscillate together, either in phase (lowest energy, symmetric mode) or in antiphase (highest energy, antisymmetric mode). By increasing the number of molecules in the gap the twin cantilevers' oscillating behaviour resembles more and more that of a double clamped beam. The symmetric mode evolves towards the first mode of the clamped beam, while the antisymmetric mode evolves towards the second mode of the double clamped beam, the one with one node in the centre of the structure. The output of the finite element analysis is displayed in figure 5.1

Thickness (μm)	f_0**(Hz)**	Δf_1**(Hz)**	Δf_2**(Hz)**	$\Delta f_1/f_0$	$\Delta f_2/f_0$
0.5	10391	0.03	64	$2.9\cdot10^{-6}$	$6.1\cdot10^{-3}$
1	20774	0.06	16	$2.9\cdot10^{-6}$	$7.7\cdot10^{-4}$
2	41572	0.08	4	$1.9\cdot10^{-6}$	$9.6\cdot10^{-5}$
4	83136	0.10	1	$1.2\cdot10^{-6}$	$1.2\cdot10^{-5}$

Table 5.1*: Main resonance response for various cantilever states and geometries as predicted by finite elements analysis. Resonance frequency* f_0 *of the first oscillating mode for 4 different cantilever thicknesses; the absolute shift for the symmetric and antisymmetric mode (*Δf_1 *and* Δf_2*) induced by bridging the gap with a 50 nm long dsDNA molecule; the relative shift for the latter two modes with respect to the unperturbed mode (*$\Delta f_1/f_0$ *and* $\Delta f_2/f_0$*)*

The results of the simulation for 4 different thicknesses are reported in table 5.1. As expected, the thinner the cantilever the higher the sensitivity, especially for the antisymmetric mode. Since the oscillation amplitude in the symmetrical mode is much larger than in the antisymmetric one, the former is much easier to detect. The frequency shift as a function of the number of molecules is displayed in figure 5.2. Both modes increase in frequency with the number of molecules linked across the gap, but the

symmetric mode is much less affected. This is the result of the stiffening of the structure induced by the molecular adsorption. The plot in Figure 5.2 clearly indicates how the stiffening is more relevant in the antisymmetric mode, where the molecules are pulled by the cantilevers in opposite directions.

Since the fabrication of thin cantilevers is technologically more challenging and since the sensitivity for the symmetrical modes does not change dramatically with cantilever thickness, we decided to fabricate a demonstrative device with a silicon thickness of 2 μm.

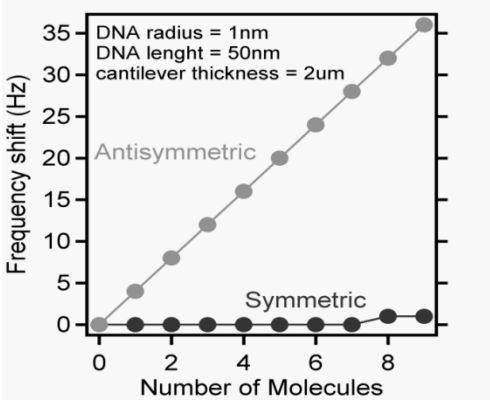

***Figure 5.2**. Frequency shift as a function of the number of molecules across the gap of a twin cantilever system*

5.3 Device fabrication

The fabrication of the twin cantilever system was based on the silicon on insulator (SOI) wafer technology. The main advantage of this choice is that the cantilever material is crystalline silicon with no residual stress. As we shall see in the following, this is of fundamental importance both for the gap fabrication and for the mutual cantilever alignment. The fabrication is based exclusively on low cost optical lithography. The lithographic process is sketched in figure 5.3. The dimensions are not drawn to scale. We first defined a twin cantilever structure on a thin layer of SiO_x deposited by PECVD. Initially, the two cantilevers were separated by a gap of 1 μm (figure 5.3a and 5.3b). The mask was carefully aligned along the 110 directions of the silicon crystal. Then we partially etched the silicon layer with KOH (figure 5.3c). Due to the anisotropy of the etching and the

symmetry of the silicon crystal, two walls at 55^{o} are formed that meet exactly at half way. Then we re-aligned a continuous bridge and removed the remaining part of silicon by CF_4:O_2 dry etching. In this way a thin and flat film of silicon is still bridging the two cantilever, and a notch is positioned exactly in the middle of the bridge (figure 5.3d). Finally the sacrificial layer of Silicon oxide was removed by wet etching in a mixture 50:50 of ethanol and buffered HF (figure 5.3e). The addition of ethanol was necessary to reduce the surface tension of the etchant and reach the silicon oxide well below the cantilevers. Samples were then blown dry and, since the cantilever were not yet formed but they were still bridged, our structure did not experience any sticking to the substrate.

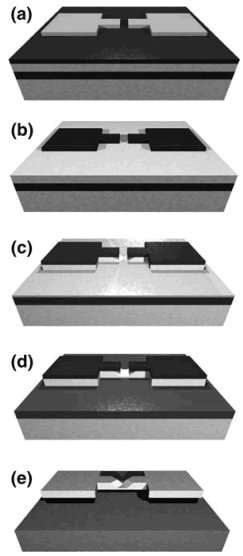

Figure 5.3 *Scheme of the main lithographic steps used to define a suspended silicon bridge with a notch in the middle.*

To separate the two cantilevers we induced a fracture along a (110) crystallographic plane by exerting a lateral force on the silicon bridge with an AFM tip. The fracture location is univocally determined by the position of the notch as defined during the previous lithographic process. In figure 5.4 we show a top view SEM image of the two cantilevers after the

cleavage. The force was applied from the top to the bottom of the picture in the position indicated by the arrow. The fracture is irregular on the top side, but is perfectly defined on the bottom side, below the notch. The above procedure breaks the chemical bonds along a crystallographic plane but does not create a gap. Because of the absence of any residual stress in the topmost crystalline layer of the SOI wafers, no relative bending of the two cantilevers was observed. A tilted SEM image is reported in figure 5.4, showing that the cantilever misalignment is negligible.

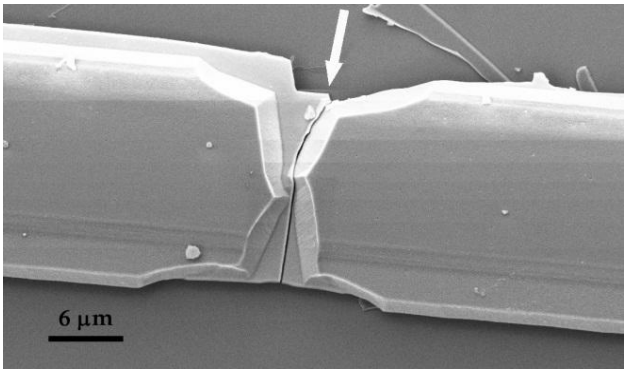

Figure 5.4 *SEM image (top view) of a twin cantilever pair just after breaking. The point where the cleaving force was applied is indicated by the white arrow.*

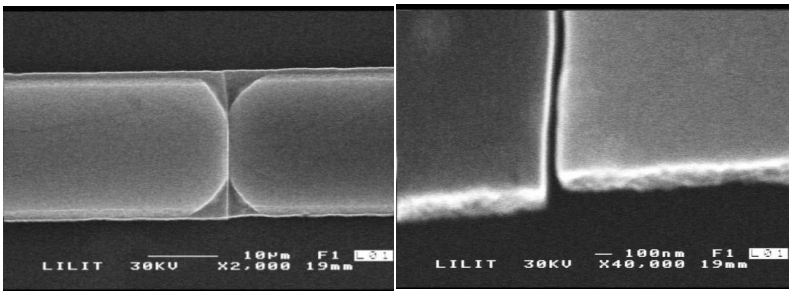

Figure 5.5 *SEM top view and lateral zoomed view of a twin cantilever structure, showing negligible vertical misalignement of the two cantilevers after cleaving.*

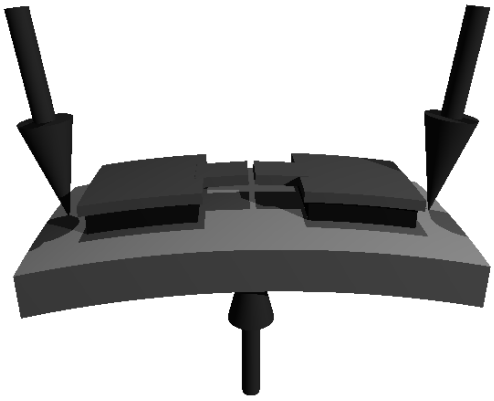

Figure 5.6 *Scheme of the break junction geometry used to separate the cantilevers in a controlled way.*

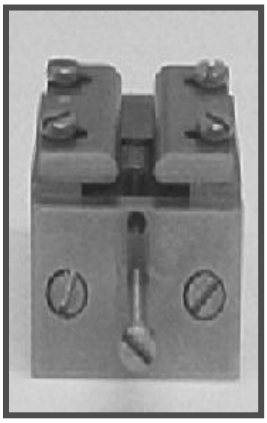

Figure 5.7 *Mechanical device used for bending the wafer chip containing the twin cantilevers*

The gap can be (and was) induced by bending mechanically the wafer in analogy with what is normally done in mechanical break junction.[Moreland 1985] A sketch of the wafer bending mechanism is

illustrated in figure 5.6. A small mechanical device used to bend the cantilever wafer during these experiments is shown in figure 5.7. With a wafer thickness of 500 μm and total twin cantilever length of 500 μm, the maximum separation achievable before breaking the substrate was 250 nm corresponding to a radius of curvature of 0.5 m. Since the demultiplication factor between the wafer pushing position and the gap opening is more than 1000 in our geometry, a stable micrometric control of the pushing screw implies a stable control in the gap opening with resolution below 1 nm.

5.4 Results and discussion

In figure 5.8a and figure 5.8b we show a detail of the separation between the same twin cantilever for two different bendings. The gap increases from 41 nm in figure 5.8a to 139 nm in figure 5.8b. The two edges of the cantilevers appears smooth and uniform to the best of the SEM resolution.

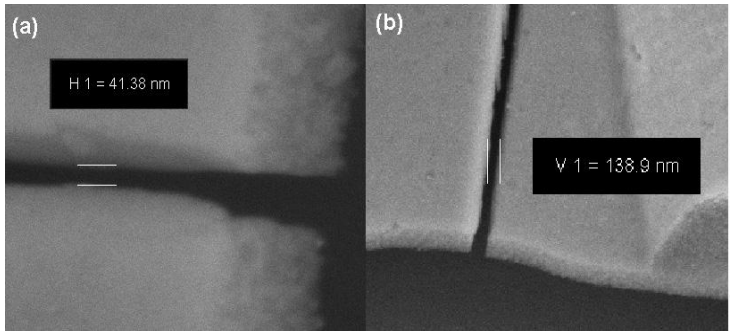

Figure 5.8 *SEM image of the gap opening for two different wafer bendings on the same twin cantilever pair. (a) 41 nm gap, (b) 139 nm gap.*

Since the image is recorded with a tilted sample, in figure 5.8b, we can observe that the two cantilevers are still vertically aligned with respect to each other, also after separation has been induced by substrate bending, which is an indirect proof that the cantilever length is identical and the wafer curvature is uniform. We also observed that, once the twin cantilever were separated by a finite gap, they could move independently from each other. In particular we measured the frequency response from couples of cantilevers at room temperature and in vacuum condition. We obtained a

resonance frequency of 75 kHz with a *Q-factor* higher than 1500, which corresponds to a full width at half maximum of 30 Hz. A representative resonance curve is displayed in figure 5.9. The small shift from the predicted value is easily explained considering that the thickness of the silicon layer in a SOI substrate is always known with an uncertainty of ± 20%. The relatively narrow amplitude vs frequency curve implies that our device can easily detect less than ten molecules. With a fine tuning of the cantilever size and geometry, we think that the single molecule sensitivity could be eventually achieved.

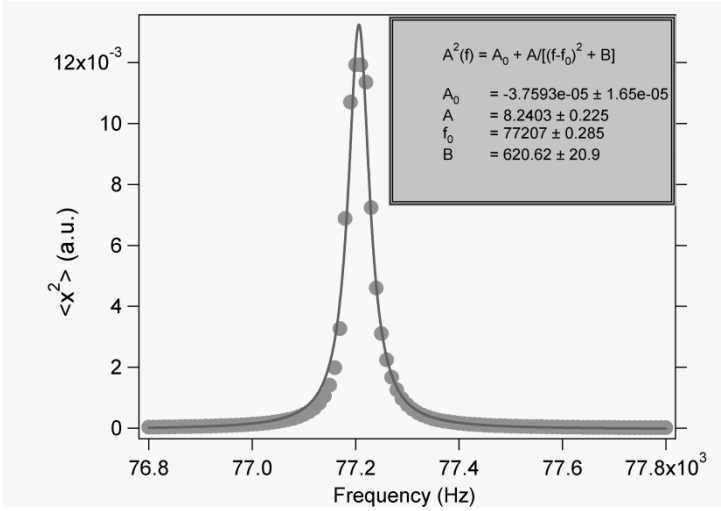

Figure 5.9 *Twin cantilever resonance frequency measured in vacuum using the optical lever technique, with a stabilized red laser, a four quadrant photodiode and a homemade electronic read-out*

5.5 Conclusion

In conclusion, in this chapter we described an alternative way to single molecule detection based on the fabrication of a couple of identical silicon cantilevers, separated by a gap tuneable with nanometric sensitivity. To fabricate the twin cantilevers we made exclusive use of optical lithography.

A nanometric gap was formed taking advantage of the crystalline structure of the silicon layer, while the size of the gap was tuned with nanometric resolution using an approach similar to that used in the operation of mechanical break junctions. We investigated the frequency response of the twin cantilever device around its fundamental resonance and showed that, in principle, the system could be used as a few molecules sensor. The main drawback of this geometry is that the fabrication of identical cantilevers is practically impossible, due to small uncertainties in the lithographic and etching processes, and in particular due to the random cleaving process. In the next chapter we shall propose a solution to this problem. The second minor difficulty concerns the way of grafting molecules to the exact edge of the cantilevers. Electron beam lithography and atomic force microscopy-based lithography and nanografting were selected in the first instance but chapters 7 and 8 will describe a different and innovative solution to this problem.

CHAPTER 6

Asymmetrical twin cantilevers[†]

Recently, there has been growing interest in sensors based on frequency shift detection of mechanical resonators that has led to extremely sensitive diagnostic methods for medicine and biology. In this chapter we propose a strategy capable of detecting the presence of few macromolecules, that uses an asymmetrical cantilever structure of several micron in size, operated at room temperature and under ordinary vacuum conditions and demonstrate that this approach can be realized. The idea is to detect the presence of one or more molecules by detecting the mechanical cross-talk induced by the molecular link between a short cantilever and an array of longer cantilevers facing the short one.

[†] This chapter is based on: A. Qazi, D. Nonis, A. Pozzato, M. Tormen, M. Lazzarino, S. Carrato and G. Scoles, *Applied Physics Letters* **90**, 173118 (2007).

6.1 Introduction

The use of nano and micro-cantilevers as molecular sensors emerged in the last few years after the pioneering work of a Swiss group showed that the absorption of DNA molecules caused the static deflection of an array of silicon cantilevers [Fritz 2000]. Since then, the rush towards single molecule detection has moved the focus of the research to the dynamic mode. Decreasing the size in the nanometric range, increasing the resonance frequency to GHz values, and forcing environmental conditions to Ultra High Vacuum and very low temperatures all proved to be crucial issues in this context. Using a single cantilever, or a single, doubly clamped beam, single virus, single molecule and zeptogram sensitivity have been demonstrated [Gupta 2004] [Ilic 2005] [Yang 2006]

A different route to improve the resolution consists in the fabrication of a resonating structure, in which the absorption of a target molecule changes the dynamical mode structure of the resonator rather than simply adding mass and shifting the resonance of a given mode. Only very few examples of this approach have appeared upto now in the literature [Lazzarino 2006] [Spletzer 2006].

In this chapter we present an alternative approach which improves the cantilever system described in the previous chapter; the basic improvement consists in the fabrication of an asymmetric couple of cantilevers facing each other with submicron separation. The two cantilevers are sized differently, so that one, the shorter or *driver*, shows the highest resonance frequency while the longer, or *follower*, has a lower resonance frequency. This overcomes the difficulty mentioned in the conclusion of the previous chapter, of fabricating structures with identical geometries and thus degenerate resonance frequencies. The actual geometry used for our experiments is shown in figure 6.1: notice that the *follower* is flanked by two identical structures in order to reduce the centre of mass displacement of the fundamental mode, reduce energy dissipation, and increase the frequency sensitivity. When the two cantilevers are connected by a molecular bridge, the actuation of the *driver* induces a displacement also on the *follower*. When this system is operated out of resonance, the force needed to cause a detectable displacement largely exceeds the strength of the molecular bonds. However, when the system is operated at the resonance frequency of the *follower* cantilever, the required force decreases dramatically and in principle the presence of a single molecule can be

observed. Recalling that the Q-factor of an oscillator can be expressed as the ratio of the energy stored in the oscillator and the amount of energy dissipated during each cycle, or, in other words, the work exerted on the cantilever to keep it in oscillation, we have:

$Q = E/\Delta E = \frac{1}{2}kx^2/Fx \rightarrow F = \frac{1}{2}kx/Q$

where x is the maximum displacement of the cantilever. Using typical values of k=1 N/m and $Q \sim 10^4$, it follows that a displacement of 10 nm in a micrometer-sized cantilever can be obtained with a force lower than 0.5 pN, *i.e.* largely below the strength of any chemical bond. A typical application of the device described above consists in the detection of organic macromolecules with different functional groups at the two ends that can selectively absorb on the two opposite cantilevers, such as DNA, proteins or protein suprastructures. It is worthwhile to stress here that the detection mechanism is based on the formation of a mechanical link between two oscillating structures rather than in a simple change of mass. Therefore it would apply more properly to the detection of molecules with very low mass but high stiffness rather than to heavy but soft ones.

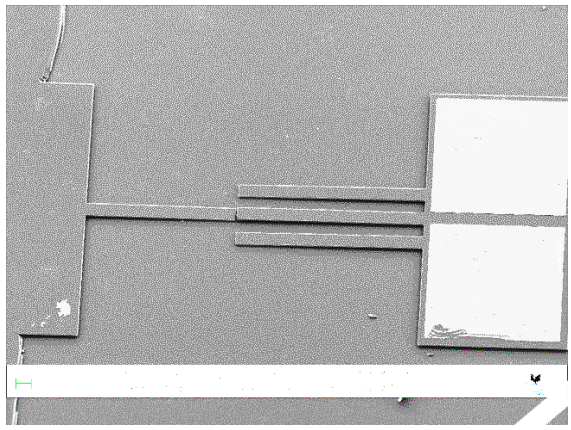

Figure.6.1. *Device geometry and experimental setup: cantilevers are actuated by applying an ac bias between the top layer and substrate. The response is detected by tracking the reflection of a laser with a four quadrant photodiode. The driver is sized 175 x 20 x 2.5 μm^3 and has a nominal resonance frequency of 88 kHz. The three followers are sized 275 x 20 x 2.5 μm^3 and have a nominal resonance frequency of 38 kHz. The separation between cantilever and substrate is determined by the thickness of the BOX layer and amounts to about 2 μm.*

6.2 Experimental details

The devices were fabricated from silicon on insulator (SOI) wafers composed of a top p-type silicon layer 2.5μm thick, with resistivity of 0.1 Ωcm, a 2.0 μm thick buried oxide (BOX) layer and a p-type silicon substrate. We used optical lithography, ICP dry etching and HF based wet etching to fabricate the structures and suspend the cantilevers. The samples were first rinsed in water, then in methanol and then gently blown dry with N_2 to minimize sticking. A detail of a fabricated structure is reported in figure 6.1. The HF etching also partially removes the BOX under the cantilever supporting pads: as a consequence the triple follower cantilevers are mechanically interacting [Spletzer 2006].

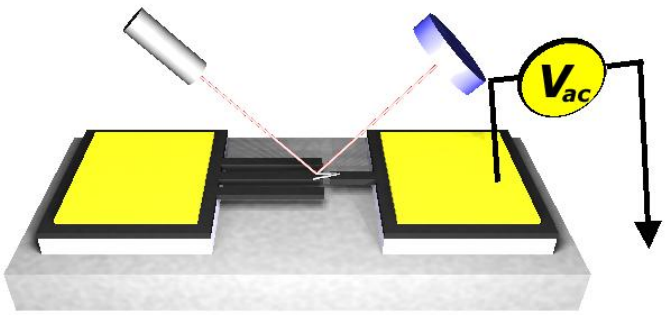

Figure.6.2. *Scheme of the experimental set up. The shorter cantilever is capacitatively actuated by applying an AC bias between the top cantilever and the substrate. A laser is focused on the longer cantilever and reflected onto a 4 quadrant photodiode. The AC bias is provided by a function generator while a lock-in amplifier is used to measure the output of the four quadrant photodiode at the same frequency.*

Ohmic contacts to the top silicon layer were fabricated by depositing a 10 nm Ni/90 nm Al film followed by rapid thermal annealing at 500^{o}C for 30 s. Contact resistances less than 10 Ω were obtained.

The actuation and detection schemes are depicted in figure 6.2. When a bias difference is applied between the substrate and the cantilever - which

are electrically insulated from each other by the BOX layer - the latter is pulled toward the substrate [Beebly 2004]. By applying an AC voltage the cantilever is forced to oscillate at the bias frequency. To avoid higher harmonics effects, the *driver* was forced to oscillate at the resonance frequency of the *follower* so that the *driver* was operated in a quasi-static regime and the operation of the device is simplified. The response of the follower was detected using the optical lever method in conjunction with a four quadrant photodiode (4-qpd), as used in atomic force microscopy with vertical sensitivity far better than 1 nm [Alexander 1989]. A wavefunction generator (Stanford Research System DS345) and a lock-in amplifier (Stanford Research System SR830) were used to generate the AC voltage and to acquire the signal from the 4-qpd, respectively. To achieve a high Q-factor and be sensitive to small frequency shifts, we operated the cantilever in a vacuum chamber with a base pressure of $4x10^{-5}$ mbar.

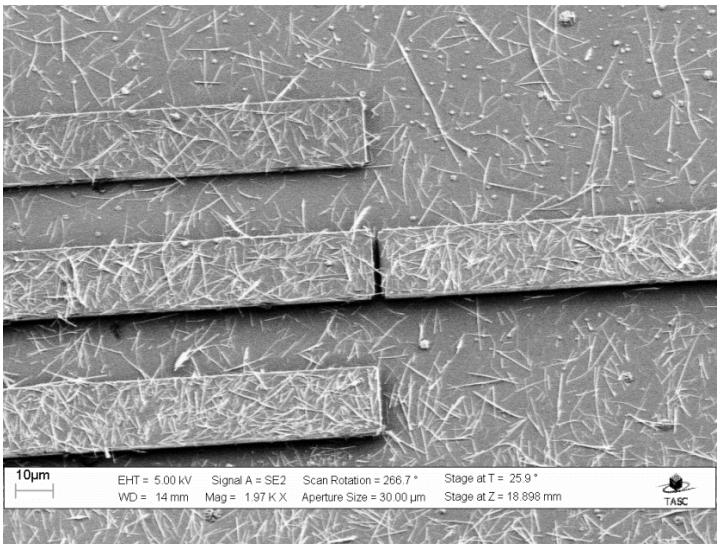

Figure 6.3. *One GaAs nanowire bridging the gap between asymmetrical cantilevers.*

6.3 Results and Discussion

A molecular bridge between the *driver* and *follower* was created on purpose, in order to test the efficiency of our detection scheme. Two different strategies were followed. GaAs nanowires were transferred by

mechanical contacts directly from the growth substrate to the cantilevers. An electron microscope image of a device with nanowires is shown in figure 6.3.

GaAs nanowires were deposited everywhere on the cantilever surface, resulting in an excess of added mass, which, in turn, made the measurement interpretation difficult. In figure 6.4 we show the resonance frequency measured on the same device before and after the deposition of nanowires. We notice three important facts: 1. The *follower* cantilevers are not actuated directly but through the nanowire link; 2. the resonance frequency is increased due to the mass addition; 3. the amplitude ratio between central and lateral cantilevers changes dramatically: before, the central cantilever had a maximum amplitude 1.5 times higher than the left one, as expected also from simulations (see insets of figure 6.6).

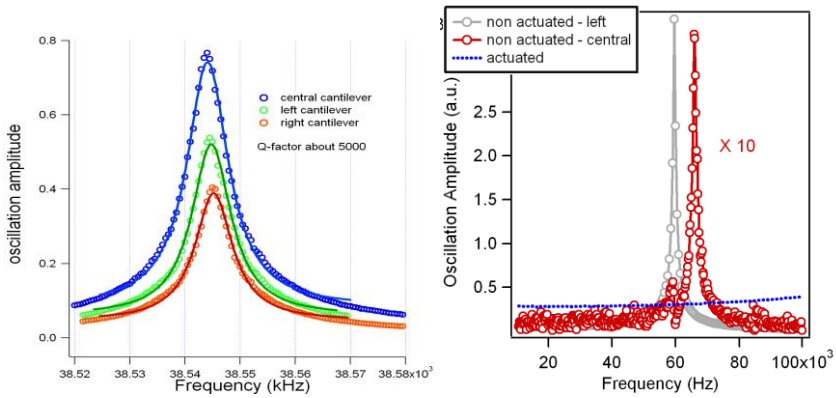

Figure.6.4 *left: oscillation amplitudes of ana symmetrical twin cantilever device before depositing nanowires. Right oscillation amplitude of the same cantilevers after NWs deposition.*

After deposition of nanowires, the central cantilever oscillates more than 10 time less than the lateral ones. This is because the nanowire damping affects only the oscillation of the central cantilever. Moreover the nanowire link made the central cantilever stiffer, shifting its resonance frequency to values higher than those of the lateral cantilevers. Notice the blue line that indicates the oscillation amplitude of the *driver*, which is out of resonance and thus negligible.

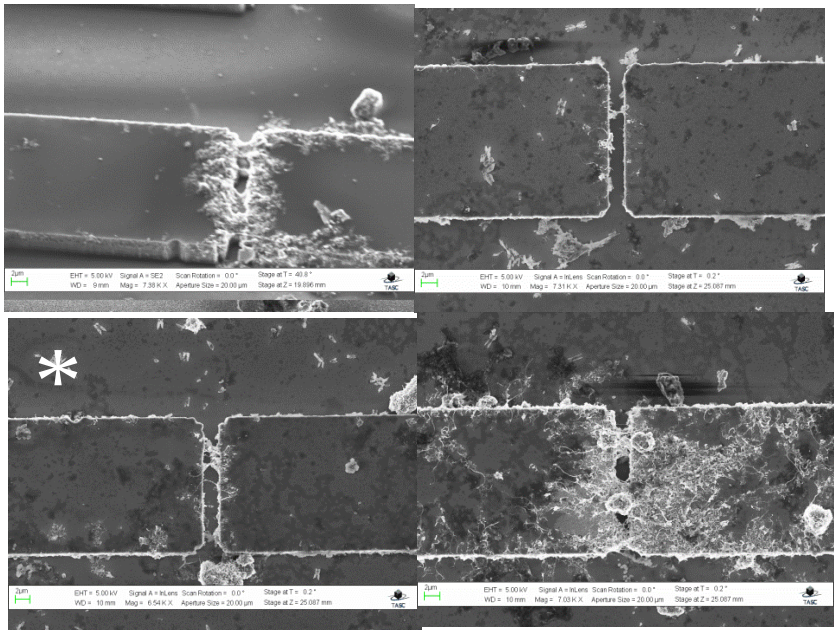

Figure.6.5. *Four examples of CNT deposition via dielectrophoresys for different time bias and concentration. By a careful choice of the parameters few MWCNT can be deposited across the gap. The surface of the cantilevers stay clean from CNT. The measurements reported in the following refers to the device marked with an *.*

In a different experiment, multiwalled carbon nanotubes (MWCNTs) were deposited from solution by dielectrophoresis. In this way it was possible to deposit the CNT only across the gap, keeping the remaining part of the cantilevers unaffected. Moreover, are a better approximation to a molecular link. After dispersing the MWCNTs in dimethylformamide. **(**DMF) at a highly diluted concentration, a droplet of the dispersion was placed across the *driver* and *follower* cantilevers, followed by the application of an RF signal (5 MHz; 5 Vpp) for 5 to 20 minutes. Thesamples were then rinsed in DMF and subsequently in chloroform, in order to minimize the sticking of the suspended structures, and then blown dry with nitrogen. The amount of deposited MWCNT varied with solution concentration, solvent and time of RF application, and only in few samples we deposited a countable number

of MWCNT. However we never observed deposition of MWCNT other than between the two extremities of the cantilevers. Examples of MWCNT molecular bridges are displayed in figure 6.5. Let us consider first the behaviour of the *follower* trio when actuated directly by applying an AC voltage between cantilevers and substrate. Due to the etching under the pad, the three nominally identical and degenerate oscillation modes are split into three different modes with well-defined symmetry. The frequency response of the *follower* trio measured on the central cantilever is shown in figure 6.6. The insets sketch the motion of the three modes. Notice that the mode at higher frequency is more pronounced because in this configuration the motion of centre of mass is very small and the dissipation at the mechanical constraints is minimized. The middle mode should not be detectable when measured on the central cantilever. However, small imperfections in the fabrication process may remove the symmetry and allow for a finite oscillation amplitude.

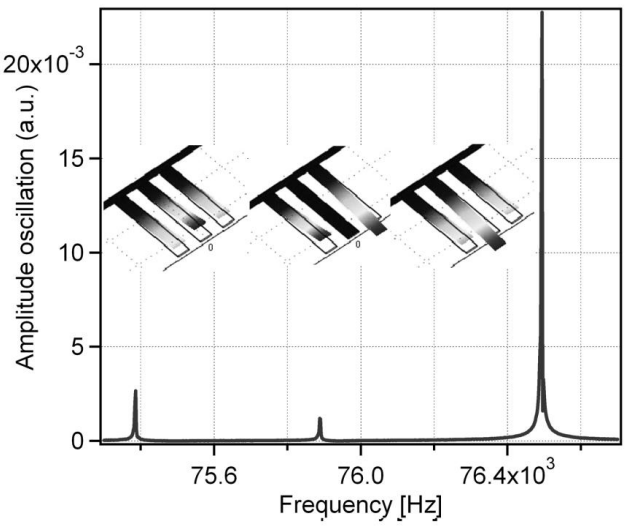

***Figure 6.6**. Typical frequency response of a device without any molecular link. The corresponding modes are drawn in the insets. The lower resonance is related to a mode where all three cantilevers move in phase; the resonance at the centre of the frequency range corresponds to a mode where the central cantilever does not move, while the left and right ones move in antiphase and finally, the higher resonance corresponds to the central cantilever moving in antiphase with respect*

to the left and right ones. The third mode shows the highest amplitude because of the smallest displacement of the centre of mass.

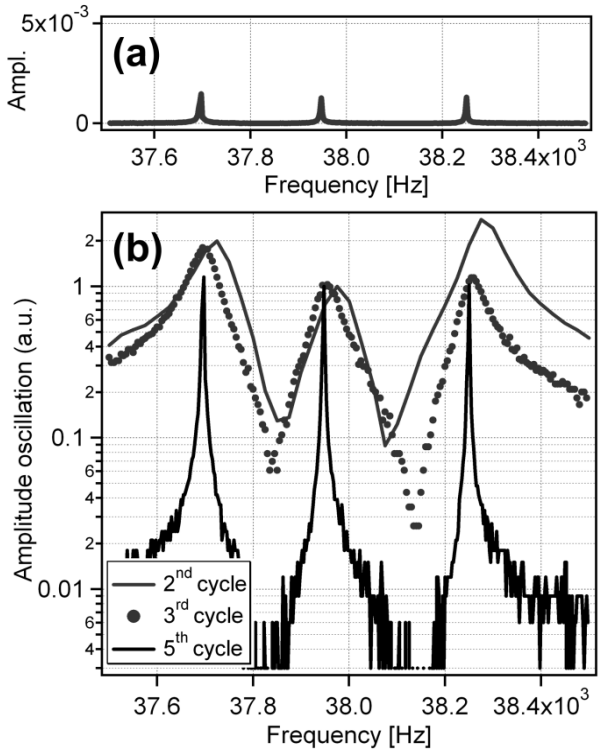

Figure 6. 7. *(a) Frequency response of the device in (c). The presence of the molecular link significantly attenuates the first and third modes. (b) Evolution of the frequency response after several measurement cycles.*

In figure 6.7a we display the frequency response of the *follower* trio represented in the third panel of figure 6.5, marked with an * measured on the central cantilever when actuated through the nearby *driver*.

First of all we noticed that the *follower* cantilevers indeed move because of the presence of the molecular link, while no motion was ever observed before the MWCNT deposition. Secondly we notice that the oscillation amplitudes are of the same magnitude for the three modes, which is consistent with the mechanical presence of a molecular link inhibiting high amplitude oscillations.

We then focused our attention on the evolution of the system under continuous "long term" actuation. Even if the force on the molecules is very small and the chemical bond with the surface or within the molecules cannot be broken, the molecules are subject to thousands of push-pulls per second. To give an estimation of the number of push-pull events in a single measurement run, the resonance spectrum of the 3rd run in figure 6.7 consists of 200 points; since each of them was integrated 100 ms, the total number of push-pull events is greater than 1.5×10^6 - even if not all with the same intensity. Eventually the molecules may detach from one of the two cantilever ends. Indeed in figure 6.7b we display the resonance curves at the 2nd, 3rd and 5th experimental run. The system clearly evolves towards narrower features and the peak position shifts towards lower resonance frequencies. The first effect can be explained considering that the molecular link is far from ideal, *i.e.* it is a highly dissipative link. Therefore the fewer MWCNT bridge the gap, the lower the dissipation and the higher the Q-factor. To understand the second effect we should consider that presence of MWCNTs on the cantilevers implies added mass and added rigidity for the system. The two factors modify the frequency in opposite directions but in our case the second contribution is dominant and the progressive reduction of the number of molecular links causes the decrease of the resonance frequency. This is consistent with the simulation reported for symmetrical twin cantilevers in the previous chapter where the addition of a molecular link always increased the resonance frequency. The evolution of the Q-factor and of the resonance frequency shift as a function of the number of cycles is plotted separately in figures 6.8a and 6.8b. A dashed line indicates the Q-factor and resonance frequency values relative to the device without MWCNTs.

Due to the unknown nature of the bond between CNT and silicon, which represents indeed the weaker point in the cantilever-CNT-cantilever link, it is rather difficult to know how many CNTs are present in each experimental run, and therefore to propose an absolute number for the sensitivity of our device. A finite element analysis was nevertheless performed on this system simulating the link between the cantilevers with small nanowires of different size and stiffness. Frequency shifts of the order of those obtained experimentally in the 3rd, 4th and 5th runs have been reproduced by using a single nanowire with a diameter of 20 nm and Young's modulus of 1 GPa. These parameters fit the typical values of polymers or structures made of proteins [Ivanovska 2004] [Gittes 1993]

much better than those made with MWCNTs, indicating that the behaviour of our system is probably dominated by the MWCNT-silicon contact. To compare our results with mass-sensitive techniques, we estimate the amount of MWCNTs in figure 6.4c to be less than 0.1 μm^3 in volume and 260 fg in mass: this compares favourably with the smallest feature - 150 pg - measured with the mode localization approach [Spletzer 2006]. When comparing with mass detection based only on frequency shift, we rather take into account the ratio between the detected and the cantilever masses: in our case it is less than $1.6x10^{-5}$ while, for instance, in [Ilic 2005], it is $0.8x10^{-5}$ indicating that our strategy is at least equivalent.

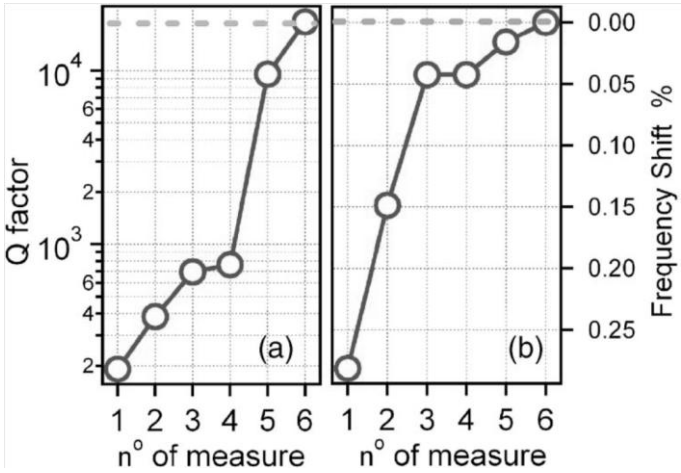

Figure 6.8*. (a) Evolution of the resonance Q-factor after several measurement cycles. (b) Plot of the frequency shift with respect of the first measurement for several measurement cycles. In both cases the gray dashed line refers to the device without molecular link.*

6.4 Conclusions

In conclusion, here we have demonstrated that, using an asymmetric cantilever system operated at room temperature and under normal vacuum conditions, in a *driver-follower* scheme, it is possible to detect the presence

of a few molecules and to follow their evolution as they change in number or strength.

Having identified a new device, which is easy to fabricate and to run, and whose performances are comparable if not better than those of other devices reported in literature, next step is to apply our device to solve a real biological problem. To do that, a more robust and controllable approach to bind molecules, other that CNT dielectrophoresis should be identified. This will be the topic of the next three chapters.

CHAPTER 7

Chemo-mechanical functionalization of twin cantilevers‡

Mechanical oscillators became a main research focus in the last years for potential applications in biomolecule detectors. In chapter 5 we demonstrated the feasibility of a scheme based on twin cantilevers with sensitivity down to the single molecule. This approach is extremely promising under the condition that the two terminals of the device can be functionalized with high selectivity and nanometric accuracy by linker molecules. In this chapter we report on the demonstration of a chemo-mechanical method to achieve the intrinsically aligned functionalization of two silicon surfaces, which can be separated by a gap controllable with nanometric precision. The chemical binding of the target molecules in the selected position was obtained through a cycloaddition reaction which exploits the reactivity of the freshly cleaved surfaces that formed when the cantilever gap was created. Finally we provide experimental evidence that below a critical size, the cleavage procedure creates step-free atomically flat silicon surfaces. The general validity of this approach is shown by the use in different chemical environments of two compounds with different reactive functional groups.

---

‡ This chapter is based on: V. Toffoli, F. Esch, M. Melli, F. Cataruzza, A. Pozzato, S. Carrato, G. Scoles, M. Tormen and M. Lazzarino, *Nanotechnology* **19**, 445502 (7pp) (2008) and on V. Toffoli, F. Esch, M. Melli, A. Pozzato, M. Tormen and M. Lazzarino, *Microelectronic Engineering* **86**, 1200–1203 (2009).

7.1 Introduction

The use of micromechanical resonators in general and especially of microcantilevers for single molecule detection and analysis has emerged in the last few years. In early experiments bacteria and viruses were placed randomly on microcantilevers and the resonance frequency shift of the system was used to monitor the presence and the number of cells. In those examples no care was taken concerning the specific location of the object to be detected on the cantilever. Since the frequency variation of the cantilever however depends on the location where mass is added – it is maximum upon mass addition at the free end of the cantilever - the precision of the measurement of the added mass is strongly affected by an unsuitable localization of the object to be detected. Ilic and coworkers [Ilic 2005] addressed this issue by defining lithographically a gold dot on the cantilever's free end and then selectively bonding double strand DNA molecules through a thiol linker, thus reaching the single molecule sensitivity and the possibility to count the DNA molecules.

Though thiol-gold interaction is perhaps the most popular functionalization strategy adopted in biosensors [Raiteri 2001], it suffers from two main disadvantages: it works only for thiolated molecules and requires a gold patterning of the substrate with nanometric accuracy. Moreover, the formation of alkanethiol self-assembled monolayers on a microcantilever surface induces a significant surface stress, whose magnitude is extremely sensitive to the gold surface roughness and more in general to growth conditions and which can be detrimental to the dynamic performances of the cantilever itself [Godin 2004].

Direct chemical functionalization of the substrate is possible mainly for polymers and semiconductors. From the technological standpoint the most relevant case is provided by silicon, for which several functionalization strategies are available: direct link with siloxane [Onclin 2005], direct covalent attachment of alkene terminated molecules [Sung 1997], acetylenylation of the chlorinated Si(111) surfaces [Rhode 2004] be integrated into a device fabrication process. All the mentioned processes require the preparation of clean reactive silicon surfaces by chemical or physical removal of the native oxide followed by a proper passivation. This adds a number of reaction steps not always compatible with the needed high spatial resolution.

An alternative approach, called chemo-mechanical functionalization and patterning, has been recently proposed [Yang 2006 and references therein]. Basically, chemo-mechanical functionalization is performed by wetting a surface with a reactive compound and then scribing the surface itself with a probe. In the case of silicon, scribing breaks the silicon oxide or the silicon passivation layer and exposes the highly reactive surface underneath that appears to react immediately with the reagent with which it is in contact. Several chemical reactions have been demonstrated to work, in particular the reaction with 1-alkenes, 1-alkynes, aldehydes, epoxides, alcohols, alkyl halides, and acid chlorides. Chemo-mechanical surface modification on silicon was first performed with a diamond-tipped rod on native oxide-coated silicon obtaining features of hundreds of micron in size. By improving the tip shape and the control of the applied force, very shallow features from one to 10 microns in size have been produced. Nanometric-sized structures have also been demonstrated to be obtainable by atomic force microscope scribing on hydrogen-passivated silicon. Recently, a similar method to functionalize silicon surfaces by laser-assisted chemical reaction instead of mechanical scratching has been proposed [Zhang 2006]. Several alkene functionalizations of silicon surfaces covered with native oxide have been shown; the minimum achievable dimensions are however in the range of several microns and cannot be pushed below the diffraction limit.

Both the chemomechanical and the laser-activated approach do not achieve nanometer-size resolution on native oxide-passivated silicon; the nanometrically controlled functionalization of silicon surfaces in micro-machined silicon cantilevers is thus still an open issue.

In this chapter we report on an alternative method that reaches this resolution. The method shares with the above described chemo-mechanical patterning the concept of mechanical modification inside a reactive medium but has the great advantage of dealing with atomically flat surfaces, generated by cleaving a crystal along a crystallographic plane. Moreover, thanks to the peculiar geometry of our experiment, we could generate two atomically flat functionalized surfaces separated by a gap controllable *with nanometric* precision owing to the atomic matching between the two cleaved surfaces. Finally, with this method, the functionalized regions are intrinsically located at the extreme end of a silicon microcantilever with atomic scale precision.

7.2 The Twin-cantilever approach

7.2.1 Operational scheme

The twin cantilever approach was described in the previous chapters for a symmetric and an asymmetric configuration. Let us just recall here the basic principles: two or more mechanical resonators (in the simplest case: cantilevers) are fabricated, close to each other but mechanically uncoupled. The dynamic behaviour, in particular the resonance frequency of each cantilever, is generally insensitive to the presence of neighbours. However,

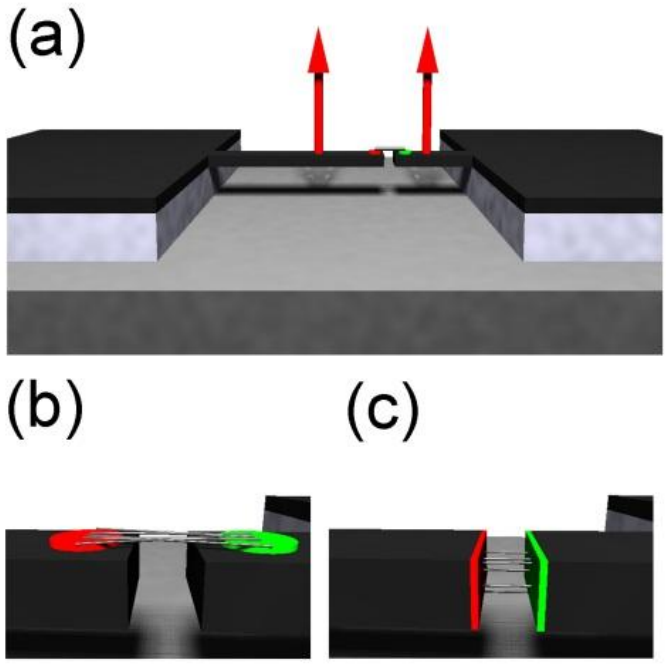

Figure 7.1 *a) Schematic description of the twin cantilever device. b) Detail of the molecular arrangement for a toplayer functionalization and c) for the proposed gap functionalization*

if any mechanical link is generated, as for instance by grafting a molecule to both resonators, the latter become coupled and their dynamic response changes. The resonance frequency of the system shifts, generally towards

higher frequency due to the increased stiffness, and the movement of one oscillator can induce a motion in a neighbouring oscillator. A model of the twin cantilever system is displayed in figure 7.1a. So far only a finite element analysis of the device [Lazzarino 2006] and a proof of concept of the detection principle with carbon nanotube linkers had been provided [Qazi 2007] since the major technical difficulty had still to be tackled before detecting biologically relevant molecules: to graft a molecule such as a protein in a way that it bridges a twin cantilever device, two opposing surfaces have to be functionalized at a relative distance of less than 10 nm.

The possibility of substrate patterning with biological molecules at nanometric resolution has been already demonstrated by dip pen lithography [Piner 1999], nanografting [Xu 1999], microcontact and nanoimprint lithography [Renault 2003] [Falconet 2004]. More recently, Huang and co-workers [Huang 2007] proposed a method to pattern a surface by electrochemically controlling the assembly/release of biomolecules on nanostructured gold electrodes, thus obtaining patterns containing several different biomolecules in a spatial configuration controlled on a nanometric scale. To implement these methods on a twin cantilever micromechanical resonator, a lithographic process with nanometer precision is required for aligning the patterns with each other and with the cantilever edges. Moreover, these methods can be applied only the top surfaces of the cantilevers leading to a geometrically inefficient process and a low probability for bound molecules to link to the opposite cantilever, as depicted in figure 7.1b. On the other hand, if the chemical reactivity of the walls of the cantilever facing each other is exploited for functionalization, a proper molecular alignment can be achieved; such a plain use of the active areas implies the intrinsic positioning within the twin cantilever gap, as illustrated in figure 7.1c.

7.2.2 Fabrication procedure and gap tuning

Let us recall here the fabrication process for the formation of a twin cantilever structure. Briefly, we started from a silicon on insulator (SOI) wafer composed of a 2.5 µm thick monocrystalline silicon layer with either <110> or <100> surface orientation, a 2 µm thick buried oxide layer and a 500 µm thick handle silicon wafer. By electron beam evaporation we

deposited a protective 50 nm thick nickel layer, on which the twin cantilever geometry was reproduced by standard optical lithography and subsequent wet etching of the Ni with a solution of HNO_3:CH_3COOH:H_2SO_4 in water. The remaining Ni structures were used as a mask for the etching of the silicon cantilever trough an inductively coupled plasma reactive ion etching which allowed for defining vertical walls through the whole thickness of the top silicon layer. Finally the oxide sacrificial layer was removed with a HF:NH_4F wet etching and the sample dried with a supercritical point drying process in order to avoid the collapse of the suspended structure.

At this stage the twin cantilevers were not yet formed and the structure is still shaped as a continuous 500 µm long, 20 µm wide and 2.5 µm thick bridge with a central region that was smoothly narrowed to a notch with a width of 10 µm (see SEM image in figure 7.2a).

We applied then a lateral mechanical stress to the bridge at its weakest point, *i.e.* at the notch, with the help of a sharp tip such as that of an AFM (see schematic illustration in figure 7.2b).

Since the bridge is monocrystalline, it cleaves along a crystallographic plane, generating - in principle- two defect-free atomically flat surfaces. A detailed discussion of the efficiency of the cleavage process will be the subject of the next chapter. Since silicon cleaves along the <111> surface, one obtains a cleavage plane tilted at 55^o with respect to the surface when starting with a <100> wafer, while vertical cleavage planes are obtained when starting with <110> wafers. If no residual stress is present in the topmost silicon layer, the two cleaved surfaces stay in contact with each other.

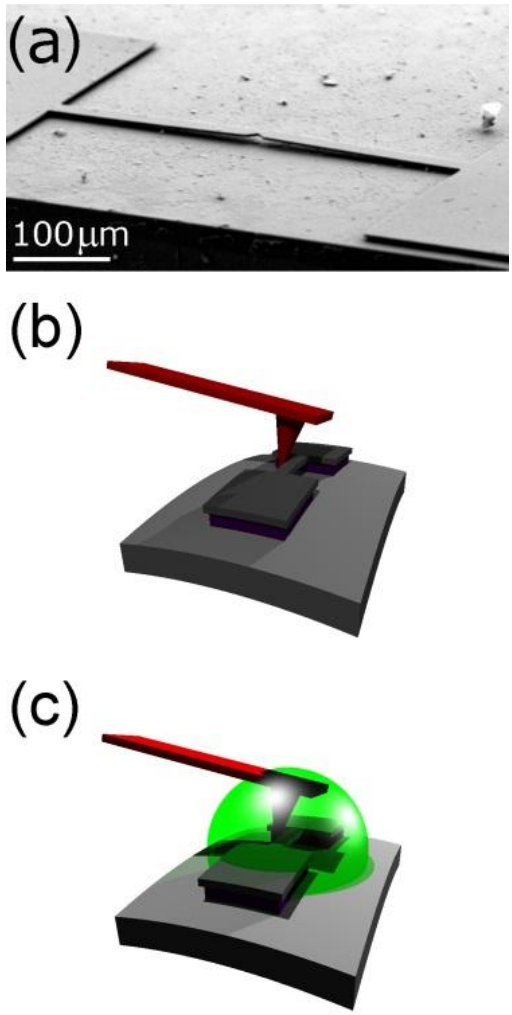

Figure 7.2 *a) SEM image of a bridge prior to the cleaving process; the small upward bow is due to residual stress in the topmost Si layer. b) Schematic of the cleaving process in air. c) Schematic of the selective gap functionalization by cleaving in a reactive environment.*

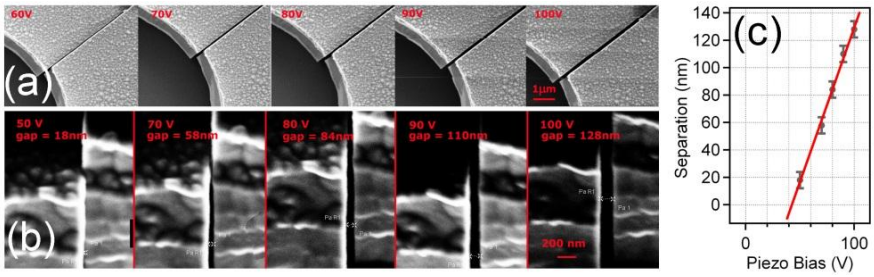

Figure 7.3 *Sequence of SEM images of a twin cantilever gap at various voltages applied to the bending piezo device. (a) top view – the images were taken with 10° tilt in order to provide also a partial image of the side walls. (b) side view – images were taken with 70° tilt which was the maximum allowed by our set-up. The gap can be tuned linearly from virtually zero to 128 nm, as indicated in the plot of the measured gap widths vs bending piezo device bias (c). Substrate: <110> Si wafer leading to a vertical gap.*

To open the gap for molecular recognition and tune it with nanometric precision, we improved the mechanism described in chapter 5 and developed a piezo-actuated device for applying a controlled bending moment to the wafer, similar to break junction experiments [Moreland 1985]. In figure 7.3 we report a series of SEM images, in top view (a) and in lateral view (b), of the gap at different bending values obtained by varying the bias applied to a piezo actuator. These data are plotted also in figure 7.3c together with a linear fit that results in a gap tunability of 2.26 nm/V. The large offset of 42 V needed to initially separate the two cantilevers originates from the residual compressive stress of the silicon top layer. The existence of a compressive stress is confirmed by the buckling of the initial bridge, clearly visible in figure 7.2a. From this measurement, the stress was estimated to be about 0.02%, in agreement with the SOI specification.

7.3 Chemical functionalization

The fabrication process described above has a technologically extremely valuable peculiarity: the formation of the gap through the cleavage of the monocrystalline silicon exposes two ideally flat, clean and extremely reactive surfaces exactly matching each other. This ideal condition cannot

be ensured by any other fabrication process such as those based on plasma etching or on focused ion beam lithography, where the edge roughness is typically in the range of several nanometres. When the cleavage is performed under ambient conditions, the two silicon (111) surfaces oxidize instantaneously and become passivated with a thin layer of amorphous silicon oxide. If the sample is instead properly cleaved in a well-controlled chemical environment, as sketched in figure 7.2c, the local reactivity can be exploited for the formation of two locally functionalized surfaces.

To demonstrate the implementation of such an idea, we looked at surface functionalization reactions that could be effective on a clean, unreacted silicon surface but that are hindered by the oxide layer that is present all over the remaining silicon surfaces, thus exploiting the intrinsic alignment of the cleaved surfaces.

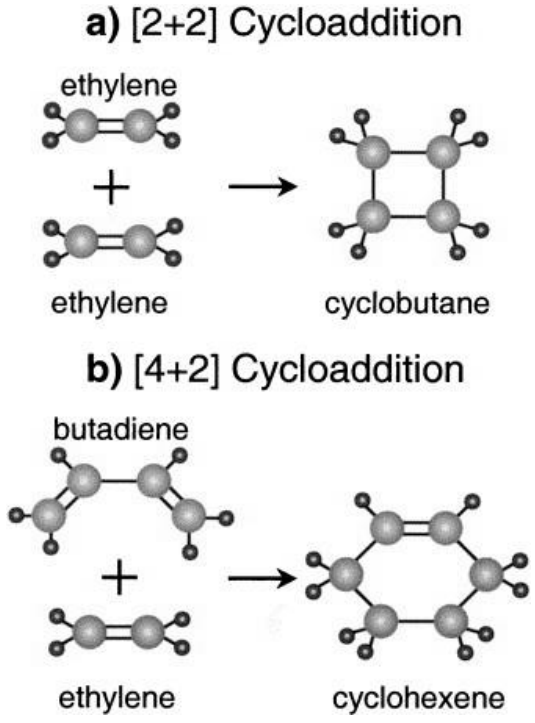

Figure 7.4 *Simple examples of cycloaddition reaction for hydrocarbures.*

Adsorption of simple unsaturated hydrocarbons on clean Si(100) surfaces has been extensively studied [Hamers 2000]. Two cycloaddition pathways are commonly accepted. In the [2+2] cycloaddition reaction the C=C double bond of a suitable organic molecule and a surface Si-Si dimer break to form a four members Si_2C_2 ring. In addition, molecules that contain at least two conjugated double bonds can instead link to silicon through a Diels-Adler [4+2] reaction. Simple and general examples of cycloaddition reaction are provided in figure 7.4. The situation at the surface can be visualized by substituting the lower component with a surface where double bonds or dangling bonds are present.

Cycloaddition reactions for compounds other than hydrocarbons have also been demonstrated. For instance Ellison and Hamers [Ellison 1999] studied the adsorption of phenylisothiocyanate on the Si(001) surface and demonstrated that the reaction involves the formation of a Si_4NC ring. In contrast to the large amount of data available for the (100) crystallographic plane of the silicon, fewer examples of cycloaddition processes are reported in literature [Tao 2004] [Leftwich 2008] for Si(111). The main difference lies in the nature of the silicon reconstructions present on the two clean, unreacted, surfaces: a symmetric one with the formation of surface Si-Si dimers in the case of Si(100)-(2x1) and a strongly asymmetric one with a adatom - rest atom pair in the case of Si(111)-(7x7). The Si-Si distance in the Si(100) dimers is 2.24 Å which matches better the C=C distance of 1.45 Å than the Si-Si distance of about 4.4 Å in Si(111). However, density functional calculations [Lu 2003] predict cycloaddition pathways for several unsaturated hydrocarbons in spite of this geometrical mismatch. Finally it should be noted that all the experiments cited above have been performed on clean reconstructed surfaces in an ultrahigh vacuum environment and no data are available on freshly cleaved silicon surfaces.

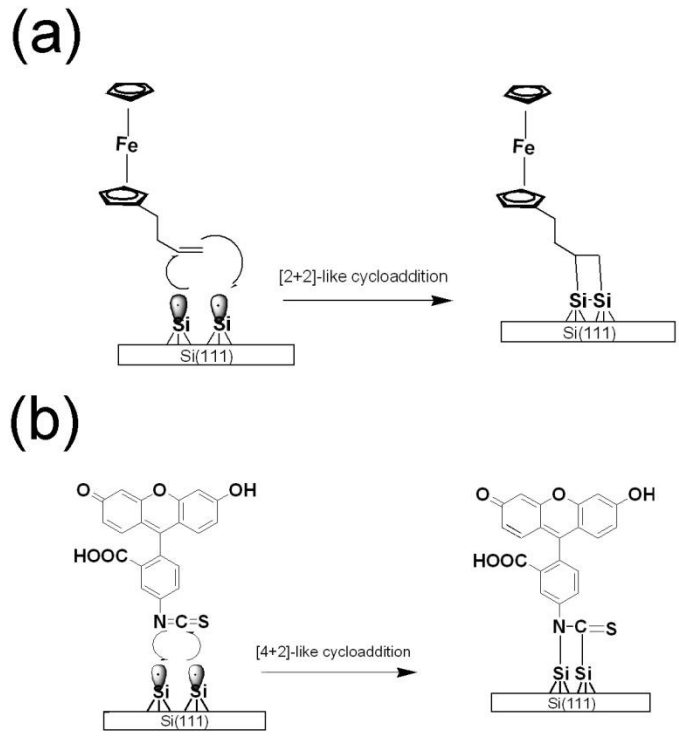

Figure 7.5 *Reaction pathways on the unsaturated Si(111) surface that results from the cleavage with reactants such as vinylferrocene (a) and FITC (b).*

7.4 Results from photoemission and EDX spectroscopy

To demonstrate the chemical functionalization upon cleaving of the twin cantilever we chose two different chemical compounds and two different cleaving strategies.

As a first approach we used vinylferrocene (see figure 7.5a). Vinylferrocene (VFC) is solid at room temperature and melts at 53°C. The Fe atom trapped between the two aromatic rings can be easily monitored by several spectroscopic methods, whereas the vinylic double bond can be used to functionalize the silicon surface through a cycloaddition process.

We mounted the sample in an Atomic Force Microscope (AFM) equipped with a heating stage. We covered the bridge with solid VFC and raised the temperature. Above the melting point the VFC changes its appearance into

a transparent reddish liquid, allowing to visualize the silicon bridge with the AFM optical microscope and to align the AFM tip to the notch in the bridge. Upon cleaving, the two opposite Si(111) flat surfaces are immediately exposed to pure VFC. After a few minutes the sample is rinsed in abundant dichloromethane to remove all non-specifically adsorbed VFC. The quality of the functionalization was studied by laterally resolved photoemission at the Nanospectroscopy beamline at Elettra, the synchrotron radiation facility in Trieste, Italy and by energy dispersive X-ray (EDX) spectroscopy in a scanning electron microscope (SEM).

The laterally-resolved chemical analysis of the twin cantilever structures was carried out with the Spectroscopic Photoemission and Low Energy Electron Microscope (SPELEEM) installed at the Nanospectroscopy Beamline. [Locatelli 2003]

The SPELEEM images a specimen that is illuminated with soft x-rays, ultra-violet (UV) radiation or low energy electrons. The emitted photoelectrons or the elastically reflected electrons are accelerated by a strong field in the objective lens, of which the specimen is an integral part. The objective produces a magnified image of the specimen, which is further magnified by several additional lenses in the imaging column of the instrument. The image is energy-filtered by the hemispherical analyser and finally projected onto an MCP detector with a phosphorous screen. The latter is imaged in real-time by a computer controlled CCD camera. The PEEM detects electrons emitted from atomic core levels with kinetic energy $E_{kin} = h\nu - E_{bin} - \varphi$, where E_{bin} is the core level binding energy, $h\nu$ the photon energy and φ the work function. Typically $h\nu$ is kept fixed, with energies in the range provided by the beamline (50-1000 eV). The energy filter is used to select the kinetic energy E_{kin} of photoelectrons, which allows measuring the binding energies of emitting atoms or accessing the surface electronic structure, including surface states and resonances. Typical kinetic energies of the photoelectrons are in the range 50 to 150 eV, *i.e.* at the minimum of the inelastic mean free path of the electrons in matter and therefore ensure good surface sensitivity. Kinetic energies are also typically well beyond the broad peak of secondary emission. Collecting a series of images at different kinetic energies allows obtaining laterally resolved (or angle resolved) spectroscopic information. The intensity of the photoemission signal is proportional to the number of emitters in the topmost layers within the energy-dependent escape depth,

and thus provides straightforward and quantitative information about the surface chemical composition. Optimal elemental sensitivity is achieved by tuning the photon energy to maximise photoionisation cross-section.

A cantilever cleaved and functionalized with vinylferrocene was places in the SPELEEM chamber and photoemission spectroscopy was performed using a photon energy of 205 eV to maximize the photoemission cross section of the Fe3*p* core level. A series of images at increasing kinetic energy were acquired, two of them are displayed in figure 7.6. The two images are formed exclusively by photoemitted electrons with well-defined energy. The contrast is clearly evident. In particular the area on the cantilever edge shows a well-defined contrast inversion.

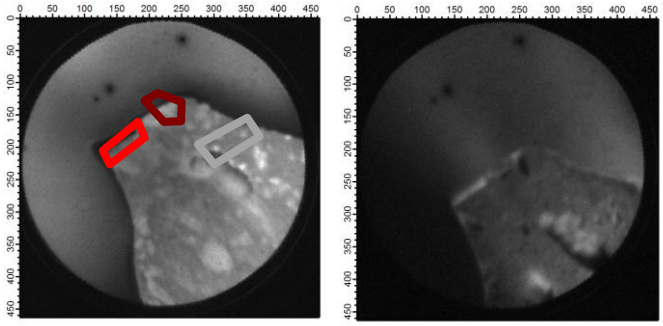

Figure 7.6 *SPELEEM images acquired at different kinetic energies, xx eV and yy eV left and righ respectively. The red area highlight the region of integration from where the full range spectra were obtained.*

Full range photoemission spectra were generated starting from the whole set of kinetic energy images, and are displayed in next figure 7.7. Firstly we observe that the SPELEEM experiments were performed a few days after the cycloaddition process, and that in the meantime the sample was exposed to air. Therefore the sample presents adventitious carbon on the surface. This constitutes a serious problem since photoemission is a surface sensitive techniques and even a few monolayers of organic residues on the surface hamper the acquisition of useful spectra.

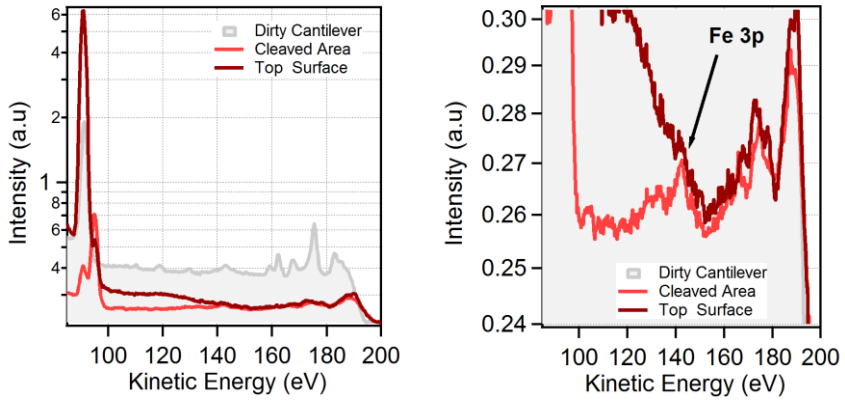

Figure 7.7 Left *Full range photoemission spectra relative to the region of integration indicated in figure 7.6.* ***Right:*** *zoom in the region of the Fe3p core level emission.*

The full range spectrum on such a contaminated area presents many peaks in the valence band, mainly related to oxygen and carbon from the impurities. However it was possible to find relatively clean regions, both on the top surface of the cantilever (purple trace) and on the cleaved area (red trace). On the cleaved area the signal from non-oxidized silicon is stronger than that of the silicon oxide, while the spectra from the top surface are dominated by the silicon oxide. This is a first indication that the cycloaddition process was successful. Indeed, if immediately after the cleavage the clean Si reacts with vynil ferrocene, subsequent exposure to air should not oxidize it any more. We also observe that the signal from the cleaved area is one order of magnitude lower than from the top surface. This is explained considering that only electrons emitted in the direction of the energy analyzer are collected, and since the cleaved area is tilted with respect to the top surface, the electrons collected from that area are reasonably less. Finally the right panel of figure 7.7 is a zoom on the Fe3*p* core level region. Here it is possible to identify a noisy peak that can be attributed to photoemission from the Fe3*p* core level. This peak is more evident on the cleaved area, again supporting the hypothesis that the functionalization process was successful. However the large noise, the poor energy resolution and the contamination of the samples did not allow to draw any definitive conclusion.

The second spectroscopic technique employed, energy dispersive X-ray (EDX) spectroscopy in a scanning electron microscope (SEM), is an

analytical technique for the elemental analysis or chemical characterization of a sample. It analyses the emission of X-rays during the decay of the core- excited states created by the impact of electrons on a sample. Its characterization capabilities are due in large part to the fundamental principle that each element has a unique atomic structure allowing unique set of peaks on its X-ray spectrum. Using the SEM beam as excitation source has the advantage of the extreme spatial resolution. The main drawbacks of this technique are that it is not resolved enough to investigate the different binding states of an element (*e.g.* bulk silicon and silicon oxide) and that the depth of interaction is only a few microns, so thin surface layers provide low signals.

To maximize the EDX signal, the two cleaved cantilevers were first positioned in a way to allow an easy access to the functionalized surface, as displayed in figure 7.8a for a device obtained from a <100> silicon layer and in figure 7.8b for a device obtained from a <110> silicon layer. The cleavage planes are tilted with respect to the device surface by 55^{o}, as shown in detail in figure 7.8c, and perpendicularly. For each sample we collected one spectrum on the cleaved area and one on the top surface as indicated by the highlighted areas in figure 7.8a and 7.8b.

Two representative spectra taken with an electron beam energy of 10 keV and an accumulation time of 10 min are shown in figure 7.8c and 7.8d for <100> and <110> surfaces, respectively. In both spectra, the continuous red line is related to the cleaved area and the black dotted line refers to the top surface. In spite of the very low surface sensitivity of the technique, we were able to observe a significant contribution of the VFC in the cleaved areas, while the VFC signal was negligible on the oxidized top surface of the cantilevers. than the VFC peak, which is in agreement with our experimental observations.

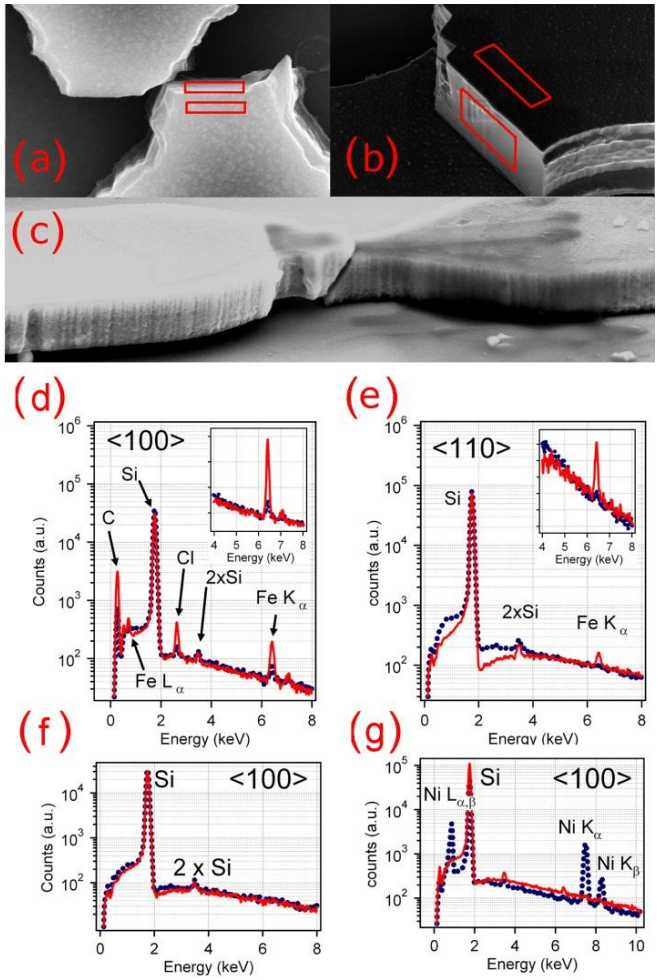

Figure 7.8 *SEM images of twin cantilever structures from a <100> (a) and from a <110> Si wafer (b) resulting in an inclined and a vertical gap, respectively which were investigated for their chemical composition by EDX after removal of the opposite cantilever (see highlighted areas). c) SEM lateral view of a <100> twin cantilever structure, showing the cleave occurring at 55^{o} with respect to the surface. d) EDX spectra for sample (a), e) EDX spectra for sample (b): continuous lines refer to the reactive gap area obtained by the cleaving procedure and exposed to vinylferrocene, dotted lines refer to the unreactive native oxide; insets highlight the ferrocene peak region. Further proof for the specificity of the procedure is the absence of functionalization in the gap obtained by cleaving in air prior to exposition to vinylferrocene (f) as well as a sample contaminated by Ni stemming from the fabrication process. The Ni signal does not show up on the cleaved surface (g).*

Indeed, since EDX spectroscopy x-rays originate from a micron-thick region, while the functionalization layer is about 1 nm thick, the bulk Si peak is expected to be several orders of magnitude more intense. In the case of <100> surface, thanks to the particularly favourable surface orientation, the VFC peak is more intense than in the case of <110> surface and the Fe L_α as well as the C K_α signal was detected. Cl contamination from the rinsing procedure with dichloromethane was also present. A zoom on the Fe signal from figure 7.8c and 7.8d, respectively, is displayed in the insets. In the case of the <110> sample, the VFC signal on the oxidized area was below the spectrum noise. In the case of the <100> sample, a VFC signal equal to 1/10 of the full signal was observed which we attributed to electrons that scatter inside the silicon cantilever and eventually reach the cleaved side of the cantilever, producing the residual VFC signal. To exclude any non-specific VFC adhesion to the cantilever surface we cleaved the silicon bridge first in air, than we exposed to VFC with the same procedure described above, and finally rinsed in abundant dichloromethane. The spectra are displayed in figure 7.8e and 7.8f. No trace of VFC was detected either in the cleaved area or on the cantilever surface. The three extra peaks in figure 7.8f correspond to residual Ni on the cantilever surfaces due to the masking procedure in the fabrication process. As expected, Ni is observed only on the cantilever surface but not on the cleaved area, which proves that the proposed procedure does not contaminate the cleaved areas.

7.6 Results from fluorescence microscopy

In a second approach we used fluorescein isothiocyanate (FITC), a dye commonly used in fluorescence microscopy (see figure 7.5b). FITC is soluble in water and other polar solvents; the latter are mostly also good oxidizing agents and therefore compete with FITC for the reaction with the freshly cleaved silicon surface. To reduce the oxygen contamination of the solution and subsequent oxidation of the cleaved surfaces, we therefore dissolved the FITC in dimethyl sulfoxide (0.13 M) directly in a sealed chamber, in which the sample and the cleaving mechanism were pre-aligned. After cleaving, the samples were rinsed in abundant methanol and water to remove all the FITC that was non-specifically absorbed on the surface. The samples were investigated by fluorescence optical

microscopy, using a xenon lamp as a light source and a set of filters for fluorescein luminescence. To facilitate the imaging, one of the two opposite cantilever was removed on purpose. In figure 7.9a and 7.9b we display two representative images obtained for cantilevers fabricated from <100> and <110> wafer, respectively. The images are the superimposition of bright field images of the sample, obtained without filters, and fluorescence images. For clarity, the fluorescence signals are indicated by arrows. We observed a fluorescence signal only in correspondence of the cleaved surfaces while the rest of the cantilevers and the substrate surfaces do not show any fluorescence, indicating the absence of non-specific absorption.

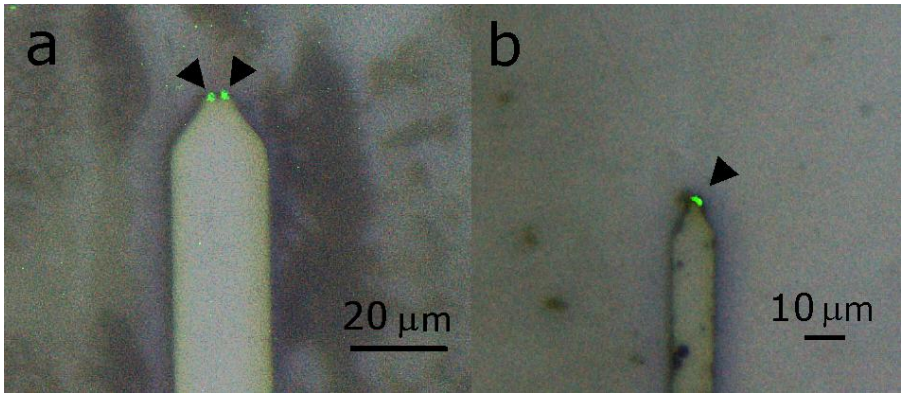

Figure 7.9 *Overlay of bright field optical images of cantilevers from a <100> (a) and from a <110> Si wafer (b) with an optical fluorescent images tuned on excitation and detection of fluorescein molecules. The opposite cantilevers were mechanically removed to facilitate the imaging. The cantilevers were cleaved in a dimethylsulfoxide solution containing FITC, and then rinsed in abundant water. We observed FITC exclusively on the cleaved region of the cantilever (black arrows)*

The fluorescence signal appears quite spotty, especially for the cantilever displayed in figure 7.9a, rather than uniformly distributed along the cleaved area. This can be ascribed to the non-optimized concentration of the FITC solution. The size of the cleaved areas, on the other hand, is comparable with the optical resolution of the fluorescence microscopy, thus hindering a more detailed optimization of the parameters.

7.5 Results concerning the morphology of the cleaved surfaces

The surface quality of the two facing surfaces generated by the cleavage process is, in principle, much better than any other surface produced through a technological process, such as those based on plasma etching or focused ion beam lithography where edge roughness is typically in the range of several nanometres. Having two atomically flat surfaces facing each other separated by a gap of few nanometers represents an incredible opportunity for a large amount of chemical and physical experiments spanning from wear and friction in confined molecular layers [Raviv 2002] to Casimir forces in Microsystems [Chan 2001]. For this reason we investigated in detail the formation of the gap and the quality of the surface involved.

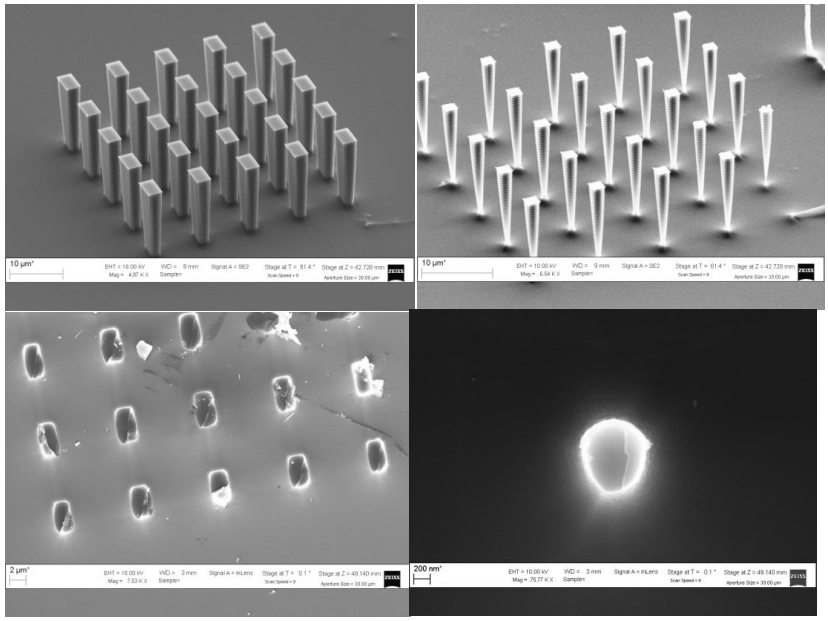

Figure 7.10 *Examples of pillar structures used for the evaluation of the performances of a scanning electron microscope to detect individual atomic steps after cleavage along a crystallographic plane. Top line: pillars with micron scale (left) and submicron scale (right) dimensions before cleavage. Bottom line: same structure after cleavage. Also submicron structures always exhibit large cleavage steps.*

To establish the actual absence of atomic steps on a cleaved surface, scanning probe microscopies offer the ideal resolution; unfortunately, in our case, the surfaces of interest are vertical with respect to the optical surface of the sample and therefore not accessible to this kind of analysis. Consequently to investigate the surfaces by AFM and SEM and then compare their performances, we fabricated by electron beam lithography and ICP etching several pillar structures of various sizes on a <111> silicon wafer and then cleaved them close to the substrate.

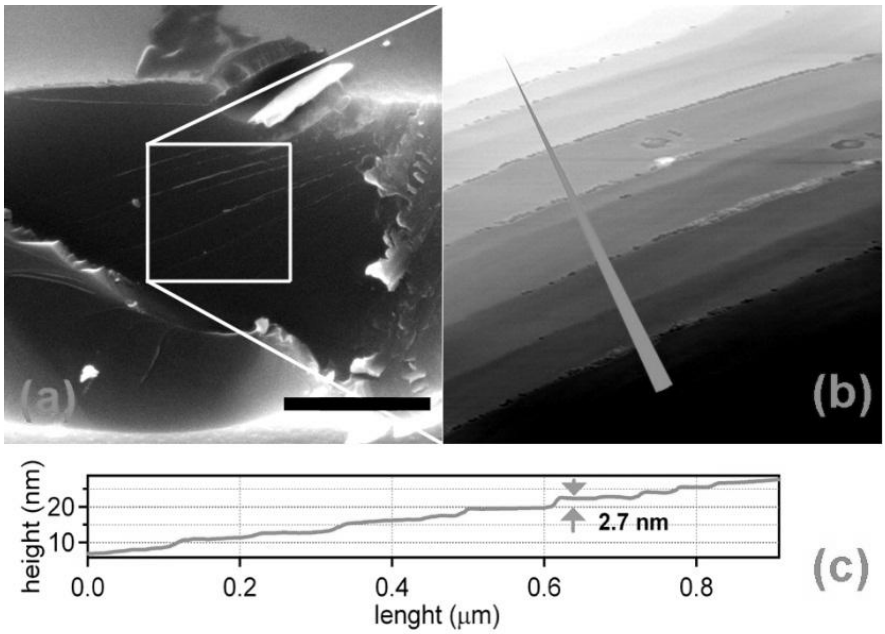

Figure 7.11 *Comparison of SEM and AFM images of cleavage defects. a) SEM image of a 2x4 μm^2 pillar, mechanically cleaved along the (111). Some steps are clearly resolved on an otherwise flat area. Scale bar 1 μm. b) AFM image of the 1x1 μm^2 area highlighted by the square in panel (a). Several flat terraces are observed. c) Height profile along the green arrow in panel (b). All the steps are smaller than 3 nm.*

In Figure 7.10 we show an SEM image of the pillar structures before and after the cleavage. Surprisingly it was impossible to obtain flat surfaces from this geometry, even for very small pillars (200 nm by side). However, this was not a problem since the purpose of this experiment was to estimate in how far the SEM is able to image the smallest cleavage steps and to

make a comparison with atomically resolved atomic force microscopy images. Figure 7.11 displays a detail of a cleaved surface exhibiting several cleavage steps. Figure 7.11a shows an SEM image while figure 7.11b presents an AFM image of the area highlighted by the square in figure 7.11a. In figure 7.11c we display the height profile obtained along the line drawn in figure 7.11b. Several steps ranging from 0.8 nm to 2.7 nm are observed, most of which can be clearly visualized also on the SEM image. We can conclude that SEM analysis can be used to assess the quality of cleaved surface down to the atomic scale.We fabricated some hundreds of bridges like the ones shown in figure 7.12 with three different notch sizes: 2.2x3.0 μm^2; 2.2x2.2 μm^2 and 1.5x1.5 μm^2.

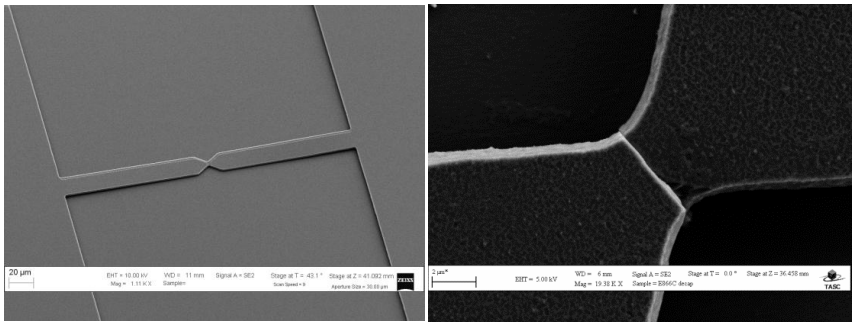

Figure 7.12 *Bridge used to investigate the cleaved surface before and after cleaving. In this condition the cleaved surfaces are not accessible, therefore the sacrifice of one of the two structures by mechanical removal was unavoidable.*

We then cleaved the bridges with the procedure described in the fabrication section and removed one of the resulting cantilevers in order to facilitate the subsequent SEM imaging. We obtained three different typologies of surfaces illustrated in figure 7.13. In figure 13a we show a 2.2x2.2 μm^2 cleavage surface where no defects are visible. Figure 7.13b presents an example of a surface with a bunch of steps indicated by the arrows. Finally figure 7.13c displays a surface with a defected cleavage where one side of the surface presents a large protrusion, indicated by the arrow. The latter geometry hinders the mutual movements of the two faces and represents a failure of a twin cantilever structure. It is worth to stress here the amazing difference between the surface roughness of the ICP-etched walls and the cleaved surfaces. Figure 7.13d displays the statistical analysis for the defect free surfaces (open symbols – red line) and the failed surfaces (full symbols – black line) plotted versus the surface area. Below 2 μm^2 the

majority of the cleaved surfaces are free of defects, opening the way for a possible engineerization of this fabrication process.

Large step free, atomically flat, surfaces are very difficult to obtain. In literature defect free cleavage procedures refer to solids whose area was in the few nm^2 range [Han 2004]. In our experiments with pillars we also never observed defect free surface for areas as small as 0.1 μm^2. We speculate that the result obtained for twin cantilevers is due to the peculiar and very elastic structure, cleaved at its half, that allows the generation of large elastic deformation distributed over the whole cleaving area, rather than have the whole stress localized in single point. However, fractures are a very complex subject, and a detailed discussion of the mechanism of cleaving in twin cantilever structures was beyond the scope of this work.

7.6 Conclusions

In this chapter we reported the demonstration of the intrinsically aligned chemo-mechanical functionalization of two silicon surface separated by a distance tunable with nanometric precision using two different chemical approaches on cantilevers cut out of silicon wafers with two different crystallographic orientations. The functionalized surfaces are flat on the atomic scale. Moreover, due the unique characteristics of the process, the localization of the functionalized regions on the structures of interest can be realized with subnanometer accuracy. The used spectroscopic methods proved the high selectivity of the process, in spite of the non-planar nature of the device under study, even if not yet allowing for a quantitative analysis of the functionalization efficiency and uniformity. In particular the experiments described do not provide any insight on the chemical nature of the functionalization observed. If a full cycloaddition reaction would occur, a covalent Si-C bond should be formed, which has a clear signature in many spectroscopic analysis, such as infrared absorption and photoelectron spectroscopy. Covalent bonds are the most stable bonds in nature, and a convincing proof of the formation of such a stable surface functionalization is of paramount importance. This will be the topic of the last chapter, before arriving at the conclusions

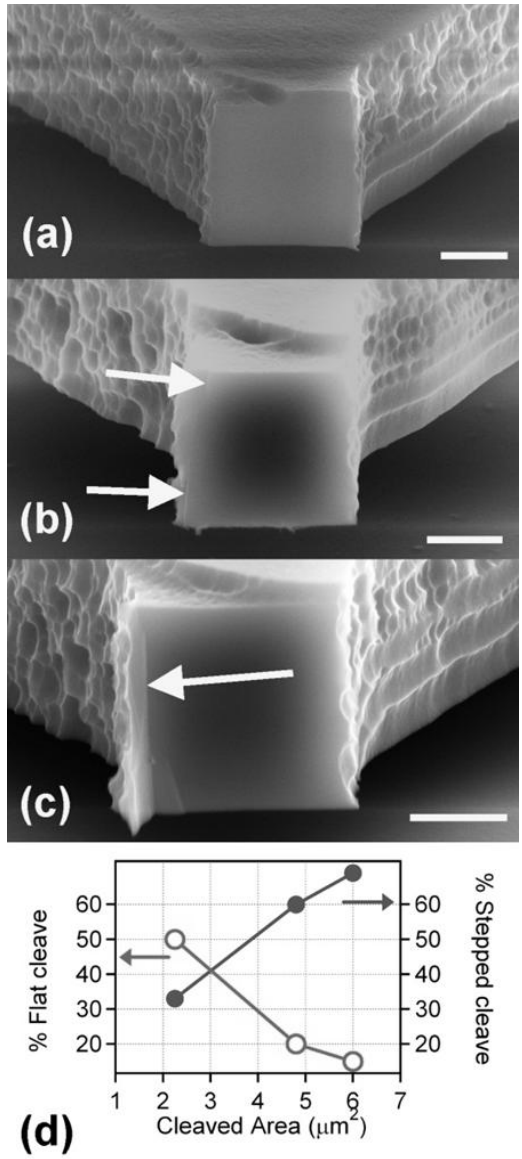

Figure 7.13 *SEM images of cleaved cantilevers with section 2.2x2.2 μm² showing different surface quality. All scale bars are 1 μm. a) Defect free surface. b) Surface with a shallow cleavage step indicated by the arrows. c) Surface with a micrometer sized protrusion indicated by an arrow. d) Plot of the percentage of defect free (open circles) and damaged (solid circles) cleavages as a function of cleavage area.*

CHAPTER 8

Cycloaddition functionalization of cleaved microstructures[§]

In chapter 7 we detailed an alternative functionalization method that relies on cleavage inside a reactive medium and is therefore intrinsically self-aligned with pre-nanofabricated structures. In this chapter we report on the chemical and physical properties of the chemical bonds originating during the cleavage in such a reactive environment and provide the evidence that our process results in an effective covalent bonding of the functional molecules with the silicon substrate. We believe that, thanks to the general character of the cycloaddition process and to the possibility to functionalize very small areas with high selectivity and a lateral resolution that is limited only by the fabrication technology used to define the sacrificial structures, this approach could find many applications in the growing field of nanotechnology.

---

§ This chapter is based on: Emanuela Carleschi, Elena Magnano, Mauro Melli, Marco Lazzarino, *ChemPhysChem* **13**, 459-462 (2012).

8.1 Introduction

The ability to provide surfaces with spatially controlled chemical properties is one of the key ingredients for many applications, ranging from the design of chemical, biochemical and biological sensors[Waggoner 2007] [Raiteri 2001] to the control of surface properties at the nanoscale such as friction, wettability [Bhushan 2008] or protein interaction [Hung 2011]. Several approaches have been proposed and demonstrated so far: from electrochemical control of biomolecular self-assembly[Huang 2007], gold-thiol interactions [Raiteri 2001], to local top-down lithography and silanization [Onclin 2005], photothermal nanopatterning [Klingbiel 2009] [Klingbiel 2010] and chemomechanical functionalization [Yang 2005].

Recently we proposed an alternative functionalization method [Toffoli 2008] that shares with the chemomechanical patterning described in [Yang 2005] the concept of mechanical modification inside a reactive medium but is intrinsically self-aligned with pre-nanofabricated structures. We used silicon sacrificial structures, fabricated for this purpose, that we cleaved inside a reactive medium, exploiting the reactivity of the freshly cleaved surface; thus we generated a chemically functionalized structure at a predefined location of a device with arbitrary shape and size, with the only constraint being the fundamental limits imposed by the lithographic techniques. This approach is fully compatible with standard MEMS production technology since the functionalization can be performed as a last step as we demonstrated in [Toffoli 2008].

In this chapter we report on the chemical and physical properties of the chemical bonds originating during the cleaving in a reactive environment and provide the evidence that our process results in an effective covalent bonding of the functional molecules with the silicon substrate. As target molecule we chose a commercially available molecule, with a perfluorinanted body and an acrylic head. The acrylic head contains an unsaturated C=C bond which may undergo a cycloaddition reaction. The perfluorinated body allows a clear identification of the molecule by measuring the C1*s* core level photoemission spectrum because the high electronegativity of the fluorine atom induces large chemical shifts. We used 1H,1H,2H,2H-perfluorodecyl acrylate, 97% purity from Sigma Aldrich (PFA); the structure is given in figure 8.1.

To investigate the chemical process that occurs at the silicon surface during the cleaving process, photoemission spectroscopy (PES) with high energy resolution is the best choice, for its surface sensitivity and its capability to discriminate between different chemical bonds that can be energetically separated by only a few hundreds of meV. On the other hand ultrasound-assisted cleavage occurs only for micron-sized structures and a spatially resolved technique should be used, which excludes other spectroscopies such as infrared-based techniques.

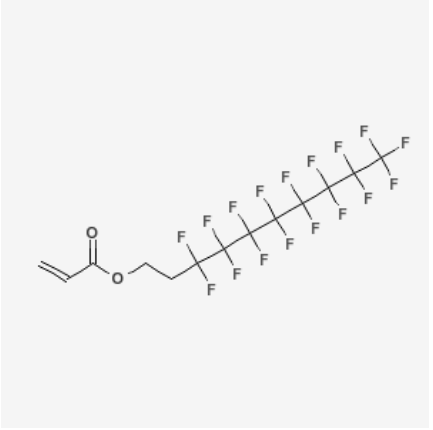

Figure 8.1 *Structure of the fluorinated organic molecule used in this experiment*

8.2 Experimental details

Micropillars were microfabricated starting from Si(111) wafers (Jocam, s.r.l Milan – Italy). The pillar in-plane geometry was produced by e-beam lithography (Zeiss Leo 30 keV) on a 400 µm x 400 µm writing field using a 500 nm thick layer of poly-methylmethacrilate (All Resist AR - 671 - 950K - Strausberg - Germany) as resist. The pillared three dimensional structure is produced by deep etching the silicon using a Bosch™-like process (C_4F_8 and SF_6 gas from SIAD, Trieste Italy) with an Inductively Coupled Plasma reactor (ICP, STS-Surface Technology). We used a process developed for the fabrication of pillar-shaped microresonators: more details on the fabrication procedure can be found on the papers based on those resonators [Melli 2010] [Melli 2011].

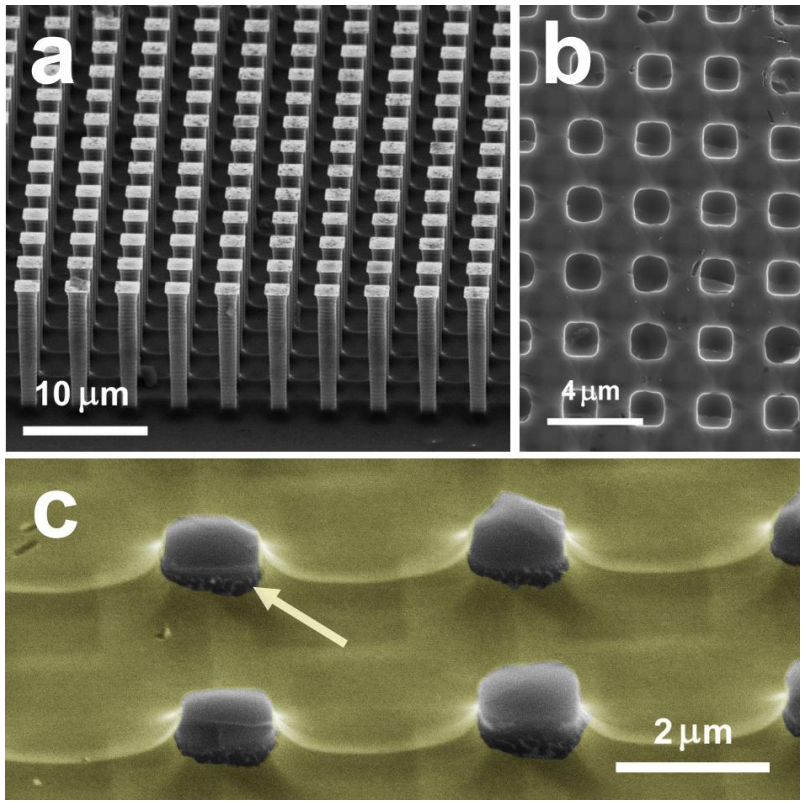

Figure 8.2 *(a) SEM image – 60° tilted view of an array of pillars before ultrasound cleavage. (b) SEM image - top view of an array of pillars after cleaving. (c) SEM image – 60° tilted view of the same sample in (b). The gold covered areas have been highlighted in false colours. Here at the base of the pillars, the portion of surface that is not cleaved nor covered by gold can be observed as a darker area as shown by an arrow for an exemplificative pillar. Even though the tilt is not necessarily the same as in the PES experiment the relative contribution of cleaved silicon and oxidized silicon can be qualitatively estimated.*

The wafer was immersed in a sealed vial containing the pure PFA. The vial was then flushed with pure nitrogen for one hour to remove any trace of moisture and oxygen that could react and passivate the silicon surface faster than the PFA. Finally the sealed vial was immersed in a commercial ultrasonic bath for 5 minutes. The ultrasound creates small gas bubbles that explode causing the cleavage of the pillars at their base, along a (111)

crystallographic plane, while keeping the vial sealed and the reactive medium clean. Ultrasonic treatment is currently used in synthetic chemistry, for longer exposure time and for more complex molecules without significant side effects [Herrero 2009]. The treatment was effective on average on one sample out of three. In the successful cases all the pillars were cleaved as shown in figure 8.2b, while in the negative cases a further exposure to ultrasounds, even for a prolonged period was ineffective. We believe that this depends strongly on the size and shape of the wafer chip on which the pillars are fabricated. Different chips may couple in different ways to the ultrasound resulting in dramatic changes in efficiency. However, further investigations are necessary to clarify this point. After cleavage, samples were rinsed in abundant methanol, immediately before being introduced in the experimental chamber of the BACH beamline and kept under ultrahigh vacuum conditions until the beginning of the experiments.

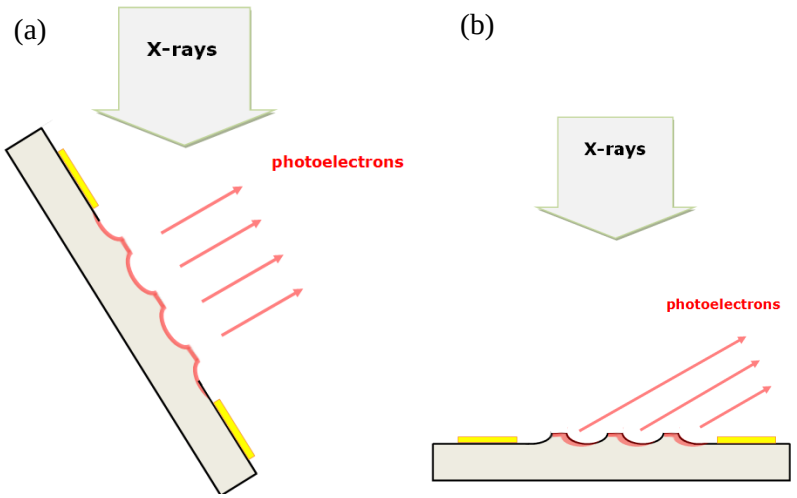

Figure 8.3 *The two different configurations, (a) normal emission and (b) grazing emission, used for these sets of photoemission spectroscopy measurements.*

Synchrotron radiation photoemission spectroscopy (PES) was performed at the BACH beamline at Elettra the Italian synchrotron radiation facility in Trieste [Zangrando 2004]. Samples were mounted on a thermally and electrically grounded sample holder and kept at room temperature and in ultrahigh vacuum conditions ($P<5x10^{-10}$mbar). The photon beam size was focused to a nominal beam size of approximately 300x20 μm^2 in order to minimize the signal from the region outside the pillars; however the PES

signal generated by the beam tails extended over a much larger area. Binding energies were calibrated using the Au 4*f* core level emission as reference. We set the photon energy to 250 eV and 340 eV, to maximize the PES cross-section for Si 2*p* and C 1*s* respectively. Energy dispersive X-ray spectroscopy (EDX) was performed with a ZEISS Supra 40 scanning electron microscope equipped with a EDAX – Genesis 4000 X-ray microanalysis system. Spectra and maps were acquired using 10 kV of accelerating bias in order to enhance surface sensitivity.

8.3 Photoemission spectroscopy

The sample consisted of high density pillar structures, designed to offer the maximum cleaved area to oxidized area ratio, which resulted in a 1:4 ratio, as shown in figure 8.2 a and b. Before cleaving, Au was evaporated on the pillar area in order to obtain a higher spectroscopic contrast. However, for geometrical reasons gold did not cover entirely the sample [Melli 2010]. After and the cleavage and exposure to PFA the sample surface consisted of three main typologies: i) clean, freshly cleaved, functionalized (111) silicon surface; ii) evaporated gold surface, (shown in false colours, figure 8.2c) on which organic molecules could physisorb a-specifically; iii) oxidized silicon surface, as left from the ICP etching process, with carbon residues originating from the etching process. The latter region is indicated by an arrow in fig 8.2c and is situated at the base of the pillars.

Two angular configurations, shown in figure 8.3 were explored. At normal emission (Figure 8.3a) PES is more bulk sensitive, and the Si 2p spectrum was dominated by the bulk silicon under the oxidized areas. At grazing emission (Figure 8.3b) PES is more surface sensitive and the bulk contribution from below the oxide was strongly reduced, however the geometric ratio was slightly worsened because of the non-planar topography of the sample and contributions from the carbon contaminated and oxidized surface indicated by the arrow in figure 8.2c and highlighted with a red shadow in figure 8.3b, are not negligible.

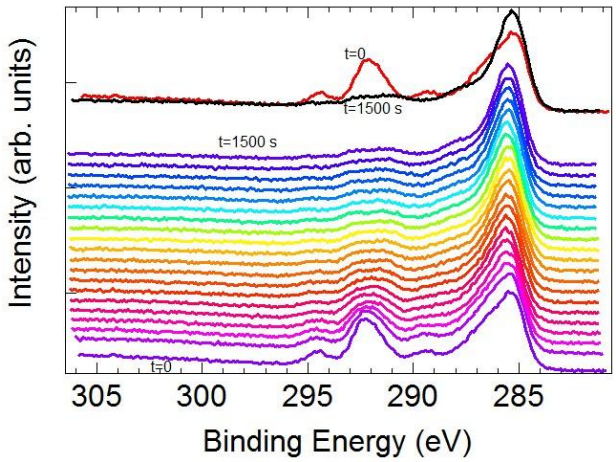

Figure 8.4 *Effect of the photon beam on a spin-cast film of PFA on silicon: temporal sequence of PE spectra relative to the C 1s core level, each with acquisition time 60 seconds is shown.*

We first performed a detailed study with PE spectra obtained from the same molecules *physisorbed* on a silicon substrate. For this, the silicon substrate was first cleaned in acetone and methanol. The native silicon oxide was removed by buffered oxide etchant and the sample was blown dry with N_2. In this way the surface is less hydrophilic and thus more affine to the highly hydrophobic fluorinated molecule. PFA was deposited on the surface and gently spun to create a uniform film. The PFA was then incubated at 80^{o}C, just below the boiling point, to evaporate the molecules in excess. The sample was loaded in the BACH beamline UHV experimental chamber and PES performed in the same conditions described in the experimental section for cleaved-assisted cycloaddition reaction discussed below.

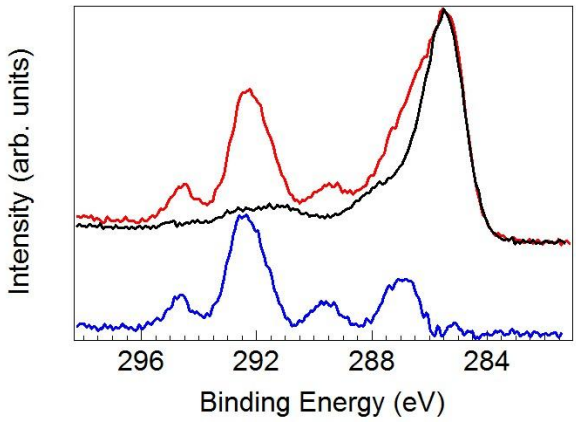

Figure 8.5 *Difference spectrum obtained by subtraction the residual PE spectrum relative to the C1s region (last in figure 8.3, black line here) from the first one acquired on the spin-cast PFA film on Si (red curve).*

Figure 8.4 shows the effect of the intense photon beam on the spin-cast PFA film. A temporal sequence of PE spectra relative to the C 1*s* core level, each with acquisition time 60 seconds is shown. The last spectrum corresponds to an overall exposure to the high photon flux, typical of synchrotron radiation source, of 1500 seconds. The inset reports a superimposition of the very first and the very last spectra. In the former, the features typical of fluorinated hydrocarbon molecule, CF_3 and CF_2 are clearly distinguishable. The component related to C=O is also clearly observed. The peaks are assigned consistently with [Winter 2002]. With increasing exposure, PFA molecules desorbed and a broad spectrum is left composed mainly by amorphous carbon. If we subtract this spectrum from the first one collected on the PFA film, as illustrated in figure 8.5, we obtain a difference spectrum where we can distinguish 4 main peaks, that according [Winter 2002] are attributed to CF_3, CF_2, C=O and CH_x. The relative intensities are about 1:5:1:2 as expected for randomly physisorbed molecules with a slight excess of the intensities of CF_3 and C=O peaks which is probably due to a slight inhomogeneity in molecule orientation with respect to the photon polarization.

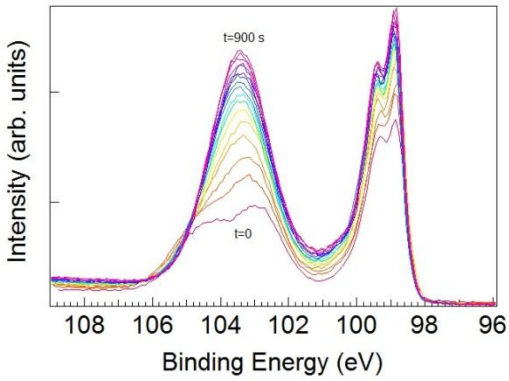

Figure 8.6 *Effect of the photon beam on a spin-cast film of PFA on Silicon: temporal sequence of PE spectra relative to the Si 2p core level spectra acquired in the same region as the C1s spectra of figure 6.3 on a spin-cast PFA film on silicon.*

Figure 8.6 shows effect of the intense photon beam on the sample as evidenced by the changes in the Si 2*p* core level photoemission spectra acquired in the same region as the C 1*s* PES of figure 8.4. Owing to the preparation procedure, only a very thin layer of silicon oxide is present which also undergoes photon-induced desorption [Ercolani 2005] as shown by the temporal sequence. However no contribution chemically shifted around 1.5 eV from the bulk silicon is evidenced; this is where one would expect a peak due to atoms participating in an Si-C bond.

Having identified the fingerprint of physisorbed PFA molecules, we can come to our main interest, namely the PE spectra of PFA chemisorbed by a cleavage-assisted cycloaddition reaction. In figure 8.7 we display the PES spectra collected from the region with the cleaved pillar (red continuous lines) and from the silicon oxidized region close to the pillar region but distant enough to avoid PES signal from the cleaved pillars and from the gold covered area (black dotted lines). A linear background is subtracted from each spectrum and the maxima are normalized to 1 for a better visual comparison. Figure 8.7a shows the C 1*s* core levels, acquired in the grazing emission geometry, which offers a higher surface sensitivity. The identification of the different peaks for PFA is in good agreement with that published in literature [Gupta 2006]. We first observe that a clear signature originating from the PFA molecule [Winter 2002] is present only in the pillar region. The ratio of the intensities of contributions originating from

CF_3 (one atom per molecule), CF_2 (7 atoms per molecule) and C=O (one atom per molecule), which should be 1:7:1 for randomly oriented physisorbed molecules [Gupta 2006], is instead about 10:20:1. This can be explained noting that the number of electrons photoemitted from atoms buried below the sample surface decreases as $\exp[-z/\lambda]$, where λ is the electron escape depth and depends on the material and the kinetic energy of the photoelectrons. In our experimental conditions $\lambda \sim 0.6$nm and the PFA length is 1.55 nm. If we consider the molecules oriented perpendicular to the surface and we sum all the contributions of CF_x moieties, we expect a CF_3/CF_2/C=O ratio of 10:30:1 close to the observed one. Therefore we conclude that PFA molecules are intact, anchored to the surface on the acrylic side and disposed nearly vertically with respect to the surface, with the CF_3 group in the outermost position.

Keeping in mind the PE spectra obtained from PFA physisorbed on a silicon substrate discussed above, we note that none of the peaks characterizing the physisorbed PFA are observed on the oxidized silicon surface, meaning that physisorbed molecules have been efficiently removed by rinsing. The strong peak at a binding energy (BE) of 285.5 eV is observed on both areas, 4.5 times stronger on the silicon oxide area. We attribute this peak to amorphous carbon (C-C bond) left by the BOSCH process used to etch the pillar structures. The difference in intensity arises because the illumination geometry is particularly sensitive to the pillar sides not coated by gold; it reflects the different portion of surface covered by this amorphous layer, which corresponds to the full area on the silicon oxide but only to roughly 1/4 on the cleaved area.

At lower BE we observed on the cleaved region a shoulder at about 283.5 eV. The presence of this shoulder is a general signature of the chemical reaction, which occurs between carbon and silicon leading to the formation of a C-Si covalent bond. This reaction has been well characterized both in the case of organic molecules [Klauser 2003] and of carbon clusters[Magnano 2003] on clean silicon surfaces.

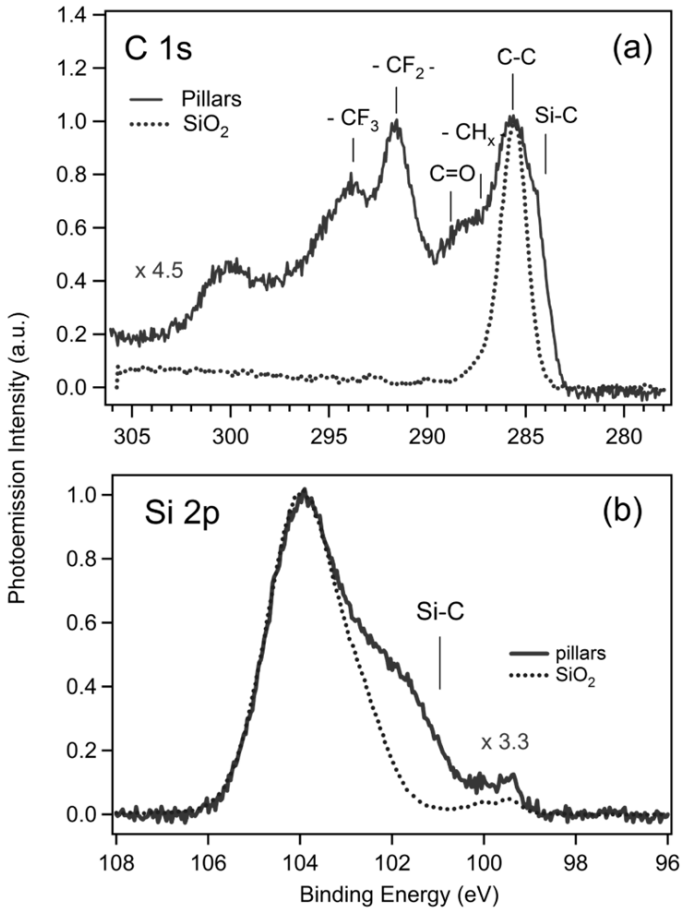

Figure 8.7 *(a) C 1s PES spectra collected in normal emission in the pillar area (black continuous curve) and on the oxidized silicon area (grey dotted curve). (b) Si 2p PES spectra collected in normal emission in the pillar area (black continuous curve) and on the oxidized silicon area (grey dotted curve). The maximum intensity has been normalized to 1 in both spectra.*

Figure 8.7b shows the PES spectra from the Si 2*p* core level, acquired in normal emission geometry, where the increased bulk sensitivity allowed us to investigate the silicon-carbon interface buried under the PFA layer. The main peak at high BE present on both spectra originates from the silicon oxide, which terminates the non-cleaved areas. As expected, the intensity is 3.3 times larger in the spectra collected on the non-patterned area. A small component from the bulk silicon is also visible around 99 eV BE in both

spectra, with the typical spin-orbit splitting of 0.6 eV. Only the spectrum acquired in the pillar region shows a shoulder at about 101 eV that can be attributed to the formation of covalent Si-C bonds at the silicon surface as already observed for organic molecules and carbon clusters reacting on silicon surfaces [Klauser 2003] [Magnano 2003]. C 1*s* and the Si 2*p* spectra acquired in the cleaved area consistently indicate the formation of a C-Si bond at the pillar surface.

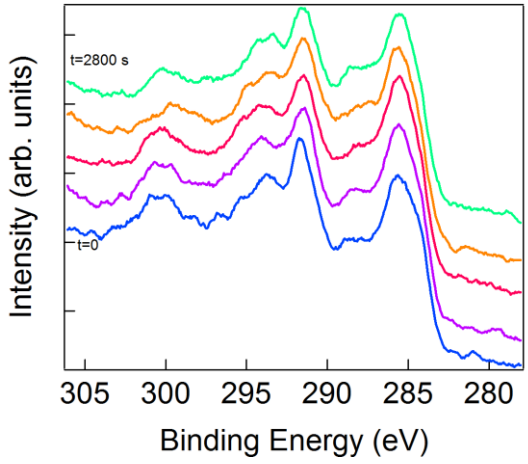

Figure 8.8 *Effect of the photon beam on PFA molecules grafted on silicon by a cleavage-assisted cycloaddition reaction: temporal sequence of PE spectra relative to the C1s core level, each collected with an acquisition time of 60 seconds.*

It is important to note that PFA chemisorbed by a cleavage-assisted cycloaddition reaction also reacts very differently to the photon beam than the physisorbed molecules discussed above. The temporal evolution of the spectra acquired on the cyclo-reacted PFA molecules is shown in figure 8.8. Here, in spite of the longer exposure, no significant changes in the PE spectra are noticed with increasing X-ray dose. This is a further indication that in this case a strong covalent bond was formed between the PFA organic molecule and the silicon surface, which cannot not be broken by X-ray irradiation, contrary to the case of physisorbed molecules.

The chemical reactions of unsaturated organic molecules with semiconductor surfaces [Filler 2003] and in particular with Si(111) [Tao

2004] have been extensively studied. It was shown that in presence of a single unsaturated C=C bond a strong [2+2] cycloaddition reaction occurs, not forbidden by the molecular symmetry [Hamers 2000] and with energy gain as high as 47.9 kcal/mol for a simple ethylene_Si(111) reaction [18]. The absence of thermal treatment rules out the possibility of a two-step process (physisorption followed by thermal bonding formation), and the absence of PFA molecules on the silicon oxide away from the pillar area excludes the possibility of ultrasound-assisted reactions. The latter can also be ruled out by the results presented in [Toffoli 2008] where local functionalization is obtained by mechanical cleaving a silicon suspended structures. Therefore we conclude that the surfaces were functionalized through a [2+2] cycloaddition process.

8.4 Scanning electron microscopy and energy dispersive X-ray analysis

To prove once more that the functionalization process occurred selectively on the silicon cleaved areas we investigated the samples with a SEM microscope equipped with chemical analysis. In figure 8.9a we show a secondary electron SEM image that provides a topographic description of the sample; the atomically flat cleaved areas are very poor electron scatterers and therefore appear dark in the image. Figures 8.9b and 8.9c present two images of the same region acquired at the X-ray energy corresponding to the K emission line of F and the M emission line of Au, respectively. The remarkable contrast observed together with the correspondence with the topographic image confirms that the cycloaddition process occurs only on the cleaved areas. Figure 8.9d displays two X-ray spectra acquired in the middle of a cleaved area (red line) and on the adjacent region covered by gold (black line). On the cleaved area we observe significant contributions from carbon, oxygen and fluorine and a large contribution from silicon, which is not surprising since EDX, contrary to PES, probes the samples up several microns in depth. All the peaks are present also on the gold area with different intensity except for the F peak which is absent. This proves that the functionalization happens only in the cleaved areas.

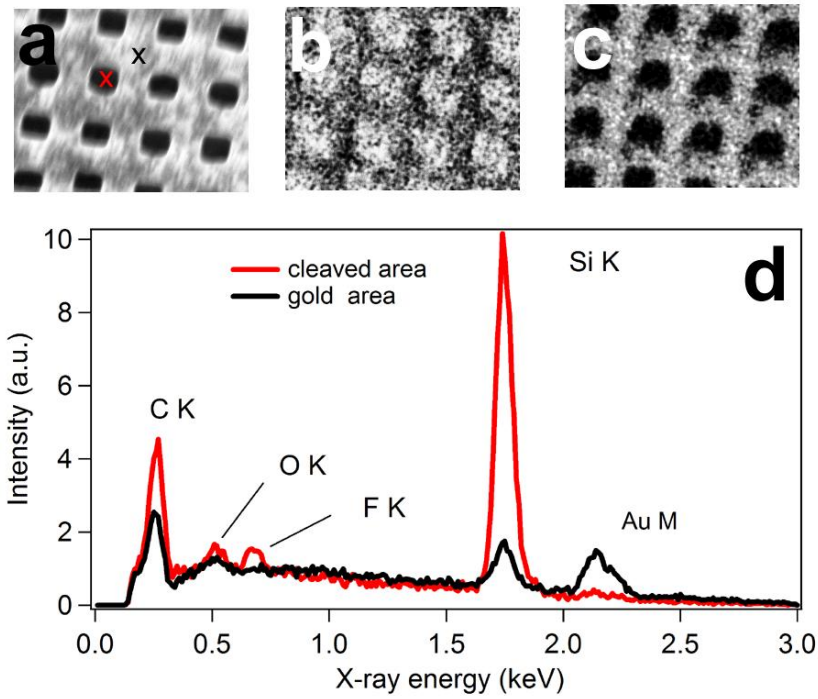

Figure 8.9 *Energy dispersive X-ray analysis of the cleaved pillars. (a) Secondary electron image; (b) F K line image; (c) Au M lines image. The three images were acquired simultaneously from the same region. (d) X-ray emission spectra acquired from a point well inside a cleaved area (grey dotted line) and on the nearest gold covered area (black line).*

8.5 Conclusions

We investigated the chemical and spatial properties of an innovative chemical functionalization method which takes advantage of the high reactivity of a freshly cleaved silicon surface to form a covalent bond with organic molecules with a C=C double bond at one end, in a wet environment. We provided evidence for the formation of the Si-C covalent bond by means of X-ray photoelectron spectroscopy and demonstrated the specificity of the functionalization process with electron microscopy and dispersive X-ray analysis. We believe that, thanks to the general character of the cycloaddition process and to the possibility of functionalizing very small areas with high selectivity and with a lateral resolution that is limited

only by the fabrication technology used to define the sacrificial structures, this approach could find many applications in the growing field of nanotechnology.

CHAPTER 9

Outlook and applications

The results collected in this thesis describe many building blocks for the design and fabrication of future nanomechanical biosensors. As already pointed out in the second chapter, in spite of the large effort devoted to the development of molecular sensitive micro- and nanomechanical sensors, only few strategies have addressed properly the problem of the molecular detection in a real biological environment, with performances suitable to be applied for biological and medical diagnostics. This requires addressing three essential points: operation in liquid, real time detection and sensitivity to low concentrations rather than few molecules. Most of the sensors reported so far in the literature operate in ultrahigh vacuum conditions and are end-point detectors, implying that the sensor is first incubated and then read out in a second separate stage. In most applications the molecules are evaporated or spayed on top of the sensor surface, circumventing the concentration issue.

It is clear that in order to develop sensors that could satisfy the three requirements listed above, new architectures should be developed, which go beyond the simple resonators, cantilevers and double clamped beam. In this work I proposed an original architecture that consists in using two cantilevers facing each other. I designed, modeled, fabricated and tested such an architecture in two different arrangements, symmetrical and antisymmetrical twin cantilevers. During this process several scientific and technical problems were raised, addressed and solved. One in particular, the chemical activation-functionalization of the opposite faces of the twin cantilever system received much attention and lead to the development of an original methodology to bind covalently an organic molecular layer on a spatially predefined semiconductor area. The design of the asymmetrical devices included three coupled cantilevers on one side, the two extra lateral

cantilevers being originally implemented as a control system. Actually the three coupled cantilevers alone revealed themselves as an interesting structure, hence they were developed in parallel and became the subject of another PhD project, the results of which were published in 2012 [Pakdast 2012].

The validity and originality of the proposed solution has been certified by a news and views commentary about of the [Qazi 2007] paper in Nature Materials [NM 2007] and the selection of the [Carleschi 2012] for the Elettra highlights 2012. Several aspects however have been addressed only marginally or not treated at all. The experiments described in this thesis are essentially proofs-of-concept, aimed at demonstrating the feasibility of the scheme proposed. A significant amount of work would be required to obtain the sensing performances in a real biological environment. A sensor should be operated in "dirty" liquid environments such as plasma, serum or full blood. The target molecules should be chosen among real biological molecules, such as proteins or nucleic acids. The surface functionalization should be applied using nucleic acid or antibody primers and in order to do that chemical synthesis should be developed since the required organic molecules are not yet commercially available. Finally a suitable instrument should be engineered to handle our devices outside a research laboratory and render them routinely accessible by technical staff. The development of biosensors into commercial prototypes is a rather complicated, time consuming and expensive undertaking and spin-off companies devoted to this task are based on millionaire budgets and employ hundreds of researchers and technicians. Examples of spin-off companies of this kind are Pacific bioscience (http://www.pacificbiosciences.com) and Oxoford Nanopore technologies (http://www.nanoporetech.com/); both are involved in the development of DNA sequencing techniques based on nanotechnologies and both have probably been beaten by the revolutionary Ion Torrent technology (http://www.iontorrent.com/) in spite of the large investments received.

We cannot play in this kind of game. On the contrary, our purpose was to contribute to the development of micromechanical sensors with new ideas, new techniques, new fabrication and chemical functionalization strategies and to run proof-of-concept experiments to demonstrate the validity of our proposal. I think we fulfilled our duty and we can leave it to bigger

companies to bring our ideas to their final exploitation if these ideas will turn out to be smart enough.

Bibliography

[Alexander 1989] Alexander, S.; Hellemans, L.; Marti, O.; Schneir, J.; Elings, V.; Hansma, P. K.; Longmire, M.; Gurley, J. *Journal of Applied Physics* **65**, 164 (1989).

[Arlett 2011] Arlett, J. L.; Myers, E. B.; Roukes, M. L. *Nature Nanotechnology* **6,** 203, **(**2011).

[Armani 2007] Armani, A. M.; Kulkarni, R. P.; Fraser, S. E.; Flagan, R. C.; Vahala, K. J. *Science* **317**, 783 (2007)

[Bashir 2004] Bashir, R. *Advanced Drug Delivery Reviews* **56**, 1565, (2004)

[Baumann 1997] Baumann, C.G.; Smith, S.B.; Bloomfield, V.A.; Bustamante C. *Proceedings of the National Academy of Sciences (U.S.A.)* **94**, 6185 (1997).

[Beebly 2004] Beeby, S.; Ensell, G.; Kraft M.; White, N. *MEMS Mechanical sensors* (Artech House, Boston, 2004)

[Bergatin 2012] Bargatin, I.; Myers, E. B.; Aldridge, J. S.; Marcoux, C.; Brianceau, C. P.; Duraffourg, L.; Colinet, E.; Hentz, S.; Andreucci, P.; Roukes M. L. *Nano Letters* **12**, 126 (2012)

[Berger 2007] Berger, R.; Delamarche, E.; Lang,H.P.; Gerber,Ch.; Gimzewski, J.K.; Meyer, E.; Güntherodt, H.-J. *Science* **276**, 2021 (1997).

[Best 2007] Best, R. *Phase Locked Loops 6/e: Design, Simulation, and Applications*, 6° ed. (McGraw-Hill Professional, New York, 2007).

[Bhushan 2008] Bhushan, B.; Jung, Y.C. *Journal of Physics: Condensed Matter* **20**, 225010 (2008).

[Binnig 1986] Binnig, G.; Quate, C. F.; Gerber, C. *Physical Review Letters* **56**, 930, (1986).

[Boef 1989] den Boef, A. J. *Applied Physics Letters* **55**, 439, (1989).

[Burg 2007] Burg, T.; Godin, M.; Knudsen, S.; Shen, W.; Carlson, G.; Foster, J.; Babcock K.; Manalis S.; *Nature* **446**, 1066 (2007)

[Burns 1998] Burns, M.A.; Brian N. Johnson, B.N.; Brahmasandra, S.N.; Handique, K.; Webster, J.R.; Krishnan, M.; Sammarco, T.S.; Man, P.M.; Jones, D.; Heldsinger,D.; Mastrangelo, C.H.; Burke D.T. *Science* **282**, 484 (1998).

[Butt 1996] Butt, H. Journal of Colloid and Interface Science **180**, 251, (1996).

[Carleschi 2012] Carleschi, E.; Magnano, E.; Melli, M.; Lazzarino M. *ChemPhysChem* **13**, 459 (2012).

[Chan 2001] Chan, H. B.; Aksyuk, V. A.; Kleiman, R. N.; Bishop D. J.; Capasso, F. *Science* **291** 1941 (2001).

[Chaste 2011] Chaste, J.; Sledzinska, M.; Zdrojek, M.; Moser, J.; Bachtold, A. *Applied Physics Letters* **99**, 213502 (2011)

[Davies 2003] Davis, Z. J.; Abadal, G.; Helbo, B.; Hansen, O.; Campabadal, F.; Pérez-Murano, F.; Esteve,J.; Figueras, E.; Verd, J.; Barniol, N.; Boisen A. *Sensors and Actuators A* **105**, 311, (2003).

[Decca 2003] Decca, R.S.; López, D.; Fischbach, E.; Krause, D. E. *Physical Review Letters*, **91**, 050402, (2003).

[Ekinci 2004] Ekinci, K. L.; Huang, X. M. H.; Roukes, M. L. *Applied Physics Letters*, **84**, 4469, (2004).

[Ellison 1999] Ellison, M. D.; Hamers, R. J. *Journal of Physical Chemistry B*, **103**, 6243 (1999).

[Ercolani 2005] Ercolani, D.; Lazzarino**,** M.; Mori, G.; Ressel, B.; Sorba, L.; Locatelli, A.; Cherifi, S.; Ballestrazzi A.; Heun S. *Advanced Functional Materials* **15**, 587(2005).

[Falconet 2004] Falconnet, D.; Pasqui, D.; Park, S.; Eckert, R.; Schift, H.; Gobrecht, J.; Barbucci, R.; Textor M. *Nano Letters* **4**, 1909 (2004).

[Fernandez 2001] Fernandez, J. M.; Chu, S.; Oberhauser, A. F. *Science* **292**, 653 (2001).

[Filler 2003] Filler, M. A.; Bent, S. F. *Progress in Surface Science* **73,** 1 (2003).

[Fritz 2000] Fritz, J.; Baller, M. K.; Lang, H. P.; Rothuizen, H.; Vettiger, P.; Meyer, E.; Guentherodt, H.J.; Gerber, Ch.; Gimzewski, J. K. *Science*, **288**, 316 (2000).

[Gevorkian 1990] Gevorkian, S.G.; Khudaverdian E.E. *Biopolymers* **30**, 279 (1990).

[Gilsantos 2009] Gil-Santos, E.; Ramos, D.; Jana, A.; Calleja, M.; Raman, A.; Tamayo, J. *Nano Letters* **29**, 4122 (2009).

[Gittes 1993] Gittes, F.; Mickey, B.; Nettleton, J.; Howard, J. *Journal of Cell Biology* **120**, 923 (1993).

[Godin 2004] Godin, M.; Williams, P. J.; Tabard-Cossa, V.; Laroche, O.; Beaulieu, L. Y.; Lennox, R. B.; Gruetter, P. *Langmuir* **20**, 7090 (2004).

[Grover 2011] Grovera, W. H.; Bryana, A. K.; Diez-Silvac, , M.; S. Suresh, S.; Higgins, J. M.; Manalis S. R.; *Proceedings of the National Academy of Sciences (U.S.A.)***108**, 10992 (2011).

[Gupta 2004] Gupta, A.; Akin, D.; Bashir, R. *Applied Physics Letters* **84**, 1976 (2004).

[Gupta 2006] Gupta, M.; Gleason, K.K. *Langmuir* **22**, 10047 (2006).

[Hamers 2000] Hamers, R. J.; Coulter, S. K.; Ellison, M. D.; Hovis, J. S.; Padowitz, D. F.; Schwartz, M. P.; Greenlief, C. M.; Russel jr, J. N. *Accounts of Chemical Research* **33**, 617 (2000).

[Han 2004] Han, W.-Q.; Zettl, A. *Applied Physics Letters* **84**, 2644 (2004).

[Herrero 2009] Herrero, M. A.; Toma, F. M.; Al-Jamal, K. T.; Kostarelos, K.; Bianco, A.; Da Ros, T.; Bano, F.; Casalis, L.; Scoles, G.; Prato, M. *Journal of the American Chemical Society* **131**, 9843 (2009).

[Huang 2007] Huang, S.; Schopf, E.; Chen, Y. *Nano Letters* **7**, 3161 (2007).

[Hung 2011] Hung, A.; Mwenifumbo, S.; Mager, M.; Kuna, J.J.; Stellacci, F.; Yarovsky, I.; Stevens, M.M. *Journal of the American Chemical Society* **133**, 1438 (2011).

[Iilic 2001] Ilic, B; Czaplewski, D.; Craighead H. G. *Applied Physics Letters* **77**, 450 (2001).

[Ilic 2004] Ilic, B.; Craighead, H. G.; Krylov, S.; Senaratne, W.; Ober, C.; Neuzil, P. *Journal of Applied Physics* **95**, 3694 (2004).

[Ilic 2005] Ilic, B.; Krylov, S.; Aubin, K.; Reichenbach, R.; Craighead, H. G. *Applied Physics Letters* **86**, 193114, (2005).

[Ilic 2005] Ilic, B.; Yang, Y.; Aubin, K.; Reichenbach, R.; Krylov, S.; Craighead, H. G. *Nano Letters* **5**, 925 (2005).

[Ivanovska 2004] Ivanovska, I.L.; de Pablo, P. J.; Ibarra, B.; Sgalari, G.; MacKintosh, F. C.; Carrascosa, J. L.; Schmidt, C. F.; Wuite, G. J. L. *Proceedings of the National Academy of Sciences (U.S.A.*) **101**, 7600 (2004).

[Jensen 2008] Jensen, K.; Kwanpyo, K.; Zettl, A. *Nature Nanotechnology* **3**, 533 (2008).

[Kajakaari 2009] Kaajakari, V. Practical MEMS: Design of microsystems, accelerometers, gyroscopes, RF MEMS, optical MEMS, and microfluidic systems (Small Gear Publishing, Las Vegas, 2009).

[Kerbush 2008] Kehrbusch, J.; Ilin, E.A.; Hullin, M.; Oesterschulze E. *Applied Physics Letters* **93**, 023102 (2008).

[Klauser 2003] Klauser, R.; Tai, Y.; Chan, Y.L.; Chuang, T.J. *Journal of Physical Chemistry B* **107**, 1387 (2003).

[Klingbiel 2009] Klingebiel, B.; Schröter, A.; Franzka, S.; Hartmann, N. *ChemPhysChem* **10,** 2000 (2009).

[Klingbiel 2010] Klingebiel, B.; Scheres, L.; Franzka, S.; Zuilhof, H.; Hartmann, N. *Langmuir* **26**, 6826 (2010).

[Knobel 2003] Knobel R. G.; Cleland, A.N. *Nature* **424**, 291 (2003).

[Krautbauer 2003] Krautbauer, R.; Rief, M.; Gaub, H. E. *Nano Letters* **3**, 493 (2003*).*

[Lahaye 2009] LaHaye, M.D.; Suh, J.; Echternach, P.M.; Schwab, K.C.; Roukes, M. L. *Nature* **459**, 7249 (2009).

[Lazzarino 2006] Lazzarino, M.; de Marchi, E.; Bressanutti, M.; Vaccari, L.; Cabrini, S.; Schmid, C.; Poetes, R.; Scoles, G. *Microelectronic Engineering* **83**, 1309 (2006).

[Leftwich 2008] Leftwich, T. R.; Teplyakov A. V. *Surface Science Reports* **63**, 1 (2008).

[Levene 2003] Levene, M. J.; Korlach, J.; Turner, S. W.; Foquet, M.; Craighead, H. G.; Webb, W. W. *Science*, **299**, 682 (2003).

[Locatelli 2003] Locatelli, A.; Bianco,A.; Cocco, D.; Cherifi, S.; Heun, S.; Marsi, M.; Pasqualetto, M.; Bauer, E. *Journal de Physique IV* **104**, 99 (2003).

[Lojek 2006] Lojek, B. *History of Semiconductor Engineering*, 1° ed. (Springer, New York, 2006).

[Lu 2003] Lu, X.; Wang, X.; Yuan, Q.; Zhang, Q. *Journal of the American Chemical Society* **125**, 7923 (2003).

[Magnano 2003] Magnano, E.; Cepek, C.; Sancrotti, M.; Silviero, F.; Vinati, S.; Lenardi, C.; Barborini, E.; Piseri, P.; Milani, P. *Applied Surface Science* **212-213**, 879 (2003).

[Melli 2010] Melli, M.; Pozzato, A.; Lazzarino M. *Microelectronic Engineering* **87**, 730 (2010).

[Melli 2011] Melli, M.; Scoles, G.; Lazzarino M. *ACS Nano* **5,** 7928 (2011).

[Moreland 1985] Moreland, J.; Ekin, J. W. *Applied Physics Letters* **47**, 175 (1985).

[Naik 2009] Naik, A. K.; Hanay, M. S.; Hiebert, W. K.; Feng, X. L.; Roukes M. L. *Nature Nanotechnology* **4**, 445 (2009).

[NM 2007] "MEMS in cross talk" *Nature Materials* **6**, 395 (2007).

[Noh 2008] Noh, J. W.; Anderson, R.; Kim, S.; Cardenas, J.; Nordin, G. P. *Optics Express*, **16**, 12114, (2008).

[Oestershultze 2012] Oesterschulze, E; Kehrbusch, P; Radzio, B.; Ilin, E. A.; Thyssen, A.; Deitmer J. W.; Kehrbusch J. *Lab Chip* **12,** 1316 (2012).

[Okamoto 2009] Okamoto, H.; Kamada, T. ; Onomitsu, K.; Mahboob, I.; Yamaguchi, H. *Applied Physics Express* **2**, 062202 (2009).

[Onclin 2005] Onclin, S.; Ravoo, B. J.; Reinhoudt, D. N. *Angewandte Chemie, International Edition* **44**, 6282 (2005).

[Pakdast 2012] Pakdast, H.; Lazzarino M. *Sensors and Actuators A* **175,** 127 (2012).

[Peng 2006] Peng, H. B.; Chang, C. W.; Aloni, S.; Yuzvinsky, T. D.; Zettl, A. *Physical Review Letters* **97**, 087203 (2006).

[Piner 1999] Piner, R. D.; Zhu, J.; Xu, F.; Hong, S.; Mirkin, C. A. *Science* **283**, 661 (1999).

[Prausnitz 2004] Prausnitz, M.R. *Advanced Drug Delivery Reviews* **56**, 581 (2004).

[Putman 1992] Putman, C. A. J.; De Grooth, B. G.; Van Hulst, N. F.; Greve, J. *Journal of Applied Physics* **72**, 6 (1992).

[Qazi 2007] Qazi, A.; Nonis, D.; Pozzato, A.; Tormen, M.; Lazzarino, M.; Carrato, S.; Scoles, G. *Applied Physics Letters* **92**, 173118 (2007).

[Raiteri 2001] Raiteri, R.; Grattarola, M.; Butt, H-J.; Skladal, P. *Sensors and Actuators B* **79**, 115 (2001).

[Ramos 2012] Ramos, D.; Gil-Santos, E.; Pini, V.; Llorens, J. M.; Fernandez-Regulez, M.; San Paulo, A.; Calleja M.; Tamayo, J. *Nano Letters* **12**, 932 (2012).

[Raviv 2002] Raviv, U.; Klein, J. *Science* **297**, 1540 (2002).

[Renault 2003] Renault, J. P.; Bernard, A.; Bietsch, A.; Michel, B.; Bosshard, H. R.; Delamarche, E.; Kreiter, M.; Hecht, B.; Wild, U. P. *Journal of Physical Chemistry B* **107**, 703 (2003).

[Rhode 2004] Rohde, R. D.; Agnew, H. D.; Yeo, W. S.; Bailey, R. C.; Heath, J. R. *Journal of the American Chemical Society* **128**, 9518 (2004).

[Rugar 2004] Rugar, D.; Budakian, R.; Mamin, H.J.; Chui, B. W. *Nature* **430**, 329 (2004).

[Schwab 2000] Schwab, K.; Henriksen, E. A.; Worlock, J. M.; Roukes, M. L. *Nature* **404**, 974 (2000).

[Smith 1996] Smith, S.B.; Finzi, L.; Bustamante C. *Science* **271,** 795 (1996).

[Spletzer 2006] Spletzer, M.; Raman, A.; Wu, Al. Q.; Xu, X.; Reifenberger R. *Applied Physics Letters* **88**, 254102 (2006).

[Stoney 1909] Stoney, G. G. *Proceedings of the Royal Society of London*. **82**, 172, (1909).

[Sung 1997] Sung, M. M.; Kluth, G. J.; Yauw, O. W.; Maboudian, R. *Langmuir* **13**, 6164 (1997).

[Tao 2004] Tao, F.; Xu, G. Q. *Accounts of Chemical Research* **37,** 882 (2004).

[Thorsen 2002] Thorsen, T.; Maerkl, S. J.; Quake, S. R. *Science* **298**, 580, (2002).

[Toffoli 2008] Toffoli, V.; Esch, F.; Melli, M.; Cataruzza, F.; Pozzato, A.; Carrato, S.; Scoles, G.; Tormen, M.; Lazzarino, M. *Nanotechnology* **19**, 445502 (2008).

[Toffoli 2009] Toffoli, V.; Esch, F.; Melli, M.; Pozzato, A.; Tormen M.; Lazzarino, M. *Microelectronic Engineering* **86**, 1200 (2009).

[Unter 2009] Unterreithmeier, Q. P.; Weig, E. M.; Kotthaus, J. P. *Nature* **458**, 1001 (2009).

[Waggoner 2007] Waggoner, P.S.; Craighead, H.G. *Lab Chip* **7**, 1238 (2007).

[Winter 2002] Winter, R.; Nixon, P.G.; Terjeson, R.J.; Mohtasham, J.; Holcomb, N.R.; Grainger, D.W.; Graham, D.; Castner, D.G.; Gard, G.L. *Journal of Fluorine Chemistry* **115**, 107 (2002).

[Wu 2001] Wu, G.; Datar, R. H.; Hansen, K. M.; Thundat, T. R.; Cote, J.; Majumdar A. *Nature Biotechnology* **19**, 856 (2001).

[Xu 1999] Xu, S.; Miller, S.; Laibinis, P. E.; Liu, G. Y. *Langmuir* **15**, 7244 (1999).

[Yang 2005] Yang, L.; Lua, Y. Y.; Lee, M. V.; Linford, M. R., *Accounts of Chemical Research* **38**, 933 (2005).

[Yang 2006] Yang, Y.T.; Callegari, C.; Feng, X.L.; Ekinci, K.L.; Roukes, M.L. *Nano Letters*, **6**, 583 (2006).

[Zangrando 2004] Zangrando, M.; Zacchigna, M.; Finazzi, M.; Cocco, D.; Rochow, R.; Parmigiani, F. *Review of Scientific Instruments* **75**, 31 (2004).

[Zhang 2006] Zhang, F.; Pei, L.; Bennion, E.; Jiang, G.; Connley, D.; Yang, L.; Lee, M.V.; Davis, R.C.; Smentkowski, V.S.; Strossman, G.; Linford M.R.; Asplund M.C. *Langmuir* **22**, 10859 (2006).

Summary

Any interactive system uses *devices* to obtain information on the environment and reacts accordingly. We humans, as nearly all animals, have devices that investigate our surroundings: we probe the mechanical properties through touch and hearing, the electromagnetic properties through vision (which is indeed limited to a very narrow band of the electromagnetic spectrum) and the chemical properties through taste and smell.

Machines, developed to help, substitute or improve human performances have been equipped in recent years with an increasing amount of *devices* to sense the environment autonomously: sensors. Wind wheels, thermometers, microphones, CCD cameras, airbags accelerometers, touch pads, are all sensors that extend our sensing capability, improve our performances and sometime substitute the human operation in automated systems.

There is a class of sensors in which humans and other animals have been more efficient than machines so far, namely chemical sensors. Current commercial ammonia sensors, for instance, are still ten times less sensitive (30 ppm) than our noses (2.6 ppm)!

In last decades, the advent of nanotechnologies and biotechnologies fuelled a tremendous development of innovative chemical sensors and in particular biosensors. Biosensors are characterized by the presence of a biological element, which can be an antibody, an enzyme, a DNA molecule etc. which interacts with the chemical element(s) to be detected and starts a transduction process which eventually provides a macroscopic signal that can be read out by a person or a machine. There are few examples of biosensors already present in our everyday life, like pregnancy tests or blood glucose monitors, together with other biosensors hidden in production lines, like food quality and water quality monitors.

However there are also hundreds of examples of biosensors that we would like to have already available, especially in medicine. From a simple flu, to an annoying allergy, to a dramatically fatal cancer, our body produces a numerous markers, mainly proteins that may indicate to us what is happening and may be used for an improvement of the treatment or a

timely prognosis. Unfortunately very often we do not know what those markers are, and when we know, we are not able to detect them, unless at a cost in terms of time and money that is hardly affordable.

There is an urgent need of safe, robust, cheap, portable, simple, easy to use biosensors, to first understand the biomarkers' significance and then detect them from time to time or continuously.

Designing a new biosensor involves many skills. There is the design of the recognition element, a biological molecule (enzyme, aptamer, antibody *etc.*) that when interacting with its target releases some kind of signal, and this is a job for a biochemist or for a biotechnologist. There is the manipulation of those biological molecules that should be bound to a surface or flown in a channel to the meeting point where the recognition takes place and this requires a chemist. There is the translation of the signal produced by the molecule into some electrical signal that can be easily manipulated, amplified and made visible in our world through our senses, and this is a job for an engineer or a physicist.

I focused on this last task, in the framework of micro-electro-mechanical systems (or MEMS) sensors. In general the acronym MEMS indicates a family of devices in which mechanical and electronic functions are tightly interconnected. This is realized by fabricating a semiconductor chip on which there are moving parts (microsprings, microcantilevers, micropaddles, *etc.*) that at the same time are also electronic components (resistors, capacitors, diodes, transistors), so that the displacement of the moving parts is immediately transduced in an electrical signal. Typical examples are the accelerometers mounted on the car airbags. When the change in the moving part is caused by an external stimulus, which can be chemical or physical, and is proportional to it, we have a MEMS sensor; a biosensor if biomolecules are involved.

Typical MEMS biosensors are oscillating cantilevers in which the resonance frequency changes when biomolecules are deposited on the cantilever surface; the latter should be treated chemically in advance to limit the adsorption exclusively to the species to be detected. This approach was adopted in the design of prototypes able to detect individual DNA molecules and even single atoms. However so far it did not go beyond the prototypal stage.

In this thesis I proposed a different approach that uses couples of cantilevers rather than single oscillators and monitors the evolution of the interaction between them, rather than the simple variation of the oscillation frequency. Two extreme cases were treated, namely the case of two nominally identical cantilevers and the case of two very different cantilevers. The behaviour of both devices was first studied by computer simulation; then devices were realized in silicon using micro- and nanofabrication strategies and their response was experimentally tested. Identical twin cantilevers are more sensitive but present a more challenging fabrication process. Asymmetrical twin cantilevers are more robust and suitable to be fabricated in large batches. A challenging technical issue was the fabrication of a gap between the cantilevers which is only few nanometer wide to match the size of a single molecule. A second even more challenging task was the tuning of the chemical reactivity of the cantilever surface exactly in front of the gap, leaving the rest un-reacted. I dedicated the second part of my thesis to this subject and was able to demonstrate a method to create a self-aligned covalent modification of the surface in question with a nanometric spatial control.

The output of my thesis was not expected to be a complete biosensor, ready to monitor real patients in a hospital. To get to this point a huge effort, affordable only by a large pharmaceutical company, would be required.

However I introduced several new concepts, never addressed before in literature, at least not in the field of biosensing, raised some questions and proposed several technical solutions to solve them.

I hope that someone in the future will reap the fruits of these little seeds I have been sowing, develop my ideas and transform them in working biosensors and thereby improve, if only just a little bit, the quality of our life.

Samenvatting

Ieder interactief systeem gebruikt apparaten om informatie over haar omgeving te verkrijgen en passend te reageren. Ook wij als mens gebruiken apparaten om onze omgeving te onderzoeken; tast & gehoor voor mechanische, zicht voor elektromagnetische (beperkt tot een zeer smalle band van het elektromagnetisch spectrum) en smaak & reuk voor chemische eigenschappen.

Machines, ontwikkeld om menselijke prestaties te helpen, vervangen of verbeteren, zijn de laatste jaren uitgerust met een toenemend aantal apparaten om hun omgeving autonoom waar te nemen: sensoren. Anemometers, thermometers, microfoons, ccd camera's, airbag versnellingsmeters en touchpads zijn voorbeelden van sensoren die onze waarnemingsmogelijkheden vergroten, prestaties verbeteren en soms zelfs de mens vervangen in autonome systemen.

In één klasse sensoren hebben machines de natuur in efficiëntie nog niet kunnen overtreffen. Onze neus is bijvoorbeeld 10 maal gevoeliger (2,6 ppm) dan commercieel verkrijgbare ammoniak sensoren (30 ppm)!

In de laatste decennia is door de opkomst van nano- en biotechnologie de ontwikkeling van chemische sensoren, in het bijzonder biosensoren, in een stroomversnelling geraakt. Biosensoren worden gekenmerkt door de aanwezigheid van een biologische component (bv. een antilichaam, enzym of DNA molecuul) welke een interactie aangaat met het te detecteren chemische element. Deze interactie wordt omgezet in een macroscopisch signaal welke vervolgens kan worden uitgelezen door een mens of machine. In ons dagelijks leven zijn biosensoren al terug te vinden in de vorm van zwangerschapstesten en glucosemeters, maar ook in minder opvallende toepassingen zoals voedsel- en waterveiligheid.

Er zijn echter nog vele gebieden, in het bijzonder in de geneeskunde, waarin biosensoren een belangrijke rol kunnen spelen. In geval van ziekte (eenvoudige griep of allergie tot levensbedreigende kanker) produceert ons lichaam biologische markers, eiwitten, welke inzicht kunnen geven in wat er zich in ons lichaam afspeelt. Hierdoor kan er een betere inschatting

worden gemaakt van de prognose en kan de therapie mogelijk specifiek op de patiënt worden afgestemd. Helaas is vaak niet bekend welke markers een rol spelen, en als dit wel bekend is, is de detectie veelal zeer kostbaar of zelfs niet mogelijk.

Er is dringende behoefte aan veilige, robuuste, goedkope, draagbare en eenvoudige biosensoren die ons helpen zowel de rol van een biomarker te begrijpen, als hun detectie mogelijk te maken.

Het ontwerpen van een biosensor gaat gepaard met vele vaardigheden. Het begint met het ontwerp van het gevoelige element, een biologisch molecuul (enzym, aptameer, antilichaam etc.) welke een signaal afgeeft bij het detecteren van een chemisch element. Dit vereist een biochemicus of biotechnoloog. Deze biologische moleculen moeten vervolgens worden aangebracht op een oppervlak of door kanaaltjes stromen naar het punt waar de detectie plaats vindt. Hiervoor is een scheikundige nodig. Ook moet het signaal dat door de biologische moleculen wordt afgegeven worden omgezet, vertaald, in een elektrisch signaal dat eenvoudig kan worden bewerkt, versterkt en zichtbaar worden gemaakt. Dit is een taak voor een mechanicus of natuurkundige.

Ik heb mij gericht op deze laatste taak, gebruik makend van micro-elektromechanische systemen (MEMS) sensoren. MEMS omvat een familie sensoren waarin mechanische en elektronische functies samenkomen. Dit wordt gerealiseerd door het vervaardigen van een halfgeleider chip waarop mechanische delen (micro-veren, -hefbomen etc.) ook een elektrisch component zijn (weerstand, condensator, diode, transistor). Hierdoor kan een mechanische prikkel direct worden omgezet in een elektrisch signaal. Een voorbeeld hiervan is de versnellingssensor in auto airbags. Als de prikkel uit een externe bron afkomstig is, dit kan chemisch of fysisch zijn, spreken we over een MEMS sensor; een biosensor als het biologische moleculen betreft.

Een typische MEMS biosensor bestaat uit een oscillerende cantilever waarvan de resonantie verandert wanneer biomoleculen op hun oppervlakte worden gedeponeerd. De biomoleculen dienen voorafgaand chemisch te worden behandeld om de absorptie te beperken tot hetgeen dat gedetecteerd dient te worden. Voor deze aanpak werd gekozen bij het ontwerp van sensoren welke in staat zijn individuele DNA moleculen, en

zelfs atomen, te detecteren. Voorbij prototypes zijn deze sensoren tot nu toe niet gekomen.

In deze thesis stel ik een ander aanpak voor waarbij gebruik wordt gemaakt van cantilever paren in tegenstelling tot enkelvoudige oscillatoren. Hierdoor kan, naast de oscillatie frequentie, ook de evolutie van de interactie tussen beide cantilevers worden gemeten. Twee extreme apparaten werden behandeld: twee identieke cantilevers, en twee asymmetrische cantilevers. Het gedrag van beide apparaten werd eerst numeriek gesimuleerd, waarna beide in silicium werden vervaardigd, gebruik makend van micro- en nano-fabricatie processen, en werd hun respons experimenteel gekarakteriseerd. Twee identieke cantilevers bleken gevoeliger, maar lastiger te fabriceren. Asymmetrische cantilevers zijn meer robuust en geschikt voor massafabricatie. Een uitdaging bij de fabricatie was het creëren van een opening tussen beide cantilevers, welke maar enkele nanometers breed is. Een nog grotere uitdaging bleek het tunen van de chemische reactiviteit van het cantilever oppervlak enkel nabij de opening, waarbij de rest onaangetast diende te blijven. Ik heb het tweede deel van mijn thesis hieraan gewijd, waarin ik een methode beschrijf om een zelf-uitgelijnde covalente modificatie van het betreffende oppervlak te creëren met nanometrische ruimtelijke controle.

Mijn thesis beschrijft niet een complete biosensor, gereed om te worden ingezet bij de behandeling van patiënten. Hiervoor zou een enorme inspanning zijn vereist, enkel betaalbaar voor een grote farmaceutische partij. Ik heb echter een aantal nieuwe, niet eerder in de literatuur in relatie tot biosensoren besproken, concepten voorgesteld. Daarnaast heb ik vragen gesteld en een technische oplossing besproken om deze te beantwoorden.

Mijn hoop is dat men in de toekomst de vruchten kan plukken van het werk dat ik heb verricht, dat ik mijn ideeën kan ontwikkelen in werkende biosensoren en dat hierdoor de kwaliteit van leven voor veel mensen kan worden verbeterd.

Acknowledgements

My first acknowledgement goes to Petra Rudolf. It is just thanks to her help, her energy and optimistic attitude that I am here filling the last pages of this thesis. I have known Petra for a very long time and it is an honour for me to have been the student of such an excellent scientist and successful woman.

My eternal gratitude goes also to Giacinto Scoles, whom I met unfortunately only in the last years of his career. However, his example has been so important to my formation and although I have been rarely able to implement his wise teachings, if I am, at least a little bit, a Scientist, I owe it to him.

Cinzia Cepek was the one who made this crazy dream become reality. I am deeply indebted to her and I think a gorgeous dinner will not be enough.

I shall try now to mention randomly all the people with whom I shared my hours in the lab, in the cleanrooms, in the meeting rooms, in my office, from the recent years going back into the past. I will definitely forget somebody, you are so many: Enrica, Srinu, Silvia, Luca, Daniele, Damiano, Laura, Elisa, Hossein, Mauro, Nicolas, Emanuela, Valeria, Alpan, Valentino, Jelena, Gianluca, Luca, Enzo, Vincent, Anneque, Davide, Pietro, Denis, Matteo, Loredana, Elena, Daniele, Giorgio, Giorgio, Barbara, Massimo, Lucia, Stefan, Onur, Andrea, Massimo, Mattia, Paola, Marco, Pascà, Silvano, Claudio, Francesco, Daniela, Silvia, Lia, Alfonso, Roberta, Alberta, Monica, John, Paolo, Fabio, Francesco, Francesca, Luca, Paolo, Mario, Corrado and Ugo: wow, that was the very beginning! Thank you all!

In this list I skipped one person with whom I spent several hours in the lab, many, too many, hours talking about science and mostly about the very annoying technical and political problems involved in our job. But then with Elena I also shared the last 12 years of my life, and I am planning to do the same for the all the coming ones. She obviously deserves a special place in this thesis as she has in my life.

Marco